

Reducing biofouling in
reverse osmosis membrane modules
by functional coatings of feed spacers

Dissertation

zur Erlangung des Doktorgrades
der Ingenieurwissenschaften (Dr.-Ing.)

der

Naturwissenschaftlichen Fakultät II
Chemie, Physik und Mathematik

der Martin-Luther-Universität
Halle-Wittenberg

vorgelegt von

Frau Magdalena Jabłońska
geb. am 14.07.1990 in Brzesko

Contents

1	Motivation and objectives	1
2	State of the art	5
2.1	Reverse osmosis (RO) for water desalination	5
2.2	Fouling in reverse osmosis (RO) membrane modules	7
2.2.1	Biofouling and biofilm formation	8
2.2.2	Effect of biofouling on RO performance	9
2.3	Material modification and surface engineering to reduce biofouling	11
2.3.1	Surface properties and susceptibility to biofouling	11
2.3.2	Zwitterionic polymers and their antifouling characteristics	14
2.3.3	Feed spacer modification for biofouling prevention	16
2.3.4	Concept of plasma assisted antifouling coatings of feed spacers	18
2.4	Technologies for surface modification	19
2.4.1	Atmospheric pressure plasma treatment with dielectric barrier discharge in air	19
2.4.2	Graft polymerization onto plasma treated polyolefin surface	24
3	Materials and methods	27
3.1	Substrates	27
3.2	Surface modification	28
3.2.1	Concept	28
3.2.2	Plasma treatment with dielectric barrier discharge (DBD) in air	28
3.2.3	Antifouling functionalization by wet coating	30
3.3	Surface characterization methods	30
3.3.1	Spectroscopic characterization	30
3.3.2	Microscopic characterization	32
3.3.3	Contact angle measurements	33
3.3.4	Time-of-flight secondary ion mass spectrometry (ToF-SIMS)	33
3.4	Preparation of polySBMA gel and its characterization	34
3.5	Evaluation of antifouling potential	35

3.5.1	Concept	35
3.5.2	Discontinuous testing	35
3.5.3	Continuous testing with membrane fouling simulation set-up	36
3.6	Summary	39
4	Results and discussion	41
4.1	Characterization of the HDPE/PP foils and feed spacers	41
4.1.1	HDPE and PP domains distribution	41
4.1.2	Surface chemistry, morphology and topography	45
4.1.3	Discussion	49
4.2	Modification of the polyolefin foils	51
4.2.1	Plasma treatment with dielectric barrier discharge (DBD) in air	51
4.2.1.1	Surface chemistry	51
4.2.1.2	Surface morphology and topography	54
4.2.2	Sulfobetaine methacrylate (SBMA) coating	57
4.2.2.1	Surface chemistry	57
4.2.2.2	Surface morphology and topography	61
4.2.2.3	Coating stability	63
4.2.3	Discussion	65
4.3	Modification of the HDPE/PP feed spacer	68
4.3.1	Surface chemistry	68
4.3.2	Surface morphology and topography	69
4.3.3	Discussion	74
4.4	Examination of antifouling effect	76
4.4.1	Concept for discontinuous and continuous testing	76
4.4.2	Discontinuous testing with <i>Pseudomonas fluorescens</i>	76
4.4.3	Study of the anti-adhesion effect of SBMA coatings	79
4.4.4	Continuous testing with fouling simulation set-up	83
4.4.5	Discussion	88
5	Summary and conclusions	91
	References	94
	Abbreviations	115
	List of chemicals	118

Acknowledgments

I would like to express my gratitude to everyone who has supported, motivated, and taught me along the way to complete this thesis. Firstly, I would like to acknowledge my supervisors. I would like to thank Prof. Dr. Ralf B. Wehrspohn for the opportunity to work on antifouling modifications for reverse osmosis membrane modules at Fraunhofer IMWS in Halle, as well as for supervising my PhD thesis at Martin-Luther-University (MLU) Halle-Wittenberg. I wish to also acknowledge the support of Prof. Dr. Andreas Heilmann. I appreciate a chance to become a member of your research group in July 2015. Thank you for your time, patience, constructive criticism, and advice. I wish to express my sincere appreciation to Prof. Dr. Wolfgang H. Binder. I am grateful for an opportunity to join your research group at Martin-Luther-University, and the knowledge I could thereby get. Thank you for your time, questions and feedback to my work. I am especially thankful to Prof. Dr. Jörg Friedrich. I was glad to learn about plasma chemistry of polymer surfaces not only from your books but also through numerous discussions. Thank you for your energy, plenty of ideas, interesting stories from the past. I wish that everyone would have such a passion for work like you.

Many thanks to my colleagues from Fraunhofer IMWS for a supportive atmosphere at my working place. I would like to thank Dr. Christian Schmelzer, my group leader. I appreciate your indulgence and time which I received to finish my thesis. I also express my gratitude to all members of a business unit Biological and Macromolecular Materials. I would like to thank Dr. Ulrike Hirsch for support at the beginning of my PhD journey, Matthias Menzel for numerous AFM analyses, Stephan Reißaus for performed ToF-SIMS measurements, Marco Rühl for construction of a fouling simulation set-up, Werner Petzold and Tobias Kürbitz for introducing me to microbiological techniques, Dr. Sven Henning for discussions about the morphology of polymer surfaces, Dr. Sandra Richter, Nico Teuscher and Sven Pohle for your guidance and help regarding plasma treatment. I would also like to thank my other colleagues: Dr. Andrea Friedmann, Marco Götze, Tobi Hedtke, Nicole Michler, Dr. Andreas Kiesow, Maria Morawietz, Dr. Sandra Sarembe, Carolin Ufer, Claudia Stehr, Heike Irrgang, Dr. Christiane Lindner, Dr. Uwe Spohn, Dr. Stefan Schwan, Dr. Jessica Klehm, Annika Thormann, Ute Heunamann, Dr. Angelika Hähnel and Maik Rudolph. Many thanks for your contribution and mental support throughout the process of working on this thesis.

I am also very grateful to my colleagues from IAB Ionenaustauscher GmbH Bitterfeld (Lanxess AG). Dear Carsten, Karina, Sasaki-san, Julien, Ruben, Celiné, Ye Wee, Jana, Stefan, Judith,

Lukasz, I am thankful for the time which I spent in Bitterfeld exploring the reverse osmosis membranes. The internship in your team has encouraged me to begin this study.

I highly appreciate the support from other PhD students at Fraunhofer IMWS as well as at MLU (research group Prof. W. H. Binder). Thank you for your feedback during our regular meetings and your expertise which you shared with me when it was needed.

I would like to thank Dr. Miriam Unger (Anasys Instruments) for performed AFM-IR analyses and Dr. Hendrik Budde (Fraunhofer PAZ) for GPC investigations.

I would also like to say a heartfelt thank-you to my family. Mum, Dad, Piotr, you always believe in me and encourage me to accomplish my goals. You went through this time, sometimes really tough, with me. Without your supportive “yes, you CAN” I wouldn’t be where I am today.

Dear friends, you also contributed to this work. Thank you for believing in my abilities, asking how is it going, and giving me reasons to smile. My friends from Halle: Vinh, Ramona, Ania, Alina, Hamed, Begnaz, Sahar, Christina, Uta, Andrea, Franzi, Asia, Michał, Tomek, I was lucky to meet you here. I am also pleased to have amazing friends in Poland. You cannot imagine how many times you have raised my spirit. Even though most of you were far away, I felt your support. I am sure that you are always on my side, regardless of which way I currently go. Dear Ala, Karolina, Michał R., Mateusz, Tomek D., Ula, I owe a lot to you.

Once you stop learning, you start dying - A. Einstein

Abstract

Reverse osmosis (RO) is an energy-efficient technology for the production of high-quality drinking water from seawater. Despite numerous advantages of reverse osmosis membrane technology, performance and durability of spiral-wound membrane modules are often negatively affected by biofouling. Biofouling is defined as the undesirable deposition of microorganisms that can build complex communities called biofilms. Besides modification of the reverse osmosis membrane, a possible strategy to postpone biofouling is chemical modification of a feed spacer surface. The feed spacer is used to separate membrane sheets and to improve mixing. Because of its grid-like structure, the feed spacer provides spots with a poor mass transfer, and therefore it is very susceptible to biofouling.

This work aimed at the development, characterization, and application-related testing of non-toxic antifouling feed spacer coatings. A two-stage procedure, combining an atmospheric plasma treatment with a subsequent wet chemical coating with zwitterionic sulfobetaine methacrylate (SBMA), was used for the chemical conditioning of feed spacer material. The feed spacer is a polymer blend consisting of high-density polyethylene (HDPE) and polypropylene (PP). Investigations were made on the original spacer grids as well as on foils made of HDPE, PP, and its blend, respectively.

It was shown that the applied plasma treatment with dielectric barrier discharge (DBD) in air increased surface hydrophilicity and introduced oxygen functional groups. Moreover, the generation of low-molecular-weight oxidized material (LMWOM) on the polyolefin surfaces exposed to DBD treatment was detected. The following wet chemical treatment with zwitterionic molecules resulted in a heterogeneous distribution of the SBMA coatings on the spacer material. The coatings were investigated using X-ray photoelectron spectroscopy (XPS) and atomic force microscopy (AFM). Short-term batch experiments were performed to demonstrate the anti-biofouling effect. With SBMA coatings, adhesion of *Pseudomonas fluorescens* bacterium was reduced by about 70%, compared to the untreated surfaces, and the production of extracellular polymeric substances postponed. At the present stage, the fouling experiments performed in a continuously operated fouling simulation set-up did not show significant biofouling mitigation of the surface-conditioned feed spacers, which is in contradiction to the short-time batch experiment. Further studies on the antifouling susceptibility of the SBMA conditioned feed spacers under various experimental conditions are suggested.

Kurzfassung

Die Umkehrosmose (RO) ist eine energieeffiziente Technologie zur Herstellung von hochwertigem Trinkwasser aus Meerwasser. Trotz der zahlreichen Vorteile der Umkehrosmosemembrantechnologie (RO) werden Leistung und Haltbarkeit der spiralförmig gewickelten Membranmodule häufig durch Biofouling negativ beeinflusst. Biofouling ist die unerwünschte Ablagerung von Mikroorganismen, deren komplexe Gemeinschaften als Biofilme bezeichnet werden. Neben der chemischen Modifizierung der Umkehrosmose-Membranen ist eine mögliche Strategie zur Verringerung des Biofoulings die chemische Modifikation der Oberfläche des Membranspacers. Der Membranspacer ist der Abstandshalter im Fließkanal des Membranmoduls. Seine gitterartige Struktur sorgt jedoch für eine inhomogene Geschwindigkeitsverteilung des fließenden Wassers und ist damit sehr anfällig für die Biofilmbildung.

Ziel der vorliegenden Arbeit war die Entwicklung, Charakterisierung und Untersuchung einer nicht toxischen Antifouling-Beschichtung für die Spaceroberflächen. Die chemische Konditionierung der Spacermaterialien wurde in einem zweistufigen Verfahren durchgeführt. Eine atmosphärische Plasmabehandlung wurde mit einer anschließenden nasschemischen Beschichtung mit zwitterionischem Sulfobetainmethacrylat (SBMA) kombiniert. Das Spacermaterial ist eine Polymermischung aus Polyethylen hoher Dichte (HDPE) und Polypropylen (PP). Die Untersuchungen wurden sowohl an dem originalen Spacermaterial als auch an Folien durchgeführt, die aus HDPE, PP und aus Mischungen aus beiden Komponenten extrudiert wurden.

Es konnte gezeigt werden, dass mit der Atmosphärendruck-Plasmabehandlung mittels dielektrischer Barriereentladung (DBD) die Oberflächenhydrophilie erhöht und sauerstofffunktionelle Gruppen an der Polymeroberfläche verankert wurden. Darüber hinaus wurde die Abscheidung von oxidierten Polymerbruchstücken mit niedrigem Molekulargewicht (LMWOM) auf den mittels DBD behandelten Polyolefinoberflächen demonstriert. Die nasschemische Behandlung in zwitterionischer SBMA-Lösung führte zu einer heterogenen Verteilung der SBMA-Beschichtung. Die SBMA-Beschichtung wurde mittels Photoelektronenspektroskopie (XPS) und Rasterkraftmikroskopie (AFM) charakterisiert. Mit Kurzzeit-Batch-Experimenten konnte nachgewiesen werden, dass die SBMA-Beschichtung die Adhäsion des *Pseudomonas fluorescens* Bakteriums um etwa 70% verringert und auch die Ablagerung von den extrazellulären polymeren Substanzen im Vergleich zu den unbehandelten Oberflächen reduziert ist. Die Fouling-Experimente, die in einem kontinuierlich betriebenen Fouling-Simulationsaufbau durchgeführt wurden, zeigten jedoch keine signifikante Biofouling-Minderung der oberflächenkonditionierten Membranspacer. Daher wer-

den weitere Untersuchungen zu den Antifouling-Eigenschaften der SBMA-konditionierten Spacer unter modifizierten Versuchsbedingungen vorgeschlagen.

1 Motivation and objectives

The depletion of available drinking water resources has been recognized as a serious global problem. Currently over 2 billion people worldwide suffer from a lack of safe drinking water at home. According to the recent World Health Organization (WHO) report, half of the world's population will be affected by water scarcity by 2025 [163]. Concerning the growing demand for drinking water, as well as decreasing available freshwater resources, an improvement of water treatment technologies efficiency becomes a very important mission. Desalination and wastewater treatment have shown a great potential to supply energy-efficient, affordable, and safe drinking water and thus overcoming drinking water scarcity [62]. Among all available desalination technologies, one of the most energy-efficient, easy to operate and commonly employed is reverse osmosis (RO). The RO process consists in the reverse of a naturally occurring osmosis phenomenon. If the pressure greater than the osmotic pressure of the saltwater is applied along a semipermeable membrane, the water molecules can be filtered from the sea or brackish water. In the majority of currently operated RO plants, desalination is carried out using spiral-wound membrane modules, an example of such is schematically presented in Figure 1. Following main elements can be distinguished in the RO membrane module: **polyamide (PA) membrane** responsible for desalination process; **feed spacer** (netting, made of polypropylene (PP) or its blends with high-density polyethylene (HDPE)), which creates the channel between the membrane sheets for the water flow; and **permeate spacer**, which collects desalinated water to the **central pipe**. Drinking water (permeate) and more concentrated salt water (concentrate) are produced by RO filtration.

One of the most severe problems affecting the performance of commercial RO membrane modules is fouling. This phenomenon is described as undesirable deposition of particles, colloids, organic matter, salts or bacteria on the membrane or the feed spacer. Fouling has plenty of negative consequences for the desalination process, among others reduces the permeate stream, increases energy consumption, destroys the membrane and shortens the RO module lifetime. Especially challenging type of fouling is microbiological fouling (biofouling), which is defined as adhesion and accumulation of microorganisms. Biofouling is hard to control due to the ability of bacteria to multiply and relocate. Furthermore, the remarkable resistance of microorganisms to disinfection agents causes the already occurred biofouling difficult to remove [68, 144]. Example of severely fouled feed spacer and RO membrane from the full-scale desalination plant are illustrated in Figure 2.

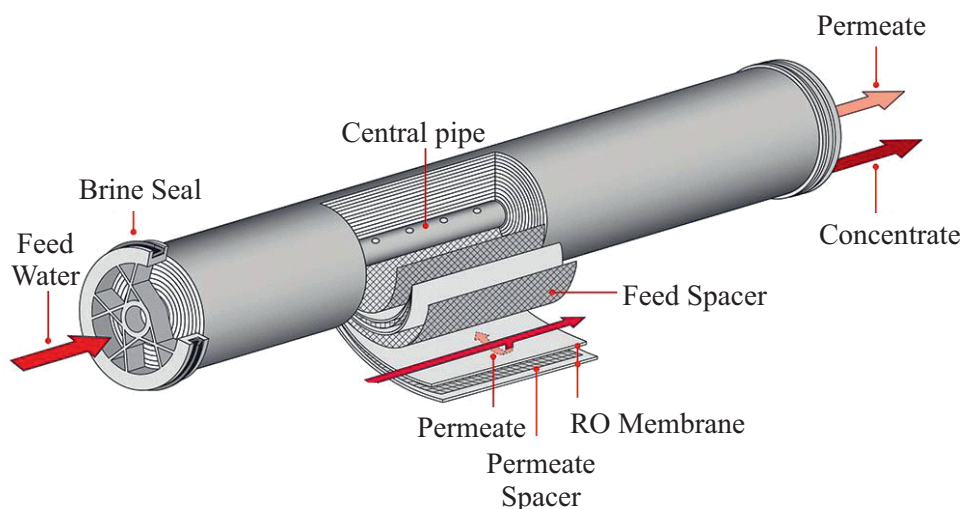


Figure 1: Spiral-wound reverse osmosis (RO) membrane module (adapted from [3]).

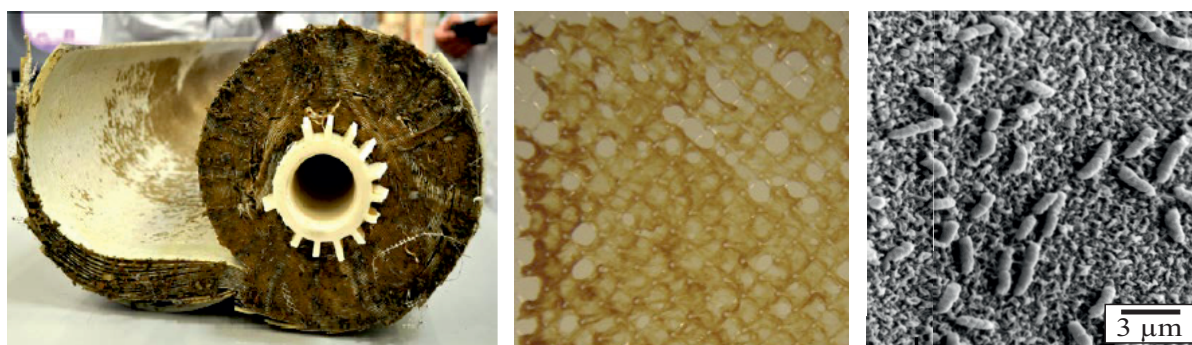


Figure 2: RO module (left), feed spacer (middle) and polyamide membrane (right) affected by microbiological fouling [223, 21].

A possible strategy to mitigate biofouling in the spiral wound RO modules is the membrane or feed spacer modification (both components depicted in Figure 3). Numerous studies on PA membrane conditioning for biofouling reduction have been already accomplished [111]. However, from the industrial point of view, the modification of the fragile membrane surface is complicated due to the potential damage of the semipermeable layer. Any defects in the PA would not only promote the bacterial adhesion but also drastically reduce desalination efficiency [5]. Moreover, according to the current reports from the autopsies on RO membrane elements, biofouling starts not on the membrane surface itself, but alongside the feed spacer situated between the membrane sheets [223, 211].

The conclusion that biofouling might be a feed spacer problem has encouraged the research community to work on the improvement of the feed spacer characteristics. The following strategies to modify the feed spacer can be distinguished: altering geometry, or changing the chemistry. RO

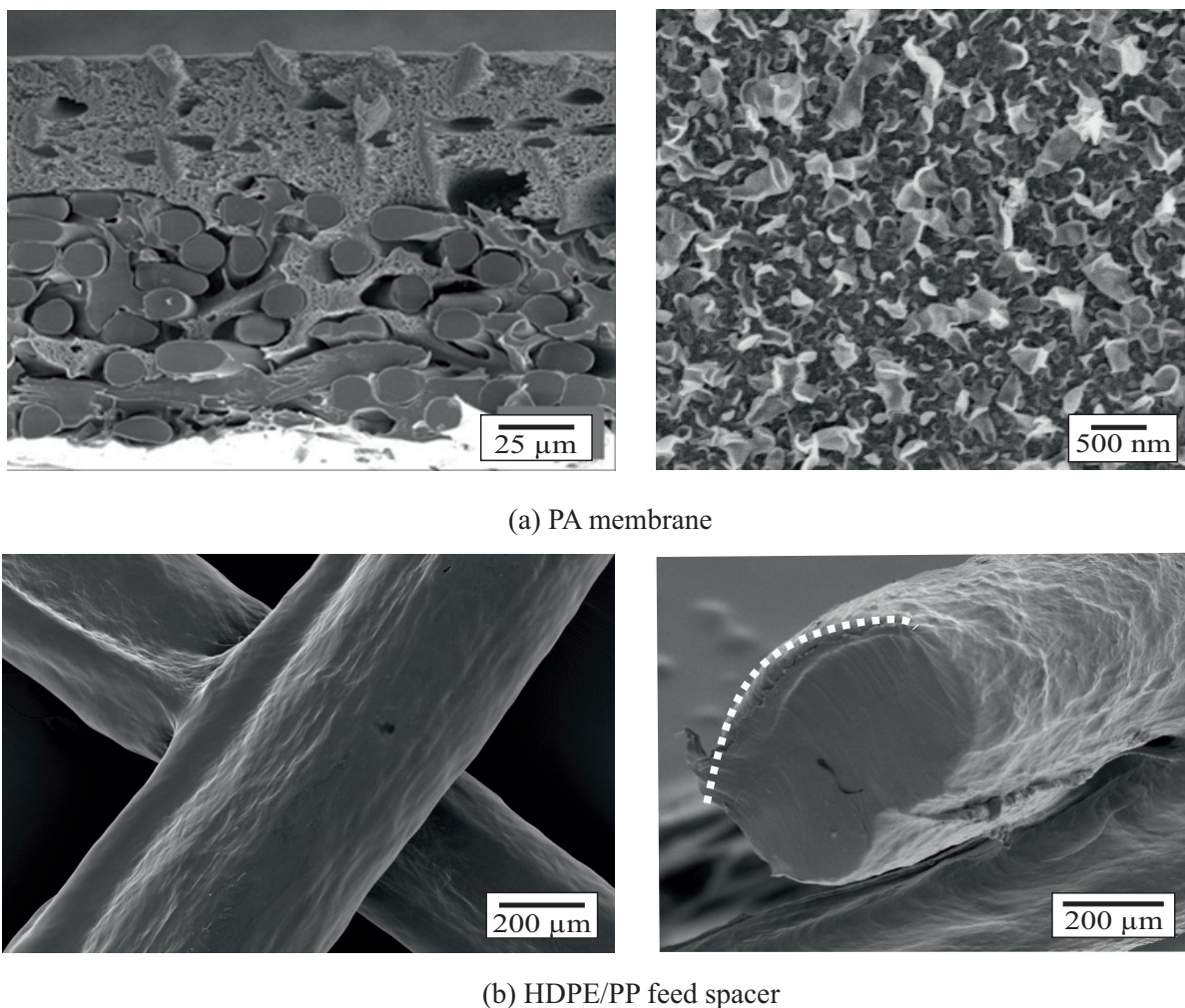


Figure 3: a: PA membrane (left: cross-section; right: surface), b: HDPE/PP feed spacer (bend structure highlighted).

membrane elements with optimized feed spacer geometry are already produced on the industrial scale (e.g. thin-thick strain design in Lewabrane[®] ASD elements from Lanxess [4]). However, none RO membrane module with antifouling feed spacer coating is currently available on the market. A combination of optimized feed spacer geometry with functional coating could be the most promising until now solution to suppress biofouling. This hypothesis prompts a study for the chemical conditioning of the feed spacer. Therefore, in the presented work the potential strategies to generate antifouling coatings of the HDPE/PP feed spacer (composition: 80 wt% HDPE; 20 wt% PP) were developed and their efficiency was examined.

The proposed process for the feed spacer modification should be economically affordable and transferable to the industrial scale. The generated antifouling coatings should be non-toxic and ensure a long-lasting effect. Considering the requirements of the process and coating characteristics, plasma treatment technologies in combination with wet chemical methods were applied for the feed spacer modification. As coating agents, zwitterionic and hydrophilic molecules were selected, well known due to their superior antifouling properties [189, 48, 94]. Chemistry, topog-

raphy, and morphology of the created coatings were analyzed. An anti-biofouling potential was tested discontinuously using commonly found in water microorganisms, as well as continuously using a fouling simulator developed for this purpose. A proposed strategy for the HDPE/PP feed spacer modification is schematically summarized in Figure 4.

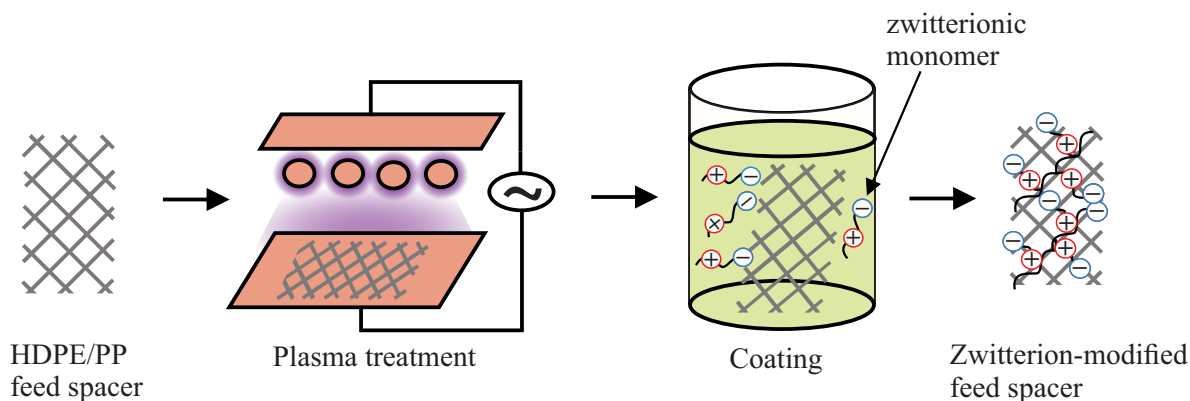


Figure 4: Plasma mediated zwitterionic coating of HDPE/PP (80/20 wt%) feed spacers.

One of the challenges in the chemical modification of the feed spacer surface is the material geometry. High irregularity and bend structure (as illustrated in Figure 3b) impede comprehensive surface characterization. To overcome this limitation and to achieve better control of the process parameters, preliminary studies were performed on the HDPE, PP and HDPE/PP foils manufactured from the same raw materials.

For the generation of the antifouling feed spacer coatings, their characterization and evaluation of antifouling properties, the following objectives were addressed in this study:

- Characterization of the HDPE/PP blend foil and feed spacer surfaces
- Plasma treatment and wet coating of the HDPE/PP substrates
- Chemical and morphological characterization of the plasma-treated and wet coated HDPE/PP substrates
- Discontinuous antifouling testing of the modified HDPE/PP blend foils and feed spacers
- Continuous antifouling testing of the modified feed spacers in fouling simulator

The organization of the thesis follows the given objectives.

2 State of the art

2.1 Reverse osmosis (RO) for water desalination

Reverse osmosis (RO) is one of the most energy-efficient methods to desalinate water [14]. It has been currently applied among others to produce drinking water from sea/brackish water, treat wastewater, generate high-purity water for pharmacy or ultra-pure water for microelectronics [116]. Figure 5 schematically illustrates the principle of reverse osmosis desalination. If two solutions with different concentrations are separated via the semipermeable membrane, a thermodynamically driven osmosis process leads to the transport of water molecules from the dilute (π_2) to the concentrated solution (π_1). The diffusion of water takes place until the equilibrium is reached. When a pressure greater than osmotic pressure ($p_f > \Delta\pi$) is applied to the feed (π_1), the transport of water can be reversed into the direction of the diluted solution. Instead of two equally concentrated solutions, as in the case of osmosis, the RO process generates concentrated saline (concentrate) and a filtrate (permeate). The quality of obtained permeate depends among others on applied pressure, salt concentration in the feed water and membrane type [77]. The osmotic pressure, which has to be overcome in RO membrane separation, is proportional to the salt concentration and temperature. If considering sodium chloride as an ionic compound, osmotic pressure is estimated at 0.7 atm per 1 g/l salt [6]. Currently performed RO membrane processes require 50–60 bar for seawater desalination (about 3.5 wt% salt), while 10–30 bar for brackish water desalination (0.1–0.5 wt% salt) [14].

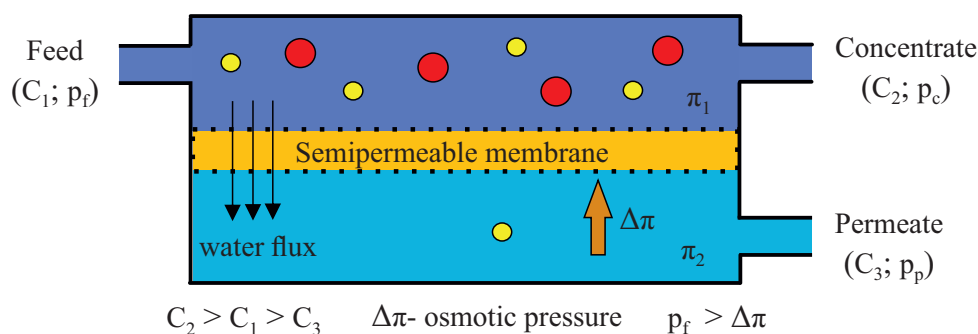


Figure 5: Principle of reverse osmosis.

The osmotic phenomenon for water desalination has been studied since the 1850s. Pfeffer and

Traube were the first who proposed ceramic membranes for salt separation [14]. In the late '60s, Reid and Breton discovered cellulose acetate (CA) as a potential semipermeable membrane material, which enabled to obtain 98% salt rejection under the pressure of 65 bar [175]. Further improvement in membrane performance (an increase of flux) was obtained via anisotropic cellulose acetate membranes. They were implemented by Loeb and Sourirajan (1963) and became commonly used until the middle of the '70s [136]. The latest achievement in the search for a suitable semipermeable membrane material is attributed to the composite membranes produced via an interfacial polymerization method [34]. In 1972 Cadotte synthesized a fully aromatic composite (thin-film composite: TFC) membrane from the reaction between m-Phenylenediamine and trimesoyl chloride [33]. The TFC membranes became a new industry standard in water desalination and remained the most often used to this day. The commercial TFC membrane consists of 3 layers: non-woven at the permeate side (made of polyethylene terephthalate: PET), followed by polysulfone (PS), and semipermeable polyamide (PA) from the feed water side. The cross-section of the TFC membrane is presented in Figure 3 a.

RO membrane *non-woven* with a thickness of 90–100 μm acts as structural membrane support. *Polysulfone* (thickness in the range of 45–60 μm) provides a smooth and highly porous surface giving membrane some mechanical strength and support for the PA layer. High hydrophilicity of PS, its good compression resistance, and stability in acidic media are beneficial for the application in RO membrane processes [128]. Highly cross-linked aromatic *polyamide* (PA) is placed on the feed water side of the membrane. This active membrane layer with a thickness of <100 nm does not possess any discrete pores. Water or small molecules with a high affinity to PA diffuse through the free volume between polymer chains (solution-diffusion transport model) [156]. The salt rejection is feasible since the effective size cutoff of the PA layer is below the hydrated radius of sodium and chloride ions (≈ 0.7 nm) [158]. Pore size distribution in the PA layer (pore understood as a PA-free volume) was shown to be pressure-dependent and affects membrane performance parameters such as flux and salt rejection [115].

Polyamide is deposited on the supporting polysulfone by the interfacial polymerization process, during which two agents (amine and acid chloride) react at an interface of two immiscible solvents. Initially, an aqueous solution of an amine-rich reactant, such as m-Phenylenediamine (mPDA), is deposited onto PS support. As next, the immersion in trimesoyl chloride (TMC) dissolved in an organic solvent, such as hexane, is performed. The reaction of mPDA with TMC leads to the formation of a highly crosslinked PA at the interface, while less dense and more permeable PA below [14]. TFC PA membranes produced by interfacial polymerization have been the industrial standard in the desalination process over the last 40 years. On the one hand, they exhibit higher stability, durability, and better performance than the asymmetric CA membranes [18]. On the other hand, however, higher affinity to fouling [63], and pure stability against common disinfectants have to be considered [82]. Recent research on the modification of the composition of the PA layer has been focused mainly on increasing the water permeability (incorporation of carbon nanotubes, zeolites, or aquaporins), reduction of the susceptibility to fouling (application of the biocides such as silver, TiO_2 nanoparticles) or increasing the hydrophilicity [83, 192, 81]. Even

if promising results for incorporated in PA layer additives have been obtained, the transfer of proposed technologies to the industrial scale process is still highly challenging and significantly more expensive than the standard interfacial polymerization process [56].

RO membrane module. Membranes for industrial applications are arranged in plate-and-frame, hollow fine-fiber, or spiral-wound configurations. Such a design leads to greater filtration area in a reduced volume. The most common are spiral wound modules. They are produced as 40 inch long elements with a diameter of 4, 8 or 16 inches and membrane-active area up to 150 m². The schematic representation of the RO membrane module with its main elements is shown in Figure 1. In the spiral-wound RO module, two membrane sheets are glued as an envelope with the PA active layer from the feed water side. Inside the envelope (non-woven side), the permeate spacer is placed. This porous material collects permeate to the perforated central pipe. Feed solution passes from one side of the module parallel to the membrane surface. Applied pressure enables the part of the feed to permeate into the envelope. As next, this part is transported as a filtrate to the collection pipe. Concentrated salt water is a RO by-product. A typical 8-inch membrane module contains about 30 membrane envelopes. The multi-short-envelope module design increases the active desalination area and minimizes a pressure drop [14, 189]. Membrane envelopes are separated from each other by feed spacer, called also netting. The feed spacer is fabricated mainly of PP or HDPE/PP blend. The presence of feed spacer creates a channel for feed water flow, increases turbulence in the module, therefore improves mixing and reduces concentration polarization [86, 108]. An anti-telescoping device (ATD) is located on the ends of the RO membrane module. ATD prevents the shifting of membrane leaves under applied pressure and inhibits bypassing the module by the feed water [14].

2.2 Fouling in reverse osmosis (RO) membrane modules

Fouling is one of the most challenging problems affecting RO membrane modules. This phenomenon can be described as an undesirable deposition of particulate matter from the feed stream on the membrane/feed spacer surface or inside membrane pores, which reduces the membrane performance and decreases permeate quality [68, 100]. The occurrence of fouling is determined by several factors, such as: feed water quality, operating parameters and applied pretreatment methods. The complexity of the fouling process results from the variety of the foulants, as well as their influence on each other [107, 106]. The following fouling types in RO membrane filtration can be distinguished [68, 100, 14]:

- *Scaling* (inorganic fouling): occurs when the solubility of salt ions in the feed water is exceeded, which results in the precipitation on the surface. The most common scalants in RO membrane filtration are: calcium carbonate, sulfate, fluoride and barium sulfate
- *Colloidal fouling*: deposition of fine suspended particles such as slit, clay, silica
- *Organic fouling*: deposition of organic matter e.g., proteins, lipids, humic acid, cell components

- *Biofouling*: accumulation and adhesion of microorganisms which can build biofilms

Accumulation of foulants appears mainly in the form of cake/gel formation, physical pore blocking or concentration polarization (an increase of salt concentration near the membrane surface relative to the bulk feed) [178]. Among all fouling types, biofouling is especially challenging due to the diversity of microorganisms in a water environment, as well as their ability to multiply and relocate [68, 100].

2.2.1 Biofouling and biofilm formation

Bacteria can form complex communities called biofilms. A biofilm in filtration processes is considered as biofouling if it occurs in an undesirable place at the wrong time and leads to unacceptable performance loss and operational problems [144]. Biofilm formation is determined by the presence of the interface, water, nutrients and microorganisms [70]. Biofilms consist of bacteria and their metabolism products: extracellular polymeric substances (EPSs), which are mainly polysaccharides, proteins, lipids and nucleic acids. The EPS promotes adhesion to the surface, cohesion in the biofilm structure and transport of nutrients within the community [71, 201]. Biofilm building allows bacteria to increase the tolerance against environmental stresses and facilitate multiplying, as well as protects the microorganisms from predators [218, 137].

The biofilm expansion is influenced by environmental factors, microbial properties, surface characteristics and surface-bacteria interactions [133, 100]. However, even if the biofilm structure differs depending on the growing conditions, the same sequence of events can be distinguished for the development of any biofilm [27, 144]. Figure 6 schematically represents the crucial steps in the colonization of the surface by microorganisms.

If microorganisms and substrates co-exist in a water environment, the surface becomes initially covered by a thin layer of adsorbed organic molecules. This „conditioning film” (step I in Figure 6) was found to impact the surface properties and facilitate an attachment of bacteria cells to the substratum. Secondly, microorganisms move in the direction of the substrate surface, which can be driven by Brownian motion, gravitation, convection, or diffusion (step II in Figure 6). If a microorganism reaches the surface, the primary bacteria attachment can occur, at this stage still reversible. In the following reproduction phase, attached cells begin to co-aggregate, form microcolonies and start producing EPS, which provides additional stability and integration to the biofilm structure (step III in Figure 6). Subsequently, part of the cells detaches to colonize a new area and increase the population density (step IV Figure 6).

Considering the biofilm development over time, three main phases can be distinguished: induction, logarithmical growth, and plateau [68, 144]. The *Induction phase* is characterized by the initial microorganisms’ adhesion and limited by the cell density in the feed water. This primary phase is followed by the *logarithmical growth* on the surface, where the biofilm expansion becomes more significant than the adhesion of new cells. Adhesion, proliferation, and detachment of the

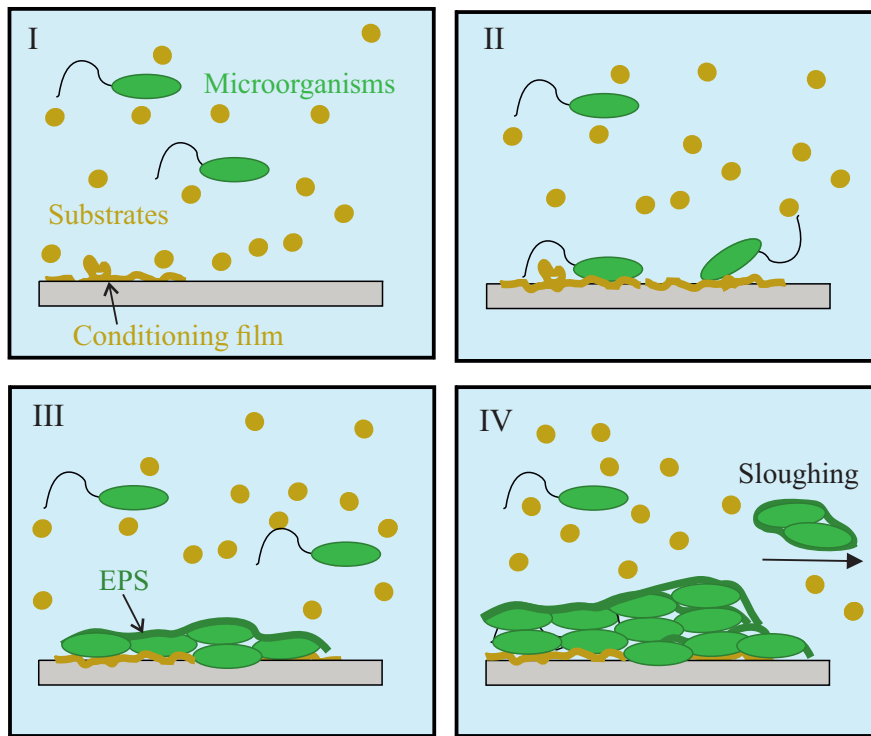


Figure 6: Schematic representation of biofilm formation on a solid surface in water environment (steps I–IV). I: Generation of „conditioning film”; II: Initial bacterial adhesion; III: Colony establishment, production of extracellular polymeric substances (EPSs); IV: Sloughing and colonization of other areas (adapted from [27]).

cells reach an equilibrium over time, which is known as the *plateau phase*. The plateau phase is regulated by nutrient concentration, the mechanical stability of the biofilm structure, as well as the involved shear forces. At this stage of biofilm development, the original properties of the affected surface are masked by microorganisms.

2.2.2 Effect of biofouling on RO performance

The biofilm on the RO membrane acts as a secondary membrane involved in the separation process. The occurrence of biofouling on the membrane or feed spacer surface has plenty of negative consequences on the filtration process, among others [68, 100]:

- decrease of permeate production due to the reduced available active membrane surface (initial rapid flux decline followed by gradual decay)
- increased energy consumption resulting from the necessity to apply higher operational pressure (higher costs)
- decrease of salt rejection
- additional costs because of used cleaning chemicals

- higher risk of concentration polarization due to reduced turbulence near the membrane surface
- decrease of module lifetime (in the worst case element replacement necessary)
- possible permeate contamination and potential microbial attack on the membrane elements such as glue lines.

Since membrane fouling leads to serious operational problems in the RO plant, its control and prevention play an important role. The probability of fouling depends greatly on the feed water quality. Control strategies are developed individually for each desalination plant [14]. A comprehensive antifouling procedure for any RO filtration system should integrate appropriate pretreatment to minimize the probability of fouling, monitoring strategies to detect its early stage, as well as membrane cleaning to handle the resulting fouling [69, 100, 144].

The feed water in RO processes contains plenty of contaminants such as colloidal suspensions, biological matter, mud, sand. To prevent fouling in RO installation and thus extend the RO membrane lifetime, various physical, mechanical, and chemical pretreatment technologies are practiced [192]. The most suitable method or their combination is chosen based on the feed water composition analysis. Disinfection, coagulation, as well as micro-, ultra-, and nanofiltration are the most commonly used approaches for biofouling prevention [100, 77].

Since the fouling phenomenon is still not fully understood, there is no versatile approach to predict the fouling in RO membrane modules [104, 111]. Nevertheless, in-situ and real-time monitoring of the filtration process is an important practice in the early detection of fouling. Parameters such as pressure drop, conductivity, and flux decline are the most often monitored. However, none of them allow identifying the threat of fouling at an early stage, which is necessary for effective prevention [100].

Membrane cleaning is another important routine in the RO plant operation [183]. Suitable physical, chemical, biological or enzymatic methods are selected based on the membrane type, foulant components and feed water chemistry [14, 100]. The chemical cleaning is applied if normalized permeate flow decreases by 10%, pressure drop increases by 15%, or normalized salt rejection decreases by 10% to the initial conditions [77]. A typical cleaning procedure for the RO membrane system consists of flushing the module with a cleaning solution at high speed, followed by soaking, and the second flush. If fouling occurs on the front part of the filtration system, reverse flushing is employed (circulation opposite to the usual feed water flow) [7, 14]. Membrane cleaning is aimed to reduce the adhesion of foulant to the surface and cohesion forces between foulant particles. Acidic cleaning agents (nitric acid, sulfuric acid) are usually applied to remove scaling. Alkaline cleaners, such as sodium hydroxide, are utilized to eliminate organic fouling and biofouling [7]. Importantly, the chemical cleaning has to be appropriately scheduled to reduce progressing membrane degradation [14].

It has been reported that all fouling types, except biofouling, can be successfully controlled

employing suitable pretreatment processes. The presence of microorganisms in industrial systems such as RO desalination plant is inevitable, which makes biofouling such a troublesome issue [68]. Even regularly applied chemical cleaning has been found insufficient to ensure complete biomass removal. Moreover, used for this purpose chemicals, cause the weakening of the PA membrane. They also might contribute to the re-growth of biofilm due to the presence of dead bacteria, which are the potential nutrient source [53]. Since the sterile conditions in the RO plant can not be maintained, and the presence of bacteria is unavoidable, a possible strategy to postpone biofouling is to impede the bacteria adhesion to the surface.

2.3 Material modification and surface engineering to reduce biofouling

2.3.1 Surface properties and susceptibility to biofouling

In order to improve the anti-biofouling properties of the surface, surface-bacteria interactions and bacterial adhesion phenomena have to be studied. Initial bacteria adhesion to the surface has been found as a crucial step in biofilm formation [144, 100]. There are plenty of factors affecting the adhesion of microorganism to the membrane or feed spacer surfaces, such as [100]:

- *microbial properties* (hydrophobicity, surface charge, structure, EPS characteristic)
- *membrane and feed spacer characteristic* (morphology, roughness, composition, charge, hydrophobicity, feed spacer configuration)
- *operating conditions* (temperature, pH, pressure, salt concentration, cross-flow velocity, permeate flux, feed water quality).

Most of the models which describe bacterial adhesion consider this phenomenon on two bases: long-range non-specific macroscopic interactions, as well as short-distance specific molecular interactions. Non-specific interactions occur between a microorganism and a surface and originate from macroscopic surface properties (e.g., charge, free energy). Considering a bacterium in the water system moving towards a solid surface, the following physicochemical forces between the cell and the surface occur: van der Waals interactions (generally attractive); electrostatic interactions (influenced by ionic strength and pH of the system); and acid-base hydrophobic interactions (depend on the system, bacterium and surface properties). When the bacterium is sufficiently close to the surface (<1 nm), the specific interactions become crucial. Those interactions exist between particular molecular groups of the bacterium cell wall and the substratum surface and enable irreversible adhesion [31, 27, 20].

The microbial structure and properties are often simplified for the studies on the adhesion phenomenon. Nevertheless, microorganisms cannot be treated as “ideal particles” with simple geometry and consistent composition, as used to apply to describe their behavior. The bacterium cell wall consists of individual layers with a specific structure and chemical nature, which may also vary depending on the environmental conditions such as pH, temperature, and access to nutrients

[140, 31]. Moreover, bacteria cell appendages (e.g., pili, fimbriae) contribute to microorganism's adhesion, which is difficult to address in general adhesion models. For these reasons, any considerations regarding the adhesion of microorganisms to the surface shall be taken from the conceptual level [218]. The absolute adhesion force between microorganisms and substratum also depends on time in contact and metabolic activity of bacteria [11]. Therefore, plenty of contradictory findings on biofilm development can be found in the literature. Published studies are often difficult to compare due to the variety of experimental conditions and fouling reagents.

Apart from the microorganisms characteristic, substratum property is another significant factor affecting bacteria adhesion. Several reports are discussing the influence of surface features on bacterial adhesion and antifouling performance [198, 242, 35, 168]. Figure 7 schematic illustrates the commonly accepted material properties influencing microorganisms' adhesion and biofilm formation.

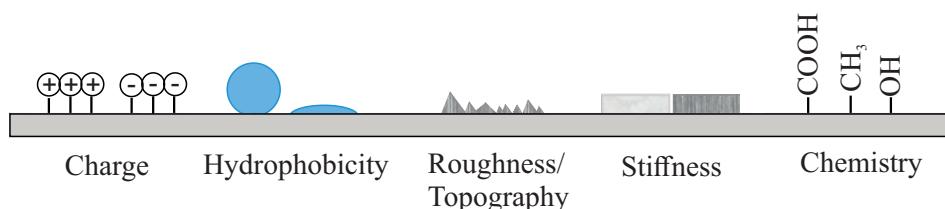


Figure 7: Schematic illustration of surface properties influencing bacterial adhesion (adapted from [198]).

Surface charge. Most bacteria cell walls are negatively charged, therefore negatively charged surfaces are believed to provide electrostatic repulsion effect and be less prone to biofouling [155]. However, charged surfaces can interact with other components in the water environment, for instance with proteins. Such attractive interactions lead potentially to organic fouling on the surface, and as a consequence, exaggerate bacterial adhesion. For this reason, a neutral surface charge is more favorable in complex water systems [35].

Surface hydrophobicity. Hydrophilic surfaces are generally less prone to fouling than hydrophobic ones. For instance, Fletcher et al. analyzed the *Pseudomonas* bacterium attachment to various hydrophilic (e.g., glass, mica) and hydrophobic (e.g., Teflon, PE, PET) substrates. They reported reduced biofouling with increasing material's hydrophilicity [72]. The formation of a dense hydration layer on the hydrophilic surface is responsible for the weakening bacteria-surface interactions [148]. The presence of water film requires previous dehydration (disruption of hydration layer) and therefore results in thermodynamically unfavorable attachment [159].

Superhydrophobic surfaces are also beneficial in biofouling mitigation. For instance, the surface of a lotus leaf exhibits superhydrophobicity. Specific micro- and nanostructure enables entrapment of air between surface features, which results in low surface free energy (water contact angle about 170°) and a high degree of foulant retention [244].

Roughness and topography. The contact area between substratum surface and bacterial cells increases with an increase in surface roughness. Moreover, higher roughness creates low shear areas. Therefore, it facilitates the microorganisms' attachment and promotes irreversible adhesion [209, 111]. As reported elsewhere, hydrophilic surface with low roughness promotes the water layer formation and thus enhances the antifouling property [50]. However, the effect of surface roughness on bacterial adhesion and biofilm formation varies depending on the bacterial cell characteristic (size and shape) and environmental factors. For this reason, an optimal roughness which enables to suppress bacterial adhesion can not be given [198]. A macro-roughness (around tens of microns) can be generally neglected for the biofouling phenomenon since this magnitude significantly overcomes a typical size of a bacterium (0.5–2 μm [141]). However, micro- and nano-roughness (around 1 μm and below) are of great importance [159]. Not only an average amplitude of surface peaks matter but also the distribution of peaks and valleys has a meaningful effect on the adhesion phenomenon [198]. Furthermore, surface defects (e.g., scratches) and irregularities promote bacterial accumulation and biofilm formation, since those are not easy to wash (so-called dead-zones) [146, 147].

Surface stiffness. An effect of material stiffness on the susceptibility to fouling is the least explored in the literature until now. Nevertheless, some studies regarding the effect of surface stiffness on bacterial attachment can be found. For instance, Song et al. analyzed an early stage of *Escherichia coli* and *Pseudomonas aeruginosa* biofilms formation on hydrophobic polydimethylsiloxane (PDMS) with various degrees of cross-linking (elastic modulus (E) between 0.1 MPa and 2.6 MPa). They observed that lower surface stiffness facilitated the attachment and growth of both tested bacterial species [199]. Dissimilar conclusions were drawn by Lichter et al., who observed a positive correlation between the adhesion of *Staphylococcus epidermidis* and *Escherichia coli* bacterial species and the stiffness of poly(allylamine hydrochloride) (PAH) and poly(acrylic acid) (PAA) thin films (elastic modulus: 1 MPa < E < 100 MPa) [134]. Saha et al. investigated the adhesion and growth of *Escherichia coli* and *Lactococcus lactis* depending on the stiffness of layer-by-layer deposited hyaluronic acid derivative grafted with vinylbenzyl groups (HAVB)-poly(L-lysine) (PLL) (considered elastic moduli: 30 kPa and 150 kPa). There was no significant difference in *Lactococcus lactis* biofilm development for investigated surfaces. However, *Escherichia coli* exhibited an enhanced growth on softer material compared to the stiffer one [184].

It is difficult to draw an unambiguous conclusion regarding the effect of material stiffness on antifouling property. Available literature addresses materials in different rigidity range, as well as with different surface chemistries. Nevertheless, the influence of material stiffness on microorganisms' attachment and biofilm formation should be considered. The underlying mechanisms are still poorly understood.

Surface chemistry. Let us consider non-toxic and non-biocide-release antifouling approaches. There are two types of antifouling surfaces. The first inhibits microbial attachment, while the second facilitates the removal of already adhered microorganisms [159].

In order to promote microorganisms' detachment, the weak adhesion strength between microorganisms and surface is required. For this purpose, poly(siloxanes) and fluoropolymers are widely used. Silicon-based materials are deprived of micro-roughness, have low critical surface energy and low glass transition temperature. Fluorine-based materials are characterized by dense packing of functional groups and permanent cross-linking, which reduces the possibility of backbone rotation and ensures longer-lasting antifouling effect [159].

To avoid microorganisms adhesion, the most commonly applied are hydrophilic compounds. Steric repulsion effect of the hydrophilic coatings and their ability to form hydration layer contribute to biofouling mitigation. Hydrophilic poly(ethylene glycol) (PEG)- based materials, zwitterionic polymers, or proteins (e.g., sericin) have been extensively studied as fouling resistant coatings for the application in RO membrane modules [50, 159, 243].

A new class of materials that combines anti-adhesion and fouling release strategies are amphiphilic copolymers. They consist of hydrophilic and hydrophobic repeating units. Such heterogeneity at the nanoscale results in unfavorable interactions between the surface and bacterium, therefore, it reduces adhesion and facilitates microorganisms' detachment. [50]. Gudipati et al. were the first who proposed amphiphilic copolymers (hyperbranched fluoropolymer (HBFP)-linear polyethylene glycol (PEG) networks) for the antifouling purpose [85, 84].

It is believed that complete biofouling prevention is not possible [11]. For this reason, a surface design that reduces bacteria attraction postpones adhesion and facilitates biofilm removal is an especially promising answer to the biofouling problem [168]. Detachment facilitating coatings require additional stress, which allows removing loosely bond microorganisms. Furthermore, removal of the cells should occur before the settlement becomes supported by the organic adhesives produced by microorganisms [159]. This requires the development of new biofouling monitoring techniques with high sensitivity. Taking into consideration amphiphilic copolymers, they showed promising results in overcoming biofouling on a laboratory scale. However, they require precise engineering (length and type of segments, structure), and complicated synthesis pathways [239]. For these reasons, their implementation in the industrial process is rather challenging.

Since the initial microorganisms adhesion is a prerequisite for biofilm formation [144, 69], an antifouling strategy based on its postpone appears as particularly favorable. According to the literature, a low-adhesion surface in the water environment should retain the following criteria: hydrophilicity, high hydration ability, and charge neutrality [35, 164, 65]. These requirements are fulfilled by zwitterionic polymers. Their chemistry was found as one of the most effective in reducing bacterial attachment [212]. The antifouling characteristic of zwitterionic molecules is described in detail in the following section.

2.3.2 Zwitterionic polymers and their antifouling characteristics

Zwitterionic polymers possess an equal number of oppositely charged moieties distributed along a polymer chain. The overall charge neutrality results in a lack of favorable interaction with positively- or negatively-charged molecules, which determines excellent antifouling properties

[148, 46]. Not only overall charge neutrality, but also a favorable distance between two charged groups in the zwitterionic polymer chain significantly contributes to the antifouling properties, as shown in the studies on the mixed charged copolymer brushes [44]. It is widely agreed that thin zwitterionic coatings reduce the nonspecific adsorption to the solid/liquid interfaces [189]. Moreover, a surface modification with zwitterions has been found as one of the most promising to reduce attachment of marine organisms, adsorption of protein, or bacterial adhesion [88, 212].

The application of zwitterions for the antifouling modifications was inspired by the composition of the mammalian cell membrane. This membrane contains phospholipids with zwitterion headgroups [189]. The most common zwitterionic building blocks contain phosphorylcholine, sulfobetaine, and carboxybetaine functional groups (see Figure 8) [88]. Phosphobetaine monomers are produced usually from the reaction of 2-Chloro-2-oxo-1,3,2-dioxaphospholane and alcohol-containing monomer, followed by the ring-opening reaction with trimethylamine. Sulfobetaines can be synthesized via the reaction of a tertiary amine with a sultone (e.g., 1,3-Propane sultone, 1,4-Butane sultone). Carboxybetaines are prepared from the reaction of tertiary amine with haloalkyl carboxylates or haloalkyl carboxylic esters [138].

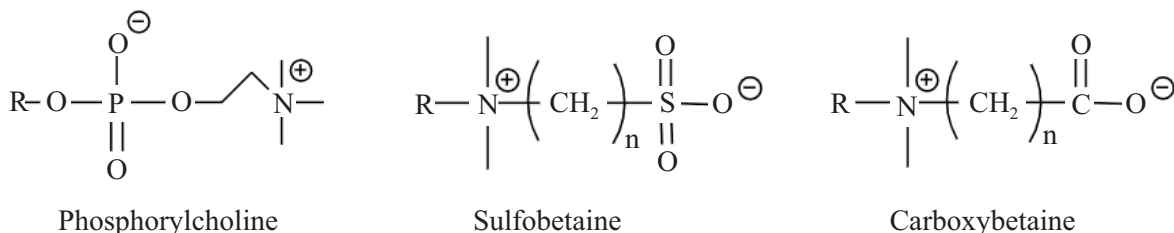


Figure 8: Examples of zwitterionic functional groups.

The antifouling behavior of zwitterions in the water environment is strongly related to the hydration mechanism. Let us consider the zwitterionic layer containing a high amount of water. In this case, no free energy can be obtained while replacing a protein/water interface with a protein/surface interface. Therefore, the adsorption process is entropically unfavorable (water generates an energy barrier). Detailed analyses of the zwitterions' antifouling behavior reported about the particular properties of water affiliated with the zwitterionic layer. First of all, there is associated water that is directly involved in the hydration of zwitterion charged groups. Secondly, unassociated water is located outside the first hydration layer and attracted by osmotic pressure [189]. It was estimated that about eight water molecules are associated with one sulfobetaine unit. Moreover, the water molecules were more tightly bound with the sulfobetaine unit in comparison to the neutral ethylene glycol unit in PEG. This is related to different mechanisms of hydration layer formation: hydrogen bonding for neutral PEG, while strong electrostatic interactions for zwitterionic polySBMA [229]. Two main effects are responsible for the non-fouling properties of the zwitterionic coatings: steric hindrance and hydration (see Figure 9).

The following factors are important to ensure the long-lasting antifouling effect of zwitterionic-

coating: coating thickness, conformation, and flexibility of the chains, as well as packing density for the brush coatings [229, 197, 49]. If a proper architecture of the zwitterionic layer is provided, the antifouling effect is stable even under high-salinity conditions [234]. There are plenty of examples in the literature demonstrating an excellent performance of zwitterionic coatings deposited on different polymer surfaces, among others on PA [94, 237], polystyrene (PS) [45], PP [47, 236], poly(tetrafluoroethylene) (PTFE) [99] and poly(vinylidene fluoride) (PVDF) [40], respectively.

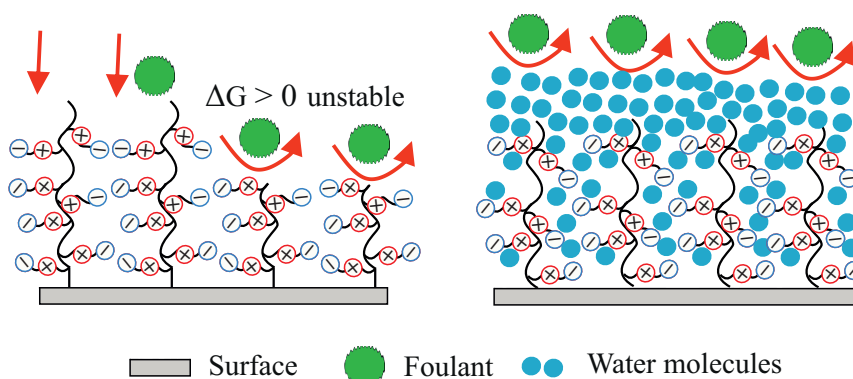


Figure 9: Schematic illustration of the fouling resistance mechanisms of zwitterionic coatings: left–steric hindrance effect, right–hydration layer formation via electrostatic interactions (adapted from [89]).

2.3.3 Feed spacer modification for biofouling prevention

Feed channel spacers are crucial for the spiral-wound RO membrane module operation. The feed spacer provides channels for feed water flow and enhances flow turbulence near the membrane surface. On the other hand, the feed spacer structure results in dead zones with the hindered mass transfer, which are more prone to biofouling [1].

Developing of feed spacers with improved antifouling characteristics is an attractive approach for reducing fouling within the RO module. The optimization of the feed spacer design includes a) geometrical modification (e.g., spacer thickness, internal strand angle, shape, mesh size) and 3D printing; and b) modification of the feed spacer surface via functional coating. Since this work aims to study the chemical conditioning of the feed spacer, the presented literature review focuses on the alteration of the feed spacer surface.

Table 1 summarizes recently reported findings on the feed spacer surface modifications. None of the proposed until now solutions for the chemical modification of the feed spacer could completely prevent the biofilm development. Biocidal approaches, such as zinc oxide or silver nanoparticles [232, 180], showed a promising reduction of biofouling. However, in the case of leakage, there is a risk of water contamination with the toxic compounds.

Material	Deposition technique	Key findings	Reference
Ag nanoparticles	Chemical reduction method	Silver-coated spacers showed slower decrease in permeate flux than unmodified spacers.	[232]
Chelating ligands charged with Cu ions	Poly(glycidyl methacrylate) was graft polymerized to the PP surface followed by reaction with iminodiacetic acid and copper chelation.	Bacteria attachment rate to the membranes with the unmodified spacers was lower than to the membrane with the Cu-modified spacer.	[178]
a) Ag, Cu, Au b) Biostatic spacer	a) Sputter coating b) Commercial product containing Triclosan (0.5 wt.%)	Lower FCPD increase for the silver and copper modified spacers, the best performance was shown by gold-modified sample. The biostatic spacer did not prevent biofouling.	[8]
PDA, PDA-g-PEG	PDA: incubation in buffered solution. PDA-g-PEG: immersion in poly(ethylene glycol) monoamine (PEG-NH ₂) solution	No difference in FCPD increase between modified and unmodified spacers while testing in a membrane fouling simulator.	[151]
ZnO nanoparticles	Sonochemical deposition	Normalized permeate flux of the modified spacer-membrane was about 50% higher than that of the unmodified spacer-membrane. Zinc leaching was detected.	[180]
Diglyme monomer	Plasma polymerization	Only high plasma energy density treatment on the spacer resulted in coating with slightly better performance than the control.	[176]
polyHEMA-co-PEG ₁₀ MA, polyD-MAEMA, polySPMA	Plasma-mediated UV-polymerization	An exponential FCPD increase observed for the polyHEMA-co-PEG ₁₀ MA-, and polyDMAEMA-coated spacers, while a linear increase for the polySPMA-coated spacer. Coating leaching after 30 days observed.	[226]
Graphene nanoplates	Treatment in SDBS, dip coating in the carbon ink containing Graphene Nano-Platelets and treatment in oven	Electrically conductive spacer enhanced the flux during electrolysis cleaning. The efficiency of the flux recovery deteriorated along with a number of fouling-cleaning intervals.	[2]

Table 1: Literature review on chemical conditioning of feed spacers. Abbreviations: FCPD–feed channel pressure drop, PDA–polydopamine, HEMA–2-Hydroxyethyl methacrylate, PEGMA–poly(ethylene glycol) methacrylate, DMAEMA–2-(Dimethylamino)ethyl methacrylate, SPMA–3-Sulfopropyl methacrylate potassium salt, SDBS–sodium dodecylbenzene sulfonate.

The possible presence of biocide in the permeate will conflict with the water quality and health regulations. Moreover, toxic coatings perform analogously to the chemical cleaning, where the first layer of dead cells can be utilized as a nutrient source for the growth of the subsequent microorganisms [226]. This encourages us to look for modification strategies that promote biofouling prevention. Employed up to now approaches were based on hydrophilic polymer coatings. The most promising results until now were obtained for the spacer modified with polySPMA. A noticeably slower feed channel pressure drop (FCPD) development was obtained for the anionic polySPMA-coated spacer compared to unmodified, neutral (polyHEMA-co-PEG₁₀MA) and cationic (polyDMAEMA) coated samples. It was claimed that even better performance could be expected from the modification with zwitterionic polymers [226]. A concept for the feed spacer modification with zwitterionic coatings is presented in the following section.

2.3.4 Concept of plasma assisted antifouling coatings of feed spacers

The commercially available feed spacers for the application in RO membrane modules are manufactured mostly from polypropylene (PP) or high-density polyethylene (HDPE)-polypropylene blends. On the one hand, both components are cost-effective, easy to process, and have good chemical and mechanical stability. On the other hand, they are highly hydrophobic and thus more prone to biofouling [233]. Moreover, both polymers do not possess any functional groups which could be utilized for a subsequent reaction with an antifouling agent (e.g., grafting to reaction). The chemical bonding of antifouling layers has an advantage over the physical deposition. It enables the generation of stable and long-lasting coatings, required for the successful biofouling mitigation.

In this work, a two-stage procedure was proposed for the chemical conditioning of the feed spacer surface. A *first modification step* was aimed at increasing the surface hydrophilicity, enhancing adhesion properties towards coating solution, and producing oxygen functional groups. For this purpose, well established atmospheric pressure plasma treatment with dielectric barrier discharge (DBD) in air was selected [74]. This approach offers quick and non-polluting surface functionalization [74, 230], favorable for scaling-up to industrial technology. A variety of oxygen functional groups is generated on the exposure of polyolefins to plasma (e.g., C-OH, CHO, COOR, COOH, and others). For instance, formed at the surface hydroperoxides, are unstable and thus capable of initiating free-radical graft polymerization onto the surface, as reported elsewhere [96, 230, 208]. The decomposition of hydroperoxides was used in a *second modification step*, where the plasma pretreated samples were immediately subjected to zwitterionic sulfobetaine methacrylate (SBMA) monomer solution. The graft polymerization of SBMA onto the plasma-treated HDPE/PP surface is schematically given in Figure 10.

Zwitterionic SBMA possesses quaternary ammonium cation and sulfonate anion at the same side chain. Besides its excellent antifouling properties (as described in section 2.3.2), it has several other advantages as a coating agent in drinking water production applications. SBMA is known because of its ease of synthesis, low costs, good chemical stability, and non-cytotoxicity [245, 41, 125].

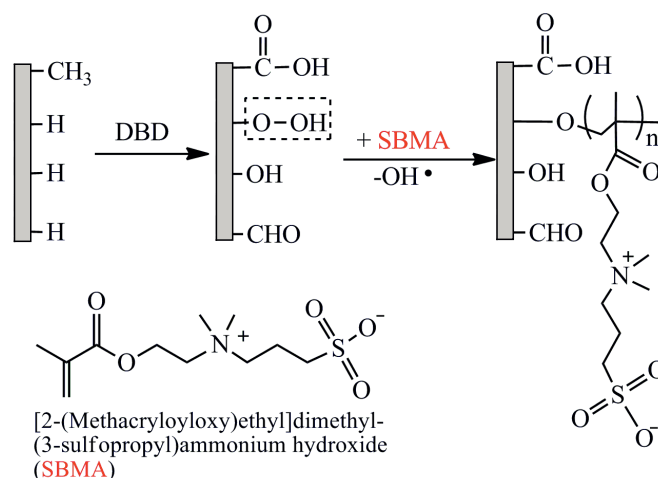


Figure 10: Suggested mechanism for the graft polymerization of SBMA ([2-(Methacryloyloxy)ethyl]dimethyl-(3-sulfopropyl)ammonium hydroxide) onto HDPE/PP surface pretreated with dielectric barrier discharge (DBD) in air (hydroperoxide group highlighted).

2.4 Technologies for surface modification

2.4.1 Atmospheric pressure plasma treatment with dielectric barrier discharge in air

Plasma is the fourth state of matter, defined as a gas in the ionized state [127]. Plasma is a highly electrically conductive mixture of electrons, ions, molecules, atoms, energy-rich neutrals and photons. It emits high-energetic vacuum-UV irradiation (VUV), forms a magnetic field and luminous glow due to the collisions of charged species. Plasma can be created under low, atmospheric and high pressure [74]. For the plasma generation, energy has to be applied to the gas to ionize it. Under atmospheric pressure, energy is transferred, from the applied electrical field, into the acceleration of electrons in the gas plasma, and therefore into their kinetic energy. The charged carriers collide with the neutral species. The energy transfer occurs, allowing the ionization, excitation, and dissociation to proceed. Inelastic collisions moderately raise the kinetic energy of neutral species, while elastic collisions can excite or ionize those neutrals. Since electrons have low mass, they move much faster than heavy particles. They more likely to participate in the collision and transition events, therefore their temperature (T_e) exceeds by orders of magnitude the temperature of heavy particles (T_h) in a plasma [210, 169, 206]. Since neutral and ionic species remain relatively cold, surface thermal damage is prevented. If $T_e \gg T_h$, plasma is identified as non-thermal, cold, low-temperature or non-local thermodynamic equilibrium plasma (non-LTE). Non-LTE plasmas include corona discharges, dielectric-barrier discharges (DBDs) and glow discharges. They are frequently applied to the polyolefin surface to improve the wetting and adhesion properties, for instance before printing or coating [112, 210]. The density of charged particles in the non-LTE plasma is in the range of 10^6 – 10^{20} particles/ m^3 , whose average energy is within 0.1–10 eV [32].

One of the most widely used atmospheric-pressure plasma systems is based on filamentary dielectric barrier discharges (DBDs), also known as "industrial corona". DBDs were originally used to generate ozone [195]. However, nowadays, they have found a wide range of applications, among others, in fluorescent excimer lamps and flat plasma displays or pollution control by the treatment of volatile organic compounds (VOCs) [112]. Non-thermal plasma generation with DBD is also commonly employed to treat polymer materials, mostly for surface cleaning, etching, activation, and functionalization [28]. The DBD treatment allows quick modification of the surface without altering the bulk properties, does not require expensive vacuum apparatus, or use of toxic solvents. During exposure to DBD, a polymer substrate is passing through the plasma zone (discharge gap) created between two electrodes separated by an insulating (dielectric) material. High voltage is required to generate a breakdown in the gas at atmospheric pressure, for most applications, in the kHz-range [196, 28]. Sinusoidal or pulsed power sources are usually employed. Distinct plasma filaments (microdischarges) are ignited when the breakdown field is reached, and extinguish when the plasma conductivity is reduced via electron attachment and recombination [112]. A discharge gap is usually in the range of 0.1–10 mm, while a microdischarge has a duration of about 10–100 nanoseconds and a diameter of tens to hundreds of micrometers [59]. The electrical breakdown results in the formation of charges on the insulator's surface. The charges created on the dielectric surface induce an opposed electric field to the currently applied, which leads to the discharge extinction. The dielectric layer hereby prevents the arc or spark formation [210].

Two different planar DBD configurations can be distinguished: volume DBD (VDBD), and surface DBD (SDBD). Considering volume DBD systems, the following set-up constructions can be found: either one or both electrodes are covered by a dielectric layer (e.g., glass, ceramics, quartz); alternatively, the insulator is placed between two electrodes and separates the discharge gap in two sections. In the SDBD configuration, plasma is generated at the exposed surface electrode and distributed along the dielectric surface. The counter electrode is placed in an additional dielectric layer [196, 28]. Figure 11 schematically illustrates the plasma species in volume DBD with double-sided dielectric configuration operating in air.

It is commonly accepted that processes involving plasma treatment are complex, and the comprehensive understanding of plasma-surface interactions is a scientifically challenging task. Taking into consideration polyolefins, they cannot distribute plasma energy over the bulk. Therefore, during exposure to plasma, energy-rich spots are formed. Those areas are characterized by increased mobility of polymer chains, side-chains, or functional groups. Consequently, the following processes on the polyolefin surface are likely to occur: functionalization, cross-linking, etching and degradation [59, 74, 28].

The active moieties of the atmospheric plasma generated in air can be divided into: (i) reactive species, which introduce new atoms at the surface, in humid air the following: O_2 , O^\bullet , HO^\bullet , O_3 , HO_2^\bullet , H_2O_2 , N^\bullet , and NO_x ; or (ii) nonreactive species, like photons, electrons, ions, etc. Their energy exceeds significantly the C–H and C–C binding energies in polyolefins (4.3 eV

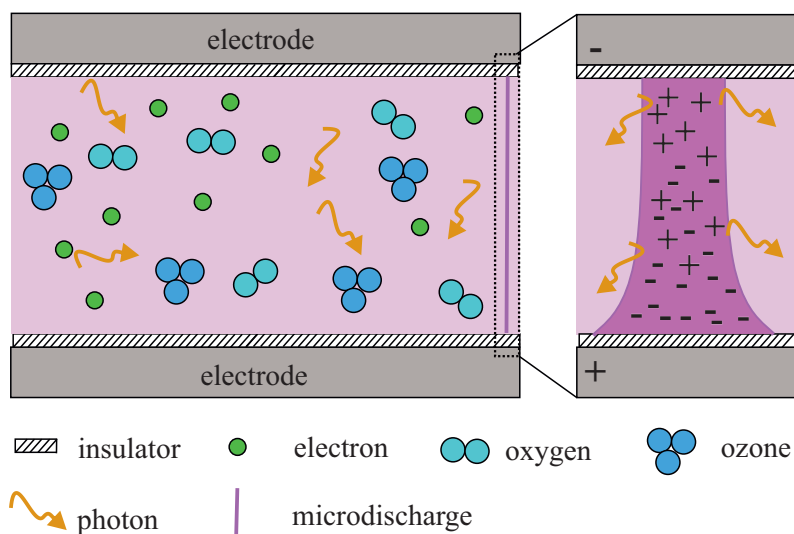
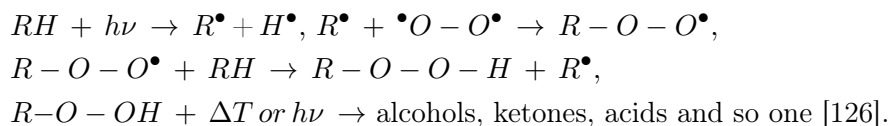


Figure 11: Schematic representation of volume DBD with double-sided dielectric configuration: left–plasma species, right–single microdischarge in a discharge gap (adapted from [74, 109]).

and 3.7 eV, respectively). Therefore, they excite the polymer or break the C–C or C–H bonds and thus create polymer radicals. These polymer radicals react: (a) between themselves, resulting in cross-linking or double bonds; or (b) with reactive species present in the discharge phase; or (c) with O₂ from air during the post-plasma oxidation processes [143, 204, 74]. Scheme 12 depicts the possible radical processes at the polymer surface upon exposure to plasma in air [74].

Taking into consideration the great energy and enthalpy excess present in plasma, polyolefin chain scission and hydrogen abstraction events occur to almost the same extend. Consequently, non-selective reactions dominate and a broad variety of functional groups are produced. For instance, the analyses performed on the plasma-treated poly(ethylene terephthalate) showed the formation of at least 12 different O-functional groups [74]. The mechanism of polyolefin oxidation in plasma is analogous to the thermal oxidation of paraffin and bases on the Engler-Bach peroxide theory [227, 64, 10]. Firstly, the C radicals react with molecular oxygen to form peroxide radicals. Subsequently, hydroperoxides are formed, and they decompose to a variety of oxidation products:



Scheme 13 illustrates the possible oxidation pathways during oxygen plasma treatment of polyolefin [75]. The reactivity of nitrogen towards the polyolefin surface is significantly smaller compared to this of oxygen. Therefore, mainly oxygen functional groups are generated at the polyolefin surfaces exposed to plasma in air. The type and concentration of functional groups depend, among others, on the plasma intensity, exposure time, relative humidity, gas temperature and composition [59].

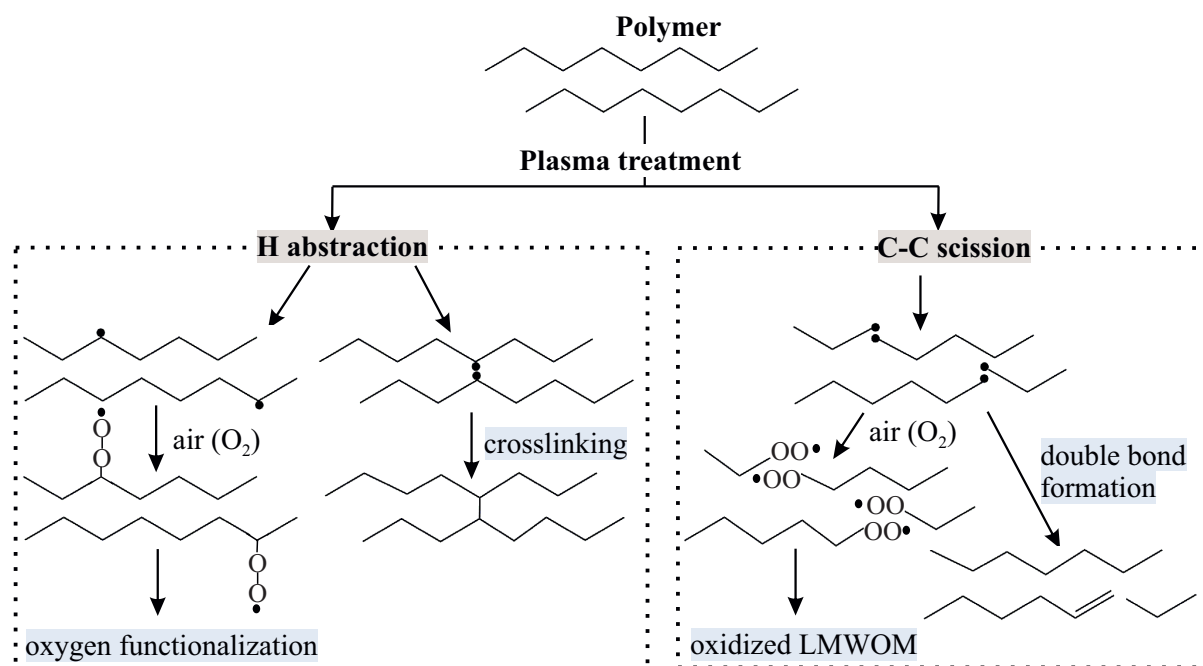


Figure 12: Chain scission reactions on polymer surface upon exposure to a plasma (adapted from [74]). LMWOM—low-molecular-weight oxidized material.

During plasma treatment, a saturation of plasma-generated C radical sites occurs. Steady-state equilibrium, between new O-functional groups introduction, and their removal by continuously proceeding oxidation to gaseous products, is established. Therefore, the oxygen introduction at the polyolefin surface is limited to about 28% O/C [74].

The etching of polymer surface occurs through chain scissions. Initially, non-volatile low-molecular-weight oxidized materials (LMWOMs), are formed. Proceeding oxidation of those reduced-molecular-weight polyolefin chains causes the formation of volatile LMWOMs, such as highly oxidized alcohols, aldehydes, ketones, and carboxylic acids (C₁–C₃). These become ultimately converted to CO₂ and H₂O [75, 59]. It was shown that the LMWOM formation occurs already when the oxidation level exceeds the O/C atomic ratio of ca. 0.07 (PP treated with DBD in air) [204].

The plasma species interact only with the topmost surface molecules. Deeper oxidation is a consequence of UV-induced radical formation and auto-oxidation processes. According to the literature reports on polyolefins treatment with DBD in air, oxidation depth should be within 20–35 nm [66, 75]. Moreover, physical aging processes should be taken into account. The functional groups generated at the surface can diffuse into the bulk of material upon rotation around the C–C bond or the segmental movements („hydrophobic recovery” process) [238]. The interaction of polar groups at the polymer surface with a polar solvent leads to the hydrogen bonds’ formation and reduces the chain mobility [74].

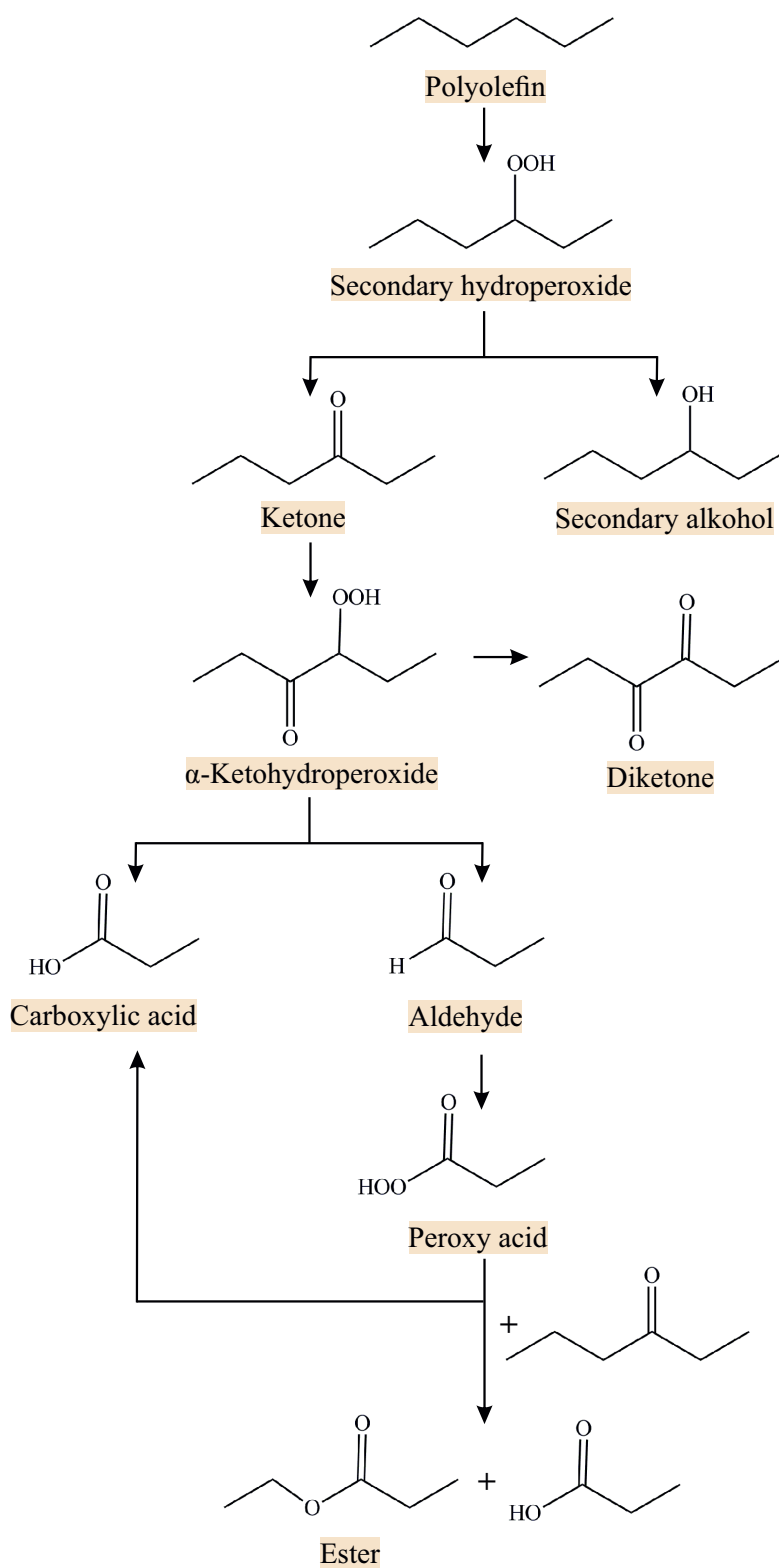


Figure 13: Schematic representation of polyolefin oxidation routes in oxygen-containing plasma [75].

2.4.2 Graft polymerization onto plasma treated polyolefin surface

The modification of polyolefin surfaces has recently gained much attention. Different chemical and physical processes have been utilized to tune the properties of those polymers for a wide variety of applications. Polymer surface grafting is one of the most promising approaches to improve surface properties without affecting the bulk characteristics. Contrary to the physically deposited coatings, grafting ensures the covalent attachment of graft moieties to the surface, therefore enables the long-lasting effect [105]. There are various synthetic paths to generate graft chains onto the polymer surface. The possible strategies utilizing plasma treatment are schematically depicted in Figure 14 (Figures 14 a and b–, „grafting from”, Figures 14 c and d–, „grafting to”).

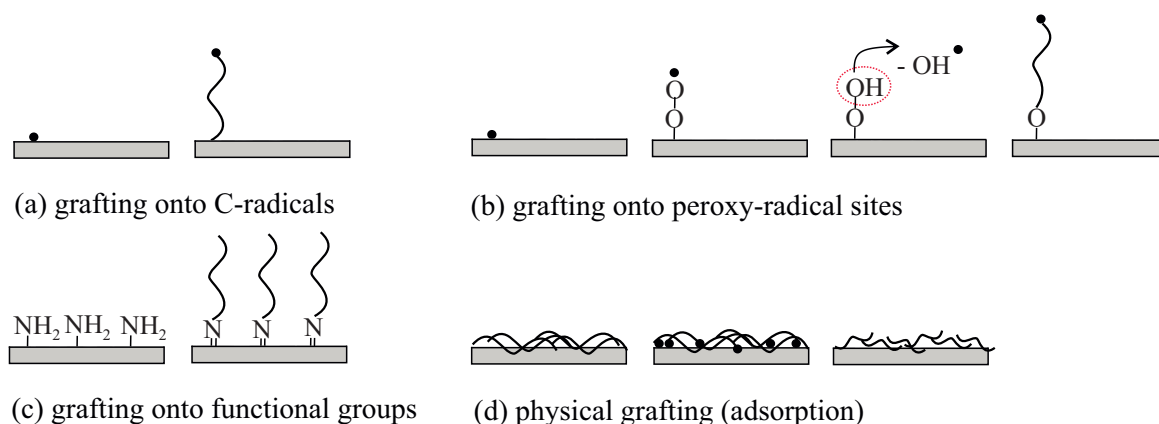


Figure 14: Possible pathways for plasma-assisted grafting onto polymer surfaces (adapted from [74]).

It is well documented that the exposure of polymer surface to plasma results in radicals’ formation [15, 120, 119]. C-radicals, generated at the polyolefin surface upon exposure to plasma, have a short lifetime (half-life of alkyl-chain radical ca. 10^{-10} s). Therefore, grafting onto radicals (Figure 14 a) should be performed in a vacuum or inert gas [92, 79, 139].

In the presence of air or oxygen, C-radicals react with biradical oxygen forming peroxy radicals. Those radicals give hydroperoxides. The hydroperoxides can further decay to a broad variety of O-functional groups (see Figure 13). Moreover, the decomposition of hydroperoxides can initiate grafting of vinyl or acrylic monomers (Figure 14 b) [208, 96]. The graft polymerization starts from hydroperoxy sides, and the grafting yield depends on the concentration of produced at the surface radicals. The radical generation differs considerably depending on the polymer and plasma type. However, the exact relationships between plasma conditions and radical formation are still unknown [74]. Generally, it is assumed that the concentration of alkoxy radicals ($-C-O\bullet$) at the surface is relatively low. Therefore, long chains are built while grafting onto the plasma-treated surface.

Alternatively, monomers (or polymers) can be physically deposited on the polymer surface, and simultaneously exposed to plasma to form free radicals (Figure 14 d) [113]. This method leads to the uncontrolled fragmentation of deposited monomer/polymer chains. Therefore, coating

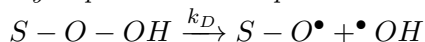
chemistry can not be well controlled.

Grafting can also be performed as a defined reaction between the introduced by plasma treatment functional groups at the surface and those of coating agents (monomers, polymers) (Figure 14 c). For this purpose, monosort surface functionalization is desirable. The following plasma processes can be applied to subsequently graft onto functional groups: (i) exposure to O-containing plasma, followed by reduction of carbonyl groups to hydroxyl groups and grafting onto OH [117]; (ii) plasma bromination (bromine, allyl bromide plasma), followed by either grafting onto Br-groups or conversion to NH₂, OH, etc. [76]; (iii) plasma polymerization, for instance of allylamine, and subsequent grafting onto –NH₂ [74]. Those techniques require several modification steps and often require toxic chemicals. For these reasons, they cannot be easily transferred to the industrial-scale processes.

Among the plasma-assisted grafting methods (see Figure 14), the grafting onto peroxy-radical sites does not require vacuum operation and has the potential to be transferred to the continuous coating process. Free radical polymerization (FRP) is widely used to polymerize acrylates and methacrylates. Free radicals possess unpaired electrons, they are highly energetic and enable rapid reactions, due to fast propagation kinetics [61]. Radicals are usually produced by the homolytic decomposition of covalent bonds, initiated either thermally or by irradiation (UV radiation, high-energy radiation). Labile bonds that can be broken, with a relatively moderate amount of energy applied, are nitrogen-nitrogen and oxygen-oxygen (dissociation energy of O–O bond is about 1.44 eV [55]). Therefore, azo compounds and peroxides are the most commonly used radical polymerization initiators.

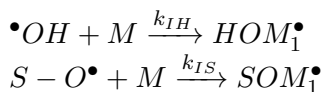
Taking into consideration grafting onto plasma-activated polyolefin surface, decomposition of hydroperoxide groups (–C–O–OH) initiates radical polymerization. The overall reaction scheme in an aqueous monomer solution can be described as follows (S–polyolefin surface, M–monomer, HP–homopolymer, G–graft copolymer, k–rate constant) [224, 37]:

Hydroperoxide decomposition:



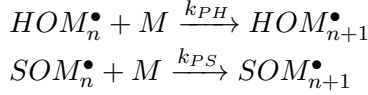
The thermal decomposition of hydroperoxides is a first-order reaction. Maximum two radicals can be formed during decomposition process (S–O[•] and [•]OH). However, the yield of free radicals is often lower because of recombination processes [154].

Initiation:



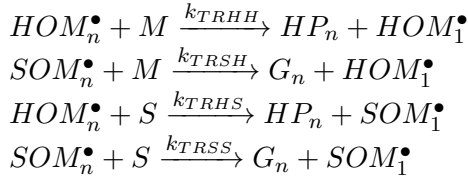
During initiation, a radical attacks a monomer, converting it into another radical (either onto the surface: SOM₁[•] or in the coating solution: HOM₁[•]).

Propagation:



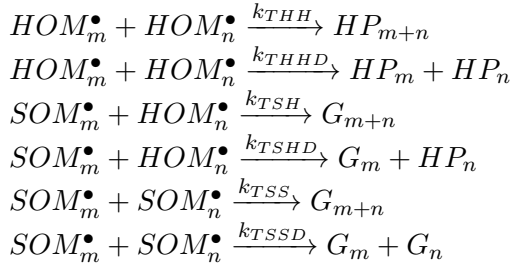
The monomer radical becomes an active species that adds subsequent monomers resulting in the chain growth (SOM_{n+1}^\bullet). For the successful propagation to proceed, favorable steric, polarization and radical stabilization conditions are required. The hydroxyl radicals ($\bullet OH$) formed from the decomposition of hydroperoxides can simultaneously induce the production of homopolymers (HOM_1^\bullet) in the solution. The growing polymer chain preserves its radical character until it does not react with another radical (chain termination).

Chain transfer:



A growing chain reacts with another molecule, abstracts a single atom, and as a consequence, a new radical is formed. If the new radical is highly reactive, a new polymer chain can grow. However, if its reactivity is low, the polymerization process is inhibited.

Termination:



In order to design the grafting onto the plasma-treated polyolefin surface in solution, several process variables should be taken into consideration. Firstly, the nature of the substrate backbone, among others its chemical composition, crystallinity, and swelling ability are of great importance. Secondly, the reactivity of the monomer (its mobility, solubility in the solvent, steric effects, susceptibility to homopolymerization, etc.) plays a significant role. The type of medium affects the generation of free radicals, as well as backbone swelling properties, monomer solubility, and diffusion. For example, water is an excellent solvent for grafting, because the occurrence of chain transfer reactions in water is reduced. The concentration of initiator also influences the grafting efficiency. Nevertheless, optimal concentration depends on the grafting system. Moreover, the presence of any additives which can react with a monomer can remarkably affect the grafting yield. The reaction temperature is another factor to consider. A higher temperature can enhance the monomer diffusion and facilitate the decomposition of initiators [22].

3 Materials and methods

3.1 Substrates

The polymer foils used in this study were isotactic polypropylene (PP), high-density polyethylene (HDPE) and HDPE/PP blend (80/20 wt%). They served as model substrates for the HDPE/PP (80/20 wt%) feed spacer. The raw components for foil manufacturing (granulates) were obtained from Conwed Global Netting Solutions. Their density, melt flow index (MFI), crystallinity and melting temperature T_m are summarized in Table 2. The degree of crystallinity and melting temperature values were determined by conventional differential scanning calorimetry (DSC 204 F1 Phoenix). Polymer foils with 150 μm thickness were manufactured by POLIFILM Extrusion GmbH within a blow film line in a single-screw extruder with a diameter of 30 mm and length 750 mm. The extrusion speed was 70 rpm (revolutions per minute), barrel temperatures in the range from 190°C to 220°C for the HDPE foil and from 190°C to 240°C for the PP and blend, respectively.

Material	Density (g/cm^3)	MFI ($\text{g}/10 \text{ min}$)	Crystallinity (%)	T_m (°C)
HDPE	0.928	1.39	81.6	134.1
PP	0.874	2.08	34.6	160.9

Table 2: Physical property of the HDPE and PP raw materials. MFI-melt flow index, T_m -melting temperature.

The HDPE/PP (80/20 wt%) feed spacer (also known as netting) was manufactured by Conwed Global Netting Solutions, from the same raw materials like PP, HDPE, and HDPE/PP foils. The feed spacer possesses an alternating thickness of the strands (average spacer thickness: $830 \pm 15 \mu\text{m}$), inner strand angle of 90° and average parallel strand distance of 2.95/2.63 mm [193]. The feed spacer was fabricated is a continuous extrusion process. In brief, an extruder melts and pressurizes raw materials. As next, the melt is forced through proper tooling in a die that contains slots for the plastic flow to create a netting profile. The extrusion process is followed by material orientation, where the netting is reheated and stretched to obtain high-strength and flat feed spacer [191].

3.2 Surface modification

3.2.1 Concept

The substrates were modified in the two-stage process which combines plasma activation with subsequent wet chemical treatment in sulfobetaine methacrylate (SBMA) solution (see Figure 4). In order to covalently immobilize SBMA on the HDPE/PP surfaces, active sites, which can initiate free-radical grafting reactions, should be first introduced onto polyolefin materials. Atmospheric pressure plasma treatment with dielectric barrier discharge (DBD) in air was proposed as a pretreatment method and hydroperoxide groups as grafting initiators. The intensity of applied plasma was varied to optimize the amount of generated at the substrates oxygen functional groups. The modification with SBMA was performed, through grafting onto radical sites during dip coating of the plasma-activated substrate in the monomer solution.

The preliminary studies, on the plasma and wet chemical treatments, were performed on the HDPE, PP, and HDPE/PP foils. Based on the obtained results, the most favorable parameters were chosen to modify the feed spacer surface.

3.2.2 Plasma treatment with dielectric barrier discharge (DBD) in air

In order to introduce oxygen functional groups, and increase the hydrophilicity of the polyolefin materials, treatment with dielectric barrier discharge (DBD) in air under atmospheric pressure was performed. For this purpose, a CORLAB-AS set-up from Kalwar CIV Innoserv GmbH equipped with four ceramic electrodes was used (schematically depicted in Figure 15). The polyolefin samples (ultrasonically cleaned in acetone and dried) with a size of $8 \times 5 \text{ cm}^2$ were fixed with adhesive tape on the glass surface of the sliding carriage and moved towards the discharge gap between two parallel electrodes, where the lower is covered by insulating glass. High voltage alternating current applied between two electrodes results in partial ionization of air (plasma generation). The distance between the upper ceramic electrodes and the counter electrode was kept constant at 3 mm. Treatment intensity was manipulated by adjusting the speed of the sliding carriage and applied current. Table 3 summarizes studied plasma treatment parameters. The applied plasma treatments were categorized based on the amount of energy transferred from plasma to the treated sample as low, middle, and high intensity. The CORLAB-AS research set-up does not allow accurate recording of current and voltage throughout discharge generation. Therefore, given plasma energy doses are roughly estimated values.

During DBD treatment in air, polyolefin surfaces are exposed to high-energy plasma particles and short-wavelength plasma radiation. This results, among others, in the formation of oxygen functional groups (addressed in detail in chapter 2.4.1) and enables further functionalization. Hydroperoxides are especially favorable for the covalent immobilization of antifouling coatings. During their decomposition, alkoxy radicals are formed [74]. These can initiate grafting onto the polyolefin surface, as shown elsewhere [96, 230, 208]. The incorporation of hydroperoxides at the

plasma-treated surfaces depending on applied plasma intensity (PL_A , PL_B , PL_C , see Table 3) was analyzed. Selective derivatization with sulfur dioxide (SO_2) was used, according to the following reaction: $R-O-O-H + SO_2 \rightarrow R-O-SO_2-OH$ [74]. In brief, the plasma-treated, as well as untreated (controls), HDPE, PP, and HDPE/PP foils, were placed in a desiccator, filled afterward with SO_2 gas. The samples were kept for 30 minutes in the SO_2 atmosphere to enable the reaction between hydroperoxide groups and SO_2 to complete. Derivatization was evaluated by analyzing sulfur content at the surface (S at%, X-ray photoelectron spectroscopy). One sulfur atom corresponds to one hydroperoxide group. Three replicates for each material, and each plasma treatment condition, were studied. The aim was, as first, to evaluate whether the hydroperoxide groups are produced. Secondly, validation if the amount of hydroperoxides varies within applied plasma treatment parameters. Particular plasma treatment parameters were selected for the subsequent antifouling coating.

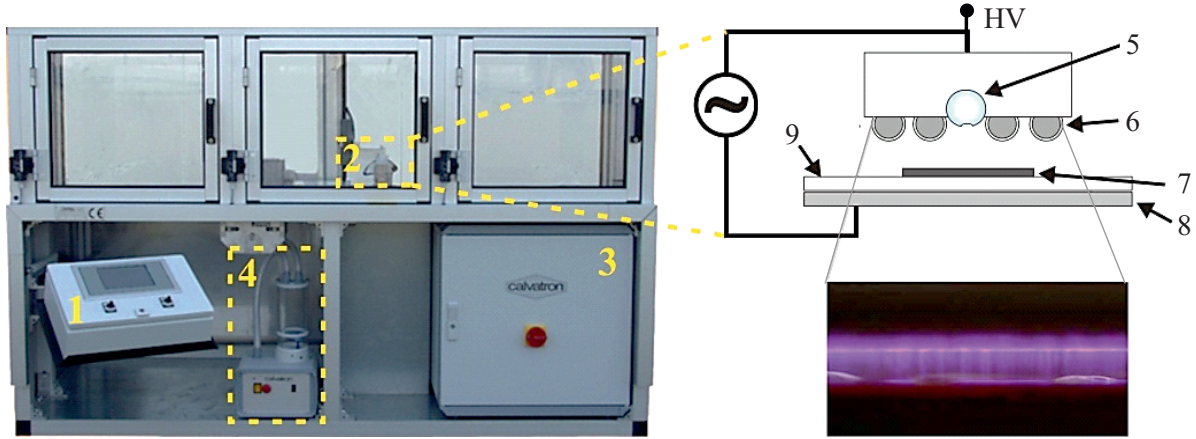


Figure 15: Left: CORLAB-AS atmospheric pressure plasma set-up: 1–control unit, 2–dielectric barrier discharge (DBD) unit, 3–high voltage generator, 4–aerosol generator. Right (above): schematic structure of the DBD unit: 5–aerosol inlet unit, 6–ceramic electrodes, 7–sample, 8–counter electrode, 9–insulating glass, HV–high voltage. Right (below): micro-filamentary discharges (photo). Adapted from [179].

Plasma treatment	Current (I)– speed (ν) (mA-m/min)	Estimated energy dose (E_D)* (J/cm ²)	Plasma intensity
Plasma A (PL_A)	25–2.6	2.2	low
Plasma B (PL_B)	25–1	5.7	middle
Plasma C (PL_C)	40–1	9.2	high

* From: $E_D = \frac{U \times I}{\nu \times B}$ [204], where: $U=8000$ V, $B=21$ cm

Table 3: Applied plasma treatment parameters (dielectric barrier discharge in air).

3.2.3 Antifouling functionalization by wet coating

The plasma-treated samples were immediately immersed in water-based sulfobetaine methacrylate (SBMA) monomer solution. Before use, the coating solution was purged with argon for 1 h to remove oxygen. Two different SBMA monomer concentrations were used for coating: 0.1 mol and 0.5 mol. These concentrations were chosen based on the literature results, obtained for graft polymerization of another zwitterionic monomer (2-Methacryloyloxyethyl phosphorylcholine) onto cross-linked polyethylene [123]. Following preliminary studies and literature research, dip coating was performed for 1 h at 70°C [93, 130]. During coating, the flask, with SBMA monomer solution and immersed specimens, was covered to minimize water evaporation. Directly after coating, the samples were soaked in distilled water and left overnight. As next, the SBMA coated samples were subjected to washing, to remove unreacted monomers: in sodium chloride (NaCl) water solution (0.1 mol) for 10 h at 60°C under stirring, followed by rinsing in distilled water (procedure adjusted from [236]). The coated samples were dried in a vacuum oven at 40°C for 2 h before surface composition and morphology analyses.

In order to evaluate the stability of the generated SBMA coatings in water, acidic and basic environments, short- and long-term immersion tests were performed on the coated HDPE/PP foils and feed spacers. As first, the SBMA coated foil with known composition was immersed in 0.1 mol NaCl solution in distilled water. Fresh solution was prepared every day. The temperature was 4°C to minimize possible bacterial growth. A sample was taken in one-week intervals, washed thoroughly in distilled water, dried, followed by the surface composition analysis by X-ray photoelectron spectroscopy (XPS). The test was carried out until the first change in surface composition.

The SBMA coating stability in acidic/basic environments was tested in H₂SO₄ (pH=1) and NaOH (pH=11) water solutions, respectively. SBMA coated foils with known compositions were immersed for 24 h in the test solutions. Subsequently, they were washed in distilled water, dried, and analyzed by XPS.

3.3 Surface characterization methods

3.3.1 Spectroscopic characterization

X-ray photoelectron spectroscopy (XPS). X-ray photoelectron spectroscopy was used to evaluate surface elemental composition, before and after each modification step.

A sample irradiated with monochromatic X-rays emits photoelectrons from the surface. The number of emitted electrons and their kinetic energy are simultaneously measured. Electron binding energy is calculated using the energy of X-ray source and the work function. Since the binding energy is element-specific, peaks can be assigned to individual elements and quantified [29]. The information depth of XPS is estimated as ca.10 nm, and the detection limit is approximately 0.1 at% [29].

In this work, XPS was performed with a Kratos UltraDLD spectrometer with a monochromated Al K α source (emission: 10 mA, anode: 15 kV). For all survey spectra (range of binding energy from 0 to 1200 eV; measured area: 300 \times 700 μm^2), pass energy of 160 eV and charge neutralization were applied. Measurements were performed at ultra-high vacuum ($p \approx 10^{-9}$ Torr). Survey spectra were taken at an electron takeoff angle of 90 $^\circ$ (normal to the sample surface). The obtained spectra were normalized to C 1s peak (285 eV). The Shirley-type background was used to fit spectra [17]. Analyses were accomplished in the software CasaXPS 2.3.15. Chemical composition was investigated at three individual positions per sample, and the average values calculated (specimen size $\approx 5 \times 5 \text{ mm}^2$).

Fourier-transform infrared spectroscopy (FTIR). Fourier-transform infrared spectroscopy was used to monitor the changes in chemical composition by the identification of specific functional groups.

The method relies on interactions between molecules and electromagnetic field in the infrared region (IR). An attenuated total reflection (ATR) sampling approach is commonly applied for surface analysis. In the ATR technique, a sample is brought into direct contact with a high-refractive-index crystal (e.g., germanium, diamond). The portion of the incident beam, which passes through the crystal, penetrates the analyzed sample. The penetration depth varies depending on the type of reflective element, the refractive index of the sample, the wavelength of light and the angle of incident [95].

In this work, the FTIR analyses were carried out with a IFS 55 EQUINOX spectrometer. Spectra were recorded in the single reflection mode in the attenuated total reflection (ATR) configuration. The ATR unit (Specac Inc., Smyrna USA) was equipped with a diamond (refractive index=2.4). The analyzed samples were cut to a size of approximately 2 \times 2 cm 2 and positioned on the 2 \times 2 mm 2 measuring spot. A pressure applicator with a torque knob was used to fix and press the samples directly onto the crystal (torque of about 0.7 Nm). The spectra were recorded over the wavenumber range 4000–650 cm $^{-1}$ and at a resolution of 4 cm $^{-1}$ (analysis software OPUS, version 6.5, Bruker Optik GmbH). At least 20 scans were acquired and averaged for each sample. Spectra analyses were performed after atmospheric compensation and baseline correction.

Nanoscale IR spectroscopy. Nanoscale IR spectroscopy was applied to analyze SBMA modified foils. This technique combines IR spectroscopy with an atomic force microscopy (AFM) and enables simultaneous topography and IR analyses. A sample is exposed to rapid pulses from a tunable IR source, which is focused near the AFM probe tip. IR absorption leads to a local transient deformation of the surface (photothermal expansion effect). This thermal expansion is detected by the deflection of AFM probe while scattering the sample surface. IR absorption spectra can be acquired while measuring the AFM probe response as a function of absorbed wavelength [57, 153].

All measurements were taken on a nanoIR2 system (Anasys Instruments, Santa Barbara, CA, USA) equipped with an optical parametric oscillator (OPO) laser over the wavenumber range 1900–1000 cm $^{-1}$. The basis of each IR measurement was the AFM investigation performed in contact mode. Multiple AFM-IR spectra were acquired using 128 co-averages at 4 cm $^{-1}$ spectral resolu-

tion. The obtained spectra were smoothed using the Savitzky-Golay algorithm with 3 side points [187].

3.3.2 Microscopic characterization

Scanning electron microscopy (SEM). Scanning electron microscopy was used to investigate the morphology of untreated HDPE/PP blend materials, and to determine the HDPE and PP domains distribution. Preceding the determination of domain distribution on the untreated HDPE/PP materials (foil and feed spacer), the surfaces were etched for 15 minutes according to permanganic etching technique of OLLEY and BASSETT using a mixture of potassium permanganate and sulfuric acid. The permanganic etching removes the amorphous polymer portion much more easily than the dense crystalline blocks [161]. Therefore, the semicrystalline blend morphology can be depicted. Furthermore, the PP phase is attacked and removed more severely by etchant than the HDPE. Consequently, the PP domains can be identified as pits, holes and trenches. The depth of permanganic etching is estimated at 10 μm .

In this study, SEM was performed using a FEI Quanta FEG 650 microscope operated at an accelerating voltage of 10 kV in the secondary electron mode. Prior investigations, the samples were sputter-coated with a conductive platinum layer.

Transmission electron microscopy (TEM). Transmission electron microscopy was employed for the morphological investigations of untreated HDPE/PP foil. Ultrathin foil sections (approximately 60 nm thickness) were prepared using a cryo-ultramicrotome (RMC PowerTome PT-PC with CRX cryo-chamber (RMC, Tucson)) with a diamond knife (angle 35°) at about 110 K. The specimen has been taken starting from the surface in the vertical direction. Prior to ultramicrotomy, the HDPE/PP foil was stained in ruthenium tetroxide (RuO_4) for four hours *en bloc* to visualize the semicrystalline morphology. Treatment with RuO_4 increases the image contrast due to oxidation of amorphous regions, while crystalline areas remain unstained. Both phases (HDPE and PP), could be distinguished because of the different appearance of lamellae after staining with ruthenium [185]. TEM investigations were performed using a FEI Tecnai G2 F20 TEM at an accelerating voltage of 200 kV. The thickness of the HDPE lamellae was analyzed in Cell^F software (Olympus Soft Imaging Solutions GmbH).

Atomic force microscopy (AFM). Atomic force microscopy was applied to verify the surface topography and morphology of untreated, plasma-treated, as well as SBMA modified materials. AFM provides a three-dimensional surface image with atomic resolution.

Surface topography can be analyzed in contact or non-contact (tapping) mode. In tapping-mode, a cantilever oscillates near its resonance frequency and taps a surface only periodically. During contact with the surface, the amplitude and phase of the cantilever's oscillation are affected. The variations in surface topography influence the oscillation amplitude. The phase-contrast image reflects heterogeneous mechanical properties. It originates from the phase difference between the cantilever's oscillations and the driving signal from a piezoelectric crystal [167].

AFM phase and height images were generated using a AFM JPK nanowizard[®] IV device. Measurements were performed in intermittent contact mode at room temperature on an area of $2.5 \times 2.5 \mu\text{m}^2$ for the foils and $2 \times 2 \mu\text{m}^2$ for the feed spacer, respectively. An arrow NC cantilever with a tip radius of 10 nm was used. The force constant calibration of used silicon cantilevers was performed by the thermal noise method [182]. Indenter tip geometry (radii and tip's shape) was verified by SEM. Surface roughness (arithmetic mean deviation of the profile: R_a and ten-point mean roughness: R_z) was determined from unprocessed height images using software Gwyddion. For this purpose, ten profiles were extracted from each obtained image and the middle R_a and R_z values were calculated.

Particular feed spacer samples were subjected to annealing in order to reduce surface roughness. The following preparation procedure was developed: a spacer sample in the size of approximately $1 \times 1 \text{cm}^2$ was initially heated on the AFM stage to 160°C for 1 minute (configuration of the single standards was not affected); secondly, the temperature was reduced to 140°C and held for 5 minutes. Next, the spacer sample was kept at 120°C for additional 5 minutes and cooled down to room temperature for 7 minutes.

3.3.3 Contact angle measurements

The contact angle (θ) is the angle formed by the liquid at a liquid-gas-solid interface and describes the wetting behavior. The surface free energy (tension) of the solid can be calculated using at least two different liquids with known surface tensions to measure the contact angle on the same surface.

Static contact angle measurements were performed to analyze the surface free energy (SFE) of foil substrates (device G10 with DSA 100 software and a CCD camera from KRÜSS). Analyses were carried out at room temperature using water ($\gamma_{H_2O} = 72.7 \text{ mN/m}$) and diiodomethane ($\gamma_{CH_2I_2} = 50.0 \text{ mN/m}$) as test liquids [121]. The individual contact angle value was determined by applying a tangent to the depicted profile of the liquid drop at the point of three-phase contact. SFE values were calculated based on the OWRK (Owens, Wendt, Rabel and Kaelble) approach using arithmetic mean values of at least five measured contact angles per test liquid. The drop volume was $3 \mu\text{L}$ each. The information depth of the method is approximated as ca. $0.5\text{--}1 \text{ nm}$ [205]. The SFE of the feed spacer, could not be evaluated using a standard sessile drop technique due to the small thickness of the spacer strands.

3.3.4 Time-of-flight secondary ion mass spectrometry (ToF-SIMS)

In time-of-flight secondary ion mass spectrometry, a pulsed primary ion beam with an energy of a few keV is applied to bombard the surface and emit chemical species from the topmost monolayers. Ejected secondary ions are extracted, then accelerated over a very short distance. This gives them virtually the same kinetic energy prior to entering a flight path towards detector. The detection limit of ToF-SIMS method is in the ppm range, while the sampling depth is below 1 nm [39].

Time-of-flight secondary ion mass spectrometry (ToF-SIMS) imaging was employed on an ION-TOF (GmbH) TOF-SIMS5 with a 25 keV primary bismuth ion beam (Bi^{3+}) at high-current bunched (high mass resolution) mode. The incident angle of ion bombardment was 45° . The secondary ions were detected from $500 \times 500 \mu\text{m}^2$. Charge compensation on the sample was obtained by low-energy electrons. The pressure of the analytical chamber during measurement was approximately 3×10^{-9} mbar. Image processing was performed in Cell^F software (Olympus Soft Imaging Solutions GmbH).

3.4 Preparation of polySBMA gel and its characterization

With the aim of a more precise analysis of the SBMA coating chemistry, SBMA polymer was prepared in the coating solution. Several coating procedures were performed using the same 0.5 mol SBMA solution (150 ml). Therefore, the SBMA homopolymer could be formed in the reaction system. The generated free radicals not only facilitate direct grafting of SBMA onto the surface but also induce homopolymerization of SBMA as a free polymer in the solution [123]. Firstly, the SBMA solution was purged with argon for one hour. Secondly, the plasma-treated blend foil was immersed in the solution and heated to 70°C for one hour. As next, cooling down to room temperature was performed, followed by setting the solution aside for at least 24 h before the procedure was repeated. The visible gel was formed in the solution after the third treatment.

The gel sample was carefully taken, dried and analyzed by gel permeation chromatography (GPC) to determine the number-average molecular weight (M_n) and the weight-average molecular weight (M_w). The SBMA monomer used for the preparation of the gel was analyzed as a control sample. The chromatograms were taken on a water-based GPC: PL-GPC 50 with a differential refractive index (RI) detector, operated at 25°C with two separating columns PSS Suprema 300×8 mm and precolumn 50×8 mm. The mobile phase used for the analysis consisted of 0.065 g/L NaN_3 , 16.998 g/L NaNO_3 and 1.38 g/L NaH_2PO_4 in water (pH 7) [124]. The gel was dissolved in the eluent at a concentration of 9.34 mg/ml. The flow rate of the mobile phase was 1.0 mL/min, while the injection volume for the polySBMA gel solutions was 50 μL . The calibration was performed using monodisperse poly(ethylene glycol) standards [124].

Apart from GPC analysis, ATR-FTIR was applied for the polySBMA gel characterization. For this purpose, SBMA was additionally free radical polymerized in order to produce a „model” polymer. IR spectrum of this „model” polymer was compared with the spectra of SBMA monomer and dried polySBMA gel. A conventional free radical polymerization reaction was performed, as follows: SBMA monomer (5 g) was dissolved in 30 mL dimethyl sulfoxide (DMSO); subsequently, 10 mg of AIBN (2,2'-Azobis(2-methylpropionitrile)) initiator was added. The reaction proceeded overnight at 70°C and the white precipitate was obtained. The reaction mixture was dissolved in hot water and precipitated in cold ethanol (20-fold volume excess). The collected solid was dried under high vacuum and the structure was confirmed by nuclear magnetic resonance spectroscopy (NMR, Varian Gemini 400 spectrometer).

3.5 Evaluation of antifouling potential

3.5.1 Concept

Antifouling testing was performed, to evaluate, if proposed surface modification with SBMA is effective to mitigate biofouling. Initially, short-term batch experiments with model bacteria culture were conducted. The untreated and SBMA modified specimens, both foils and spacers, were simultaneously investigated to assess whether the surface coating can delay bacterial adhesion. As next, the modified feed spacers were subjected to long-term antifouling testing in constructed for this purpose fouling simulation set-up (MeFoS). The MeFoS was designed based on the knowledge derived from the numerous publications of J. S. Vrouwenvelder, who first established this testing procedure [219, 222, 221]. Two parallel working cells, containing membrane and feed spacer coupons, enable us to investigate untreated and modified feed spacer under the same conditions. Detailed description of the set-up and testing principle is given in chapter 3.5.3.

3.5.2 Discontinuous testing

Procedure. A short-term adhesion assay is a common practice to determine the susceptibility of a surface to biofouling [174, 129] since the initial adhesion has been recognized as a critical step in biofilm formation [144, 100, 69]. In this work, gram-negative green fluorescent protein (gfp)-tagged *Pseudomonas fluorescens* were used in the short-term adhesion tests. These microorganisms were chosen based on the work from Baker and Dudley. They announced *Pseudomonas* bacterium as one of the most commonly occurring on the fouled membranes and feed spacers [13]. Moreover, *Pseudomonas fluorescens* bacteria build more severe biofilms than *Escherichia coli* or *Staphylococcus aureus*. Therefore, they serve as convenient model to analyze the bacterial deposition [236]. In order to prepare *Pseudomonas fluorescens* culture, a freezer stock of strain (ARQ1, starting strain DSM 19095), preserved at -80°C , was used. The culture was prepared in a sterile CASO bouillon at room temperature by shaking at 120 rpm for 18 hours. The suspension was diluted with sterile medium to adjust the optical density to 0.1 at 600 nm (approximately 10^8 CFU/ml). The untreated and SBMA modified samples were cut into coupons with diameter of 1 cm, sterilized in 70% isopropanol and placed in 12-well plates. The bacteria suspension was uniformly distributed on each investigated sample (50 μl on the foils, while 100 μl on the feed spacers). After 40 minutes of exposure, the samples were gently washed in sterile water, transferred to the new well plates with fresh CASO medium (3 ml per sample) and incubated for 24 hours at room temperature with stirring (about 120 rpm). Next, the samples were gently washed in distilled water and directly subjected to biofilm analyses.

Biofilm examination on the foils. The fouled foils were gently dried and the gfp-tagged *Pseudomonas* were imaged using their fluorescence. For this purpose, a fluorescence microscope BX53 (Olympus) with cellSense Dimension1.9 software equipped with a mercury vapor arc lamp (X-Cite™ 120 PC Q) and a CCD camera (XC10) was used.

For the investigations, the 460–480 nm excitation and 495–540 nm emission filter set (ET-EGFP

filter from Chroma Technology) was adapted. The light output intensity was kept constant (iris opening 50%), while integration time was 5 sec. At least five independent positions per sample were visualized (objective M-Plan N 50 \times /0.75) and evaluated. The examined area was about 220 \times 170 μm^2 per image. The surface coverage by microorganisms was quantified with the software Cell^F version 2.6 (AnalySIS, Olympus) using the following procedure: each image was converted to a gray 8 bits image, followed by determination of threshold values for the fluorescence signal. The applied binarization process resulted in a two-phase image: black-background and white-biofilm. The phase analysis gave the percentage of surface coverage by biofilm. An average surface coverage value was calculated from five images taken at different positions.

Biofilm examination on the feed spacers. Biofilms on the spacers were stained with safranin O dye according to the procedure proposed by Ommen et al. [162]. In brief, dried samples were placed in the well plates with freshly prepared 2 ml of 0.5% safranin solution in each. After 10 minutes of soaking time, the spacer samples were gently washed by immersing twice in demineralized water for 30 seconds, and then let dry. Safranin was extracted from the biofilms by immersion in 2 ml of acetic acid (33%) for 10 minutes. The optical density of the solutions was measured at 530 nm (OD₅₃₀, spectrometer SPECORD 210 from Analytik Jena AG). The untreated, as well as SBMA coated spacers that were not exposed to bacteria suspension, were used as negative controls in this experiment. The relative attachment of bacteria to the SBMA coated spacer samples was obtained by the normalization of the OD₅₃₀ values for SBMA coated spacers to the untreated samples, as proposed elsewhere [226]. The presented results are the average values from five replicates.

To visualize the biofilm developed on the untreated and SBMA coated spacers, scanning electron microscopy (SEM) was performed (JEOL JSM-7401F microscope, an acceleration voltage of 3 kV). The biofilms were fixed according to the following procedure: the fouled samples were rinsed 5 times in sterile distilled water and then incubated overnight in 2 ml solution of 2.5% (v/v) glutaraldehyde in 0.1 mol phosphate-buffered saline at 4°C. Next, the samples were washed thoroughly in distilled water and cooled in liquid nitrogen at -20°C for 2 h. As the last step, freeze-drying at 0.1 mbar for 18 h was performed (ALPHA 2-4 LSCplus, Christ).

3.5.3 Continuous testing with membrane fouling simulation set-up

Continuous testing in fouling simulation set-up (MeFoS) was performed to verify the fouling propensity of SBMA modified feed spacers under practical flow conditions. The MeFoS can mimic hydrodynamic conditions in industrial membrane modules, which made it a valuable tool to study biofouling. The test principle relies on constant monitoring of feed channel pressure drop (FCPD), which is a difference between the inlet and outlet pressure at the test cell [221]. The pressure drop increase over time indicates the biofilm building. Several reports have already shown that the FCPD increase in the RO membrane element is predominately caused by feed spacer fouling [12, 216]. Therefore, monitoring of this particular parameter became a commonly accepted practice in studying the antifouling potential of feed spacers [151, 9, 176, 193]. During testing, the biomass is accumulated on the membrane surface and between the feed spacer fila-

ments, which increases the hydraulic resistance in the feed channel and creates flow stagnation zones and thus causes the FCPD increase [194].

The fouling simulation set-up (MeFoS) constructed to study the antifouling potential of the modified feed spacers consists of:

- *feed water pretreatment apparatus*: cartridge filter (10 μm pore-size), backflow preventer (BA295S, Honeywell GmbH), pressure regulator (type 586, GF Piping Systems Ltd.), pressure damper (WD165, Reflex Winkelmann GmbH), plate heat exchanger (EWT-B3-12x12, EWT Handel Beratung), thermostat (RE 104 Ecoline, LAUDA DR. R. WOBSE & CO. KG), pressure reducing valve (Type 582, GF Piping Systems Ltd.)
- *two analogous fouling simulation systems* (see Figure 16): two fouling simulation cells (FS1-fouling simulation cell 1, FS2-fouling simulation cell 2; from Global Membrains BV, Netherlands), each of them possessed separate differential pressure transducer to monitor the feed channel pressure drop (Deltabar S PMD75, Endress+Hauser GmbH+Co. KG), flow controller (FC 8800, Brooks Instrument B.V), flow meter (RS 185-998, Parker Hannifin Manufacturing Ltd.), pump for nutrient dosage (Simdos 02 diaphragm metering pump, VWR International GmbH).

The fouling simulation cells (FS1 and FS2) were made of polyvinyl chloride (PVC) bottom and poly(methyl methacrylate) (PMMA) top ($280 \times 85 \times 55 \text{ mm}^3$). The viewing windows of the cells were covered while testing to minimize the impact of light on biofilm development. The untreated and SBMA coated spacers together with membranes (coupons size $20 \times 4 \text{ cm}^2$) were tested in parallel under the same conditions. Therefore, the performance of unmodified and coated feed spacers could be directly compared. The tested spacer samples were sterilized in 70% isopropanol before installing. The spatial orientation of the spacer in the fouling simulation cell corresponded with the full-size RO module to ensure similar hydrodynamic conditions. The biofilm development was indicated by feed channel pressure drop (FCPD) increase over time. Fouling experiments were performed without filtrate collection since it has been shown that the FCPD is independent on permeate production [223].

Drinking water from plant Wienrode/Harz (supplied by Elbaue-Ostharz GmbH; treated by flocculation with aluminum sulphate, sand filtration and softening) was used as feed water in the long-term fouling experiments. Parameters such as inlet pressure, pressure drop and temperature for both fouling simulation cells (FS1, FS2) were recorded by data loggers at 1-minute intervals. Each fouling simulation cell was operated at a pressure of 1.7 bar without recirculation. The feed water temperature was kept constant at 20°C , while the flow rate adjusted to $16 \text{ L} \times \text{h}^{-1}$, which agrees with industrial practice [220]. To accelerate biofilm growth, a nutrient solution containing sodium acetate (0.922 g/L), nitrate (0.325 g/L) and anhydrous monobasic sodium phosphate (0.104 g/L) in distilled water (C:N:P ratio of 100:20:10) was dosed. Bacteria growth in the stock solution was prevented by adjusting pH to 11 with 40% NaOH. The nutrient solution was replaced with a fresh one every fifth day.

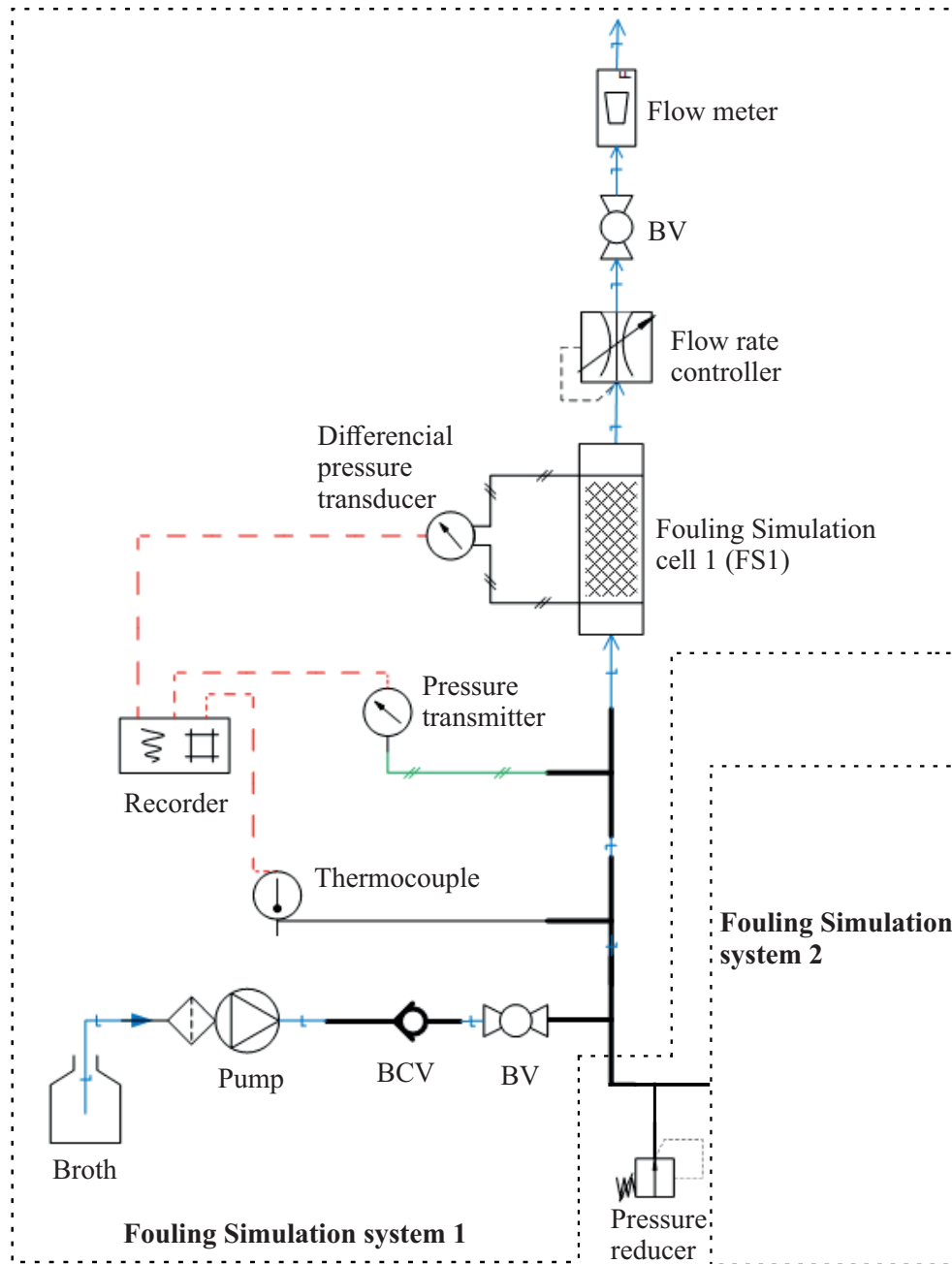


Figure 16: Schematic representation of two parallel-working fouling simulation systems: Fouling Simulation system 1 and Fouling Simulation system 2 (identical to system 1). BV–ball valve; BVC–check valve.

Microbial load in tap water. The microbiological examination of drinking (tap) water used for continuous fouling simulation tests was performed applying sterile filtration followed by the filter incubation on an agar plate. For each experiment, 200 ml of tap water was collected to a sterile, weighted bottle. The bottle with the collected water sample was again weighed. Next, water was sterile filtrated through a cellulose acetate membrane filter (pore size 0.2 μm), followed by incubation of this filter in a CASO-agar-filled sterile petri dish at 37°C for 24 h. Thereafter, the total number of colonies on each plate was counted and colony-forming unit (CFU) per 100 g of tested water was calculated. The experiments were performed over six days. The obtained

bacterial colonies in tap water ranged from 366 CFU/100g to 44 CFU/100g. The middle value from 6 independent studies was 175 ± 116 CFU/100g.

Coating stability under experimental conditions. In order to evaluate the stability of the SBMA feed spacer coating under examination in fouling simulation set-up, three weeks of continuous testing with tap water without nutrient dosage was performed. Two fouling simulation cells operated in parallel, one contained the SBMA modified feed spacer and membrane, while second included the untreated feed spacer and membrane. The surface elemental composition of each sample was evaluated before and after testing by XPS. The specimens exposed to continuous study were measured at three positions (inlet, middle and outlet of the fouling simulation cell), and the average atomic concentrations were calculated.

3.6 Summary

Figure 17 schematically illustrates the structure of this thesis.

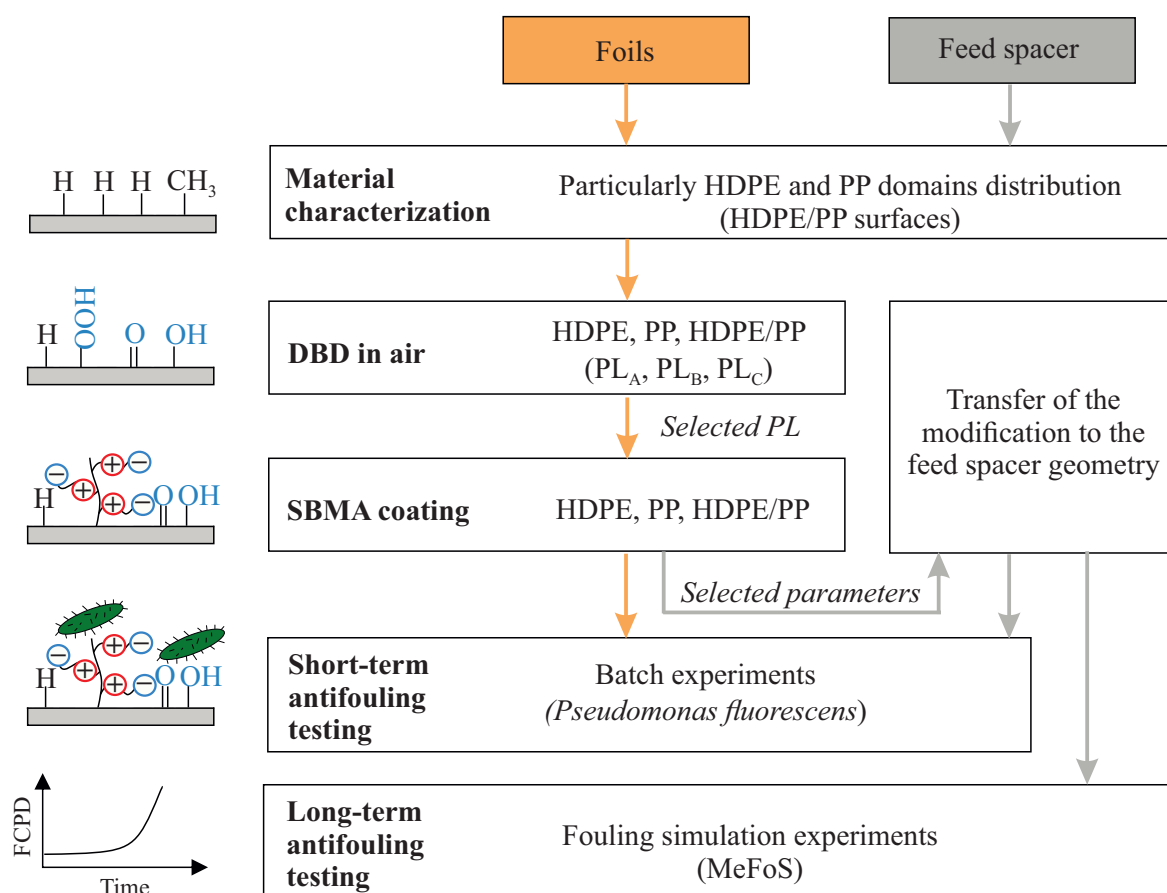


Figure 17: Schematic proceedings of the thesis including performed modifications and applied materials. Abbreviations: HDPE–high-density polyethylene, PP–polypropylene, HDPE/PP–high-density polyethylene/polypropylene blend (80/20 wt%), DBD–dielectric barrier discharge, PL_A, PL_B, PL_C–applied DBD treatment parameters (for detailed description see Table 3), SBMA–[2-(Methacryloyloxy)ethyl]dimethyl-(3-sulfopropyl)ammonium hydroxide, FCPD–feed channel pressure drop, MeFoS–membrane fouling simulation set-up.

The geometry and topography of the HDPE/PP feed spacer are challenging for the microscopic or spectroscopic analyses, as already mentioned in the introduction part. Therefore, HDPE/PP foil extruded from the same raw materials was used as a model substrate for the preliminary studies. The most favorable DBD treatment and coating parameters were selected, based on the surface chemistry and morphology analyses, and applied for the feed spacer modification.

The preliminary modifications were carried out not only on the HDPE/PP foils but also on the HDPE and PP foils. It was aimed, at: i) understanding of the blend oxidation in plasma, and ii) investigation, if there is a better coating affinity to one of the phases, either HDPE or PP.

4 Results and discussion

4.1 Characterization of the HDPE/PP foils and feed spacers

4.1.1 HDPE and PP domains distribution

HDPE and PP are immiscible and their blends form a complex morphology [78]. Therefore, the domain distribution of the HDPE/PP model foil and feed spacer is an important aspect to investigate. Moreover, the morphology, chemistry, and topography of untreated materials have to be determined in order to discuss the effects of performed surface modifications.

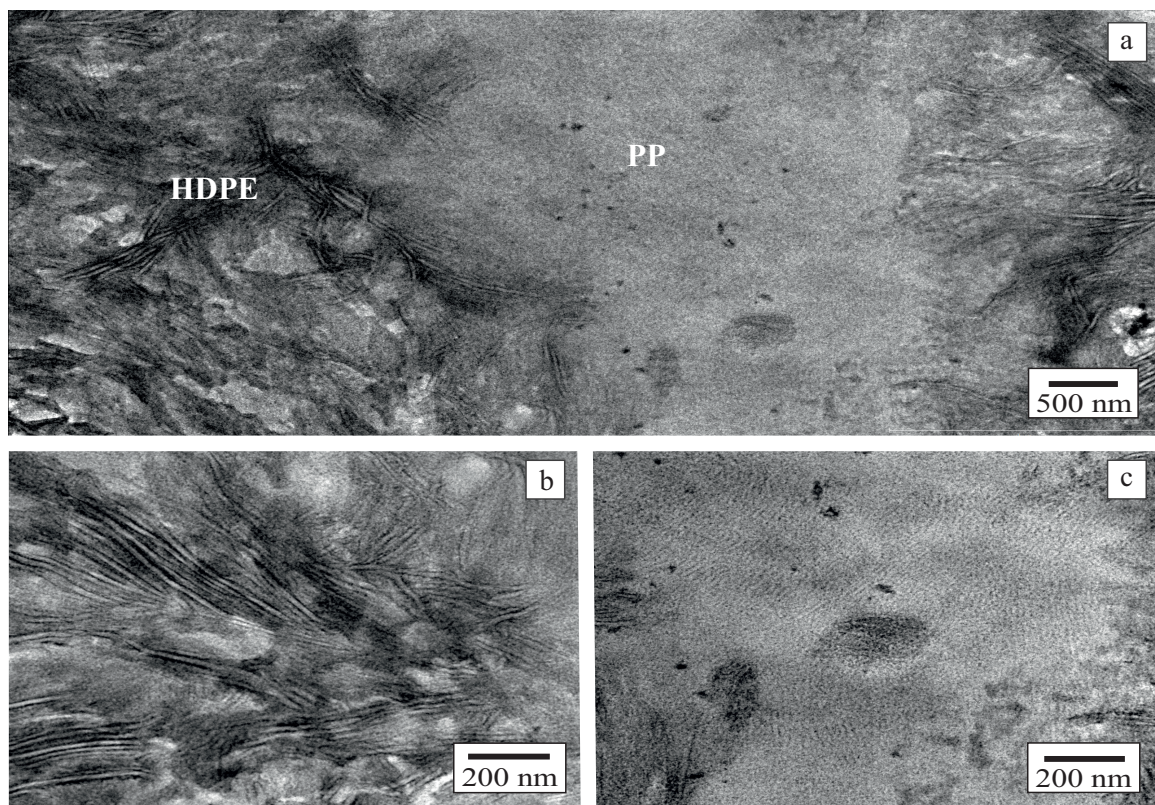


Figure 18: TEM images of the HDPE/PP (80/20 wt%) blend foil (microtomed sample stained in RuO_4): a–overview, b–enlargement on HDPE domain, c–enlargement on PP domain.

Morphology of blend materials can vary locally. The lateral and vertical structure can be different at different positions. Moreover, surface properties can vary from bulk characteristics [38]. For this reason, various HDPE and PP distributions at the surface and in the bulk of the HDPE/PP (80/20 wt%) blend should be investigated and considered.

First, the investigation of the blend film morphology in higher resolution using TEM revealed the incompatibility of the two components (see Figures 18). The HDPE and PP phases could be well-distinguished after staining with ruthenium, mainly because of the different sizes and appearance of lamellae [185]. In Figures 18 b and 18 c, the semi-crystalline structures of both components are presented in higher magnification. The average thickness of the lamellae depicted in Figure 18 b is 16 ± 2 nm, which corresponds well with literature values for crystalline HDPE [248]. In Figure 18 c, image processing, to determine lamellae thickness, was not performed because of low phase contrast. However, thinner cross-hatched lamellae can be attributed to the PP phase [165]. It is concluded from TEM investigations, that PP occurs as the minor phase in a bulk of the blend, forming domains without sharp boundaries. Nevertheless, due to the method requirements, the film sample was microtomed, and thus the analyzed specimen represents the near-surface structures, not the surface itself. It is possible that during material blending one of the phases, either PP or HDPE, migrated towards the interface, and as a consequence one phase dominates at the surface. To reveal the shape and distribution of the domains on the blend film and the feed spacer surfaces, surface analysis methods with low sampling depths, such as SEM and ToF-SIMS, were applied.

Before SEM, the HDPE/PP surfaces were etched [161], aimed to reveal the semicrystalline blend morphology. On the one hand, an amorphous phase is removed more easily by permanganic etchant than crystalline polymer structures. On the other hand, the PP phase is attacked more severely than the HDPE phase [161], which allows its easier identification (occurrence as pitch, holes, etc.). Figures 19 depict the matrix-dispersed phase morphologies of the HDPE/PP foil and feed spacer obtained by SEM.

SEM imaging on the permanganic-etched materials showed the occurrence of HDPE as a matrix, while PP is a minor phase. This is in good agreement with material composition. Similar shape and distribution of PP domains for both, foil (Figures 19 a1 and a2) and feed spacer (Figures 19 b1 and b2), can be observed. Smaller PP domains, partially removed by the etchant, formed holes in the HDPE matrix (highlighted in Figure 19), while elongated PP domains appear as trenches (marked with arrows in Figure 19).

It has to be noted that investigated by SEM surfaces were altered by permanganic preceding etching, aimed to improve the contrast between the two phases. Considering the depth of SEM analysis (about 10 nm) and the depth of etching (approximately 10 μ m), SEM on the permanganic-etched HDPE/PP materials cannot be considered as thoroughly surface representation. If there was a few nm thick PP layer on the blend surface, it would be completely removed during permanganic etching.

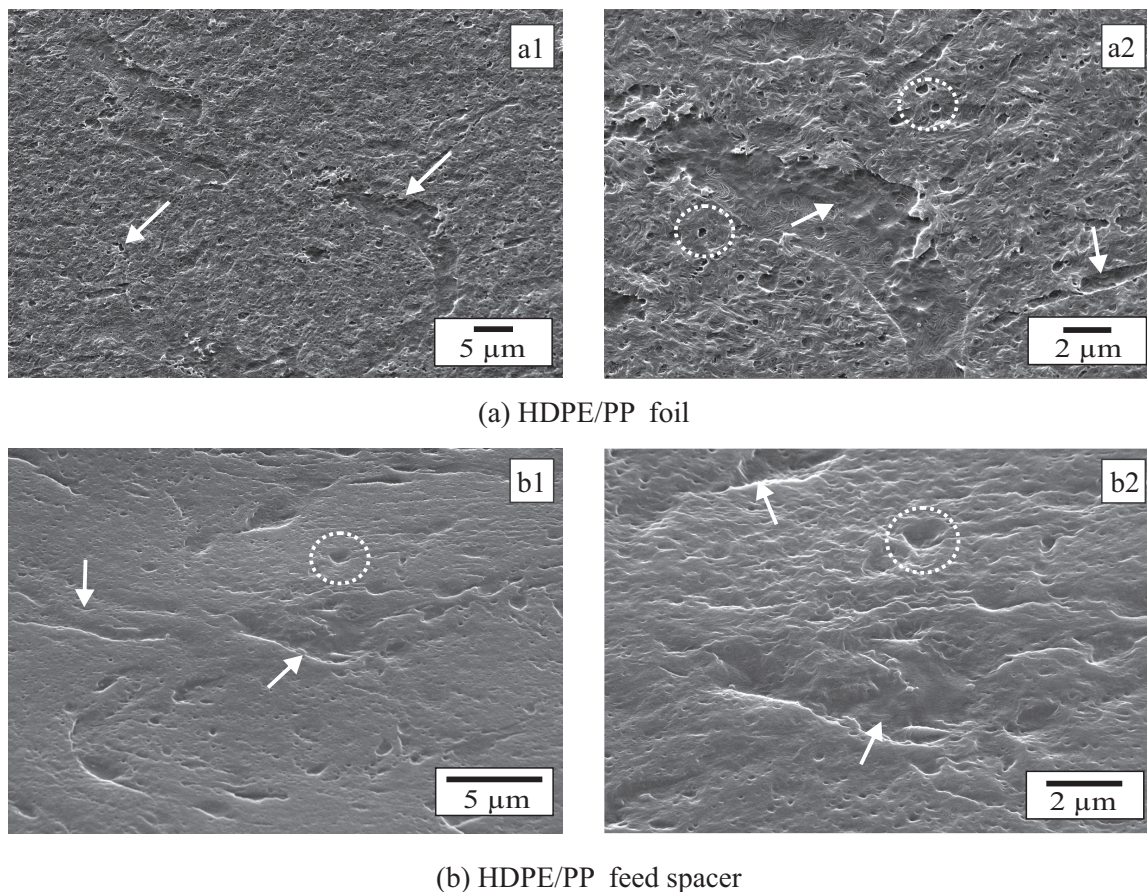


Figure 19: SEM micrographs of the permanganic-etched HDPE/PP (80/20 wt%) blend foil (a1 and a2 at higher magnification) and feed spacer (b1 and b2 at higher magnification) (PP domains highlighted and marked with arrows).

To analyze the upper nanometers of the HDPE/PP materials, ToF-SIMS with an information depth from the topmost monolayers (1–3 nm) was used [157]. Characterization of the HDPE/PP blend morphology utilizing ToF-SIMS imaging is much more complex than with conventional microscopic methods. To discriminate PP and HDPE by ToF-SIMS, a particular examination procedure was used [97]. In brief, pure polyolefin foils extruded from the same raw materials, were initially studied, to determine the characteristic peaks for either PP or HDPE. Both polymers show similar mass spectra, however, differences in the intensities of individual peaks are noticeable [152]. The peaks which showed significantly higher intensity for HDPE were assigned as HDPE characteristic; PP characteristic peaks were chosen analogously. Figure 20 displays some characteristic HDPE and PP peaks, while Table 4 summarizes all peaks which showed significantly different intensities (mass range 0–120 atomic units).

Taking into consideration only the characteristic HDPE and PP peaks (see Table 4), imaging of the blend foil was performed. The visualization after normalization to the total intensity and applying 4-pixel binning is presented in Figures 21. Complementary areas of characteristic HDPE (Figure 21 a) and PP peaks (Figure 21 b) are distinguishable on the HDPE/PP blended

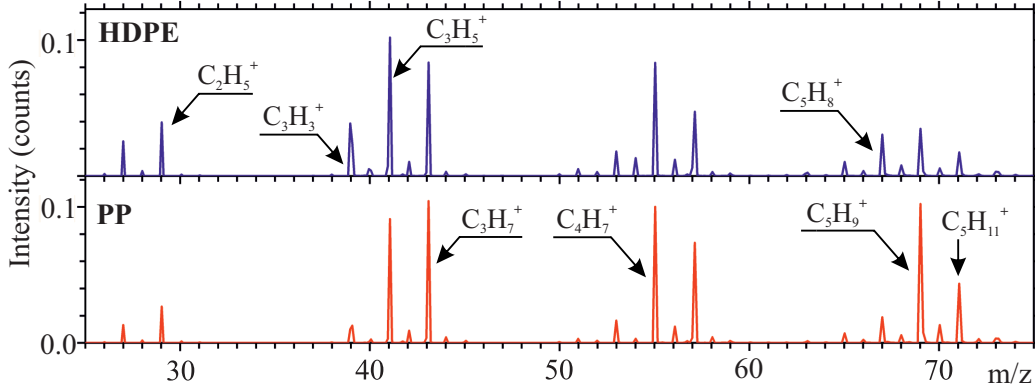


Figure 20: Positive ToF-SIMS spectra of HDPE (above) and PP (below) foils normalized by total intensity, mass range (m/z) from 25 to 75 atomic units (au).

Material	Characteristic peaks
HDPE	CH_2^+ , CH_3^+ , C_2H_2^+ , C_2H_3^+ , C_2H_4^+ , C_2H_5^+ , C_3H_2^+ , C_3H_3^+ , C_3H_4^+ , C_3H_5^+ , C_3H_6^+ , C_4H_2^+ , C_4H_3^+ , C_4H_4^+ , C_4H_5^+ , C_4H_6^+ , C_5H_3^+ , C_5H_4^+ , C_5H_5^+ , C_5H_7^+ , C_5H_8^+ , C_6H_5^+ , C_6H_6^+ , C_6H_7^+ , C_6H_8^+ , C_7H_7^+ , C_7H_8^+
PP	C_3H_7^+ , C_3H_8^+ , C_4H_7^+ , C_4H_9^+ , $\text{C}_4\text{H}_{10}^+$, $\text{C}_4\text{H}_{11}^+$, C_5H_9^+ , $\text{C}_5\text{H}_{10}^+$, $\text{C}_5\text{H}_{11}^+$, $\text{C}_6\text{H}_{10}^+$, $\text{C}_6\text{H}_{11}^+$, $\text{C}_6\text{H}_{12}^+$, $\text{C}_6\text{H}_{13}^+$, $\text{C}_7\text{H}_{11}^+$, $\text{C}_7\text{H}_{13}^+$, $\text{C}_8\text{H}_{13}^+$, $\text{C}_8\text{H}_{15}^+$

Table 4: List of characteristic HDPE and PP peaks (ToF-SIMS positive spectra, mass range (m/z): 0–120 au)

foil. Owing to the limited lateral resolution, the surface morphology determined by ToF-SIMS imaging varies from a typical matrix-dispersed phase morphology. However, a significant occurrence of the PP phase at the surface was demonstrated (area shown in red in Figure 21 c). The share of HDPE on the examined blend surface (depicted in blue in Figure 21 c) is estimated at $\approx 35\%$ (evaluation performed in software Cell^F).

The same procedure was applied to analyze the morphology of the HDPE/PP feed spacer surface. The distribution of the characteristic HDPE and PP peaks is given in Figures 22. ToF-SIMS positive imaging of the feed spacer surface showed PP as the main phase (presented in red in Figure 22 c). This finding is in good agreement with the results obtained for the HDPE/PP foil (Figure 21 c). However, the distribution of the HDPE phase varies between those two materials. The HDPE domains are finely dispersed on the foil surface, while they appear as a larger cluster/island on the feed spacer (blue region in Figure 22 c). This discrepancy in domains' distribution, is possibly caused by different manufacturing processes of the foil and feed spacer materials.

ToF-SIMS positive imaging, performed on the HDPE/PP (80/20 wt%) foil and feed spacer, showed primarily the presence of PP on these surfaces, despite its lower percentage in the material's composition. The majority of PP can be caused by its lower density. Therefore, PP can migrate towards the surface during blending aimed to minimize the surface energy of the blend system [39, 181].

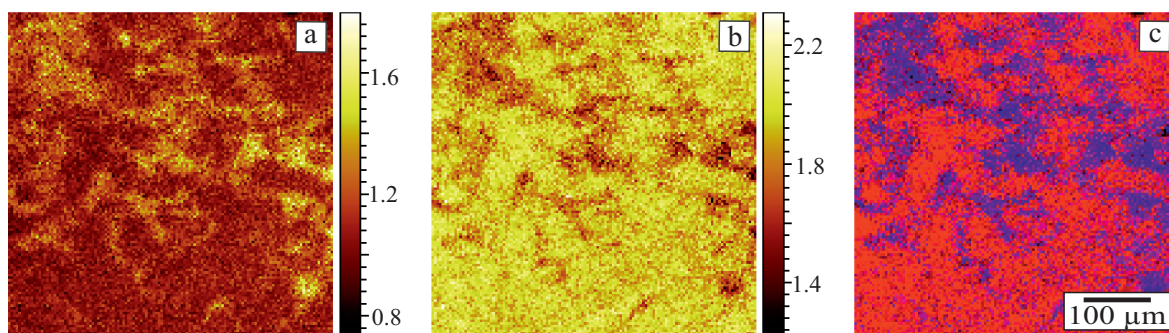


Figure 21: ToF-SIMS positive imaging of the HDPE/PP **blend foil** surface (normalized by total intensity, investigated area $500 \times 500 \mu\text{m}^2$): a–sum of the intensities of characteristic HDPE peaks, b–sum of the intensities of characteristic PP peaks, c–overlay with final materials’ allocation: HDPE (blue) and PP (red). Color scale from black, to red to yellow depending on the characteristic peaks’ content.

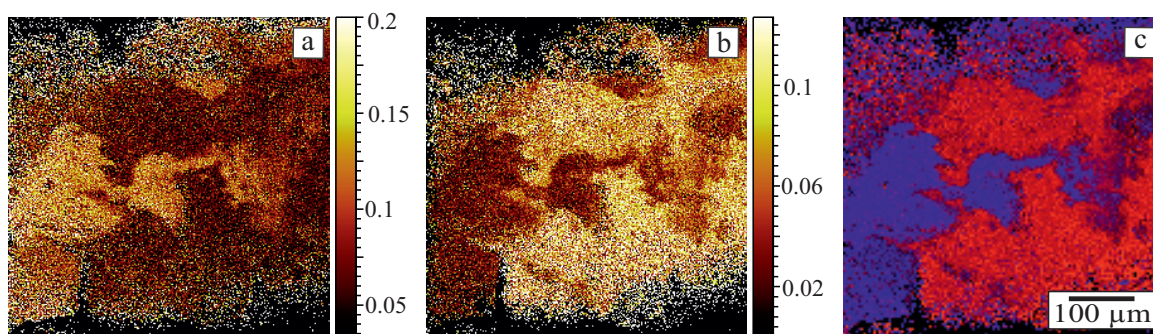


Figure 22: ToF-SIMS positive imaging of the HDPE/PP **feed spacer** surface (normalized by total intensity, investigated area $500 \times 500 \mu\text{m}^2$): a–sum of the intensities of characteristic HDPE peaks, b–sum of the intensities of characteristic PP peaks, c–overlay with final materials’ allocation: HDPE (blue) and PP (red). Color scale from black, to red to yellow depending on the characteristic peaks’ content.

4.1.2 Surface chemistry, morphology and topography

The HDPE/PP foils and feed spacers were manufactured from the same raw materials, however by different companies. Therefore, they might possess some additives, be affected by photoaging or difficult to remove contamination. To analyze the elemental compositions of the foil and feed spacer surfaces, XPS was applied. Obtained results are summarized in Table 5, while example spectra, with highlighted characteristic peaks, are depicted in Figure 23. Oxygen was detected, at both surfaces, in significantly higher concentration at the feed spacer. A certain amount of oxygen highly probable correlates with detected silicon, which can originate from silicon-containing slip agents. Argon sputtering was applied in order to release surface contamination (up to 7 minutes of sputtering). Despite Si concentration, was significantly reduced over sputtering time, oxygen content remained at about 5 at%. Therefore, besides Si-based surface contamination, the

possible presence of some organic additives, containing oxygen, should be considered.

Material	C (at%)	O (at%)	Si (at%)
HDPE/PP foil	99.8 ± 0.1	0.2 ± 0.1	x
HDPE/PP spacer	89.9 ± 4.1	7.5 ± 2.1	2.6 ± 2.6

Table 5: Surface elemental composition of the untreated HDPE/PP blend foil and feed spacer (XPS).

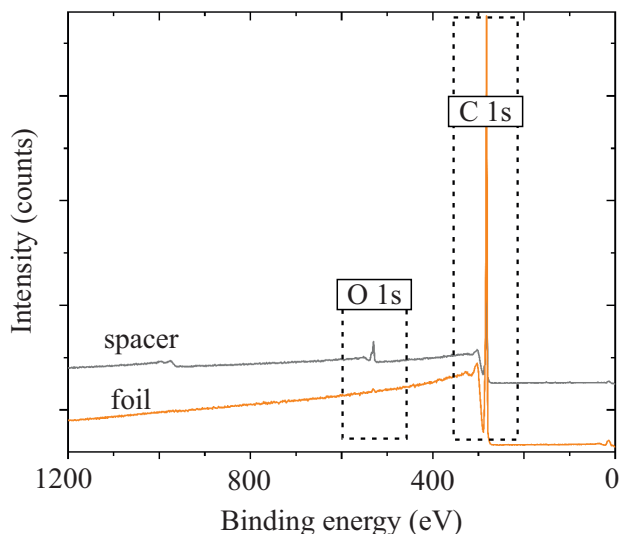


Figure 23: XPS survey spectra of the untreated HDPE/PP film and feed spacer (highlighted O 1s and C 1s peaks).

Furthermore, the HDPE/PP materials were analyzed by ATR-FTIR. Figure 24 illustrates an example spectrum of the untreated blend foil. All characteristic absorption bands for HDPE and PP polyolefins could be assigned. They are summarized in Table 6 [103, 247].

Contact angle measurements were performed to estimate the surface free energy (SFE) of the HDPE/PP blend foil. The obtained value was 33 mN/m, which is in good agreement with the SFE values reported in the literature for PP (29 mN/m) and HDPE (33 mN/m) [215]. The surface free energy of the feed spacer, could not be evaluated, using a standard sessile drop technique, due to the small thickness of the spacer strands.

AFM phase, and height imaging, were carried out to analyze the morphology and roughness of the HDPE/PP foil and feed spacer. The obtained morphologies are presented in Figures 25. Taking into consideration the morphology of the HDPE/PP foil (Figure 25 a), crystalline structures are visible, and two types of lamellae can be distinguished. Thicker lamellae (examples marked with arrows in Figure 25 a) are attributed to the HDPE phase, while thin lamellae represent the PP material (examples highlighted in Figure 25 a) [149, 248]. The examined by AFM untreated feed spacer surface (Figure 25 b) showed a heterogeneous morphology. Besides crystalline structures

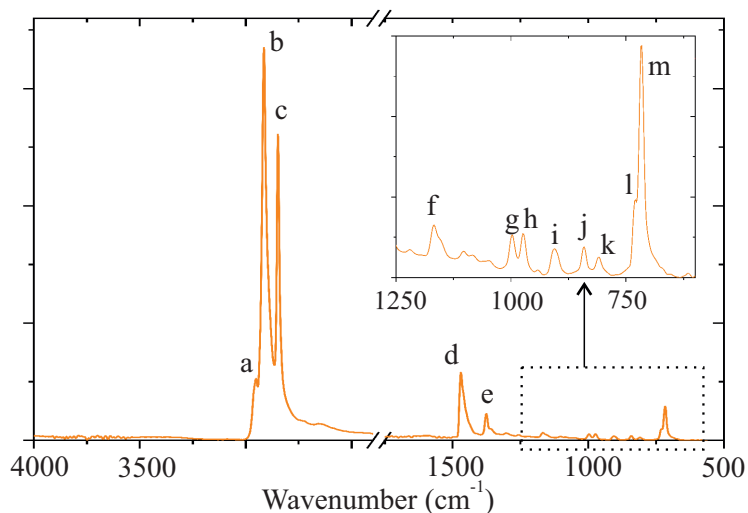


Figure 24: ATR-FTIR spectrum of the untreated HDPE/PP foil.

(based on the estimated lamellae thickness, most probably HDPE [149]), unusual amorphous regions could be assigned (examples marked with arrows in Figure 25 b). These are likely some extrusion additives that diffused to the surface; or impurities, possibly containing silicon, as can be concluded from the surface composition analysis (see Table 5). Inhomogeneously distributed contaminations are likely to occur at polymer surfaces manufactured on the industrial scale. Not only contamination from handling is possible, but also an application of slip agents or stabilizers while processing, what is a common practice [74].

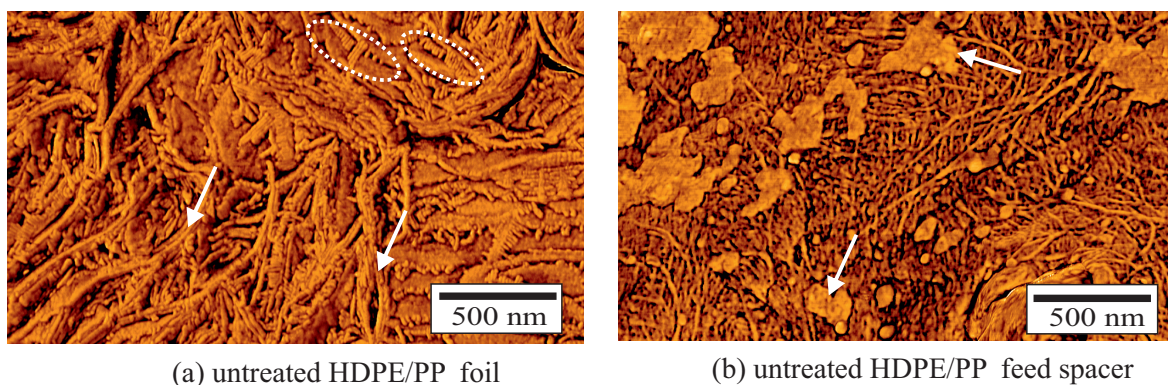


Figure 25: AFM phase imaging: a–untreated HDPE/PP foil (PP lamellae highlighted, HDPE lamellae marked with arrows), b–untreated feed spacer (unusual amorphous islands marked with arrows).

A comparison between surface morphology of the untreated blend film (Figure 25 a) and untreated feed spacer (Figure 25 b) is not straight forward. However, considering that different technologies were used to manufacture both materials, various surface morphologies can be expected [135]. The feed spacer and foil investigations by AFM indicated the majority of HDPE at both surfaces. This finding is contrary to ToF-SIMS positive imaging, which showed PP as the main phase at the outermost blend surfaces (Figures 21 c and 22 c). Therefore, local changes in

4.1 Characterization of the HDPE/PP foils and feed spacers

Absorption band (cm ⁻¹)	Vibration modes	PP	HDPE
(a) 2949	C–H stretch	x	
(b) 2910	C–H stretch	x	x
(c) 2845	C–H stretch	x	x
(d) 1468	CH ₂ bend	x	x
(e) 1378	CH ₃ bend	x	
(f) 1166	CH bend, CH ₃ rock, C–C stretch	x	
(g) 997	CH ₃ rock, CH ₃ bend, CH bend	x	
(h) 973	CH ₃ rock, C–C stretch	x	
(i) 904	CH ₃ rock	x	
(j) 840	CH ₂ rock, C–CH ₃ stretch	x	
(k) 809	CH ₂ rock, C–C stretch, C–CH stretch	x	
(l) 730	CH ₂ rock		x
(m) 715	CH ₂ rock		x

Table 6: List of absorption bands with their assignment for the ATR-FTIR analysis of the untreated HDPE/PP foil and feed spacer [103, 247].

composition (the HDPE phase vs. the PP phase), have to be considered, while studying those blend substrates.

To evaluate the surface roughness of the HDPE/PP substrates, AFM height imaging was used. Determined R_a for the foil was 8.7 ± 1.1 nm and for the spacer was 5.1 ± 3.4 nm, while R_z was 41.4 ± 5.8 nm and 28.2 ± 18.8 nm, respectively. It cannot be assumed from those results that the spacer surface is, significantly rougher. The reason why, significant feed spacer roughness, could not be revealed by AFM, is too short sampling length. AFM is one the one hand, well suited to investigate surface topography due to its high sensitivity and resolution. However, on the other hand, the method is not well-suited to analyze larger areas [225].

Considering the standard ISO 4288:1996 [73], which describes the rules and procedures for the assessment of the surface texture, the evaluation length (l_n) for the profiles having R_a values between 6 nm and 20 nm, should be at least 0.4 mm. Since, in this study, shorter l_n were analyzed (2.5 μ m for the foil, while 2 μ m for the spacer), obtained using AFM roughness parameters, are not standardized. Nevertheless, they can be used for a comparison purpose, to assess an effect of applied modifications on the surface topography.

A contact profilometry (DektakXT contact stylus profilometer) was applied, to determine the R_a value for the blend foil according to ISO 4288:1996 [73] (evaluation length of 4 mm). The obtained R_a was 219.4 ± 9.3 nm. The feed spacer geometry was not suitable to be analyzed by contact profilometry.

4.1.3 Discussion

It was shown that the distribution of the HDPE and PP domains is different for the blend foil and feed spacer surfaces. According to the results obtained by ToF-SIMS analyses, HDPE is more evenly distributed on the foil surface, and it generates islands on the spacer surface (Figure 21 and Figure 22, respectively). The chemical composition analyses showed the presence of oxygen on both materials, a very low concentration at the foil surface, and considerably higher concentration at the spacer surface. Furthermore, the feed spacer possesses significantly more heterogeneous topography. Table 7 summarizes some key parameters determined for the HDPE/PP foils and feed spacers.

Parameter	HDPE/PP foil	HDPE/PP spacer
O (at%)	0.2±0.1	7.5±2.1
SFE (mN/m)	33±1	x
R _a (nm)	8.7±1.1	5.1±3.4

Table 7: Parameters determined for the untreated HDPE/PP foils and feed spacers.

The following aspects will be discussed in more detail: first, the comparison of different methods for surface characterization; second, the challenges of chemical modification of the spacer.

Some of the challenging properties of the investigated HDPE/PP substrates, such as surface contamination or defects, can be generally attributed to the industrially manufactured materials. Their surface characteristic can vary depending on the position on the sample. Therefore, surface characterization, obtained by different methods with various areas of interest, might be inconsistent. To better illustrate this objective, a schematic overview, for applied in this work characterization methods with the fields of the examination, was prepared (see Figure 26).

For instance, let us compare the following analyses: surface free energy by contact angle measurements, a chemical composition by XPS, and surface morphology by AFM. Contact angle measurements allow investigation of relatively large surface areas with good surface sensitivity (about 0.5–1 nm [207, 214]). Test liquid droplets are placed on the analyzed material and occupy the specific surface area, larger for the better affinity between liquid and surface. Since an overall surface free energy is calculated, based on several individual contact angles (at least 10 for both test liquids), the local changes in surface characteristics, might remain "unnoticed". The elemental composition obtained by XPS represents about 300×700 μm² of the surface (per position), while AFM performed on the same specimen does not depict even one-hundredth of this field (analyzed area 2.5×2.5 μm²). Consequently, an interpretation of surface analyses carried out on the industrially manufactured materials, has to be performed, taking into consideration the limitations of the applied characterization methods. Not only the area of the analyzed surface is of great importance, but also the sampling depth, and the detection limit of the applied technique. For example, oxygen was detected at the feed spacer surface by XPS (Table 5), while

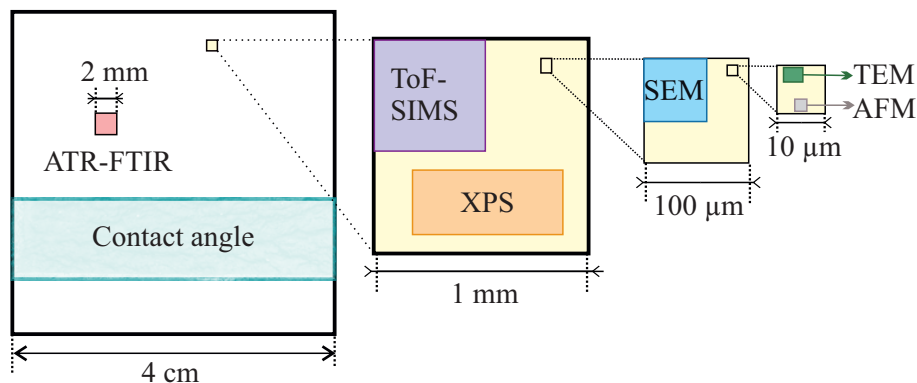


Figure 26: Overview of the applied methods to characterize the HDPE/PP surfaces with an emphasis on the size of the examined area. Abbreviations: ATR-FTIR: attenuated total reflection Fourier-transform infrared spectroscopy, ToF-SIMS: time-of-flight secondary ion mass spectrometry, XPS: X-ray photoelectron spectroscopy, SEM: scanning electron microscopy, TEM: transmission electron microscopy, AFM: atomic force microscopy.

it was not revealed by ATR-FTIR (sampling depth: XPS—about 10 nm, ATR-FTIR—about 1 μm [207, 29]). This indicates, either that oxygen is accumulated more at the feed spacer surface, or the concentration of oxygen functional groups is not high enough, to be detected by less sensitive ATR-FTIR. Therefore, various characterization methods were employed in this work, to obtain possibly comprehensive information about used materials, and subsequently about the effect of performed modifications.

The chemical modification of the feed spacer surface is not bearing the risk of deterioration of the filtration properties, as it could be for the polyamide membrane modification. However, the feed spacers are made of PP or HDPE/PP blends. Therefore, they do not possess any functional groups, which could be, used for the grafting of antifouling agents. Attempts to produce some functional groups at the PP or HDPE surfaces, for example utilizing plasma treatment, are often associated with material degradation via chain scission [74]. The functionalization of the PA membrane provides much more reaction pathways, for instance, via amino or carboxylic groups [213].

The chemical modification of the feed spacer is highly challenging not only, because of material composition, but also its heterogeneous topography (see Figure 3b). Plenty of grooves, high overall specimen roughness and waviness, are desirable for improving flow conditions. Nevertheless, they are troublesome for the generation of thin functional coatings.

A further difficulty, in the feed spacer modification, is related to its 3D structure. For instance, there is a lack of appropriate methods to detect and analyze generated coatings at material junctions, where the initial bacterial adhesion occurs [211, 223]. The coatings' quality control at those problematic spots is very challenging. According to the author's knowledge, there is no analytical method that provides complete information about the surface chemistry for such type of sample geometry. Proposed in this work, preliminary modifications of the model foils enabled

using a broader spectrum of characterization methods. Nevertheless, analogously conducted on both substrates modifications, can perform differently. The reason for this may be different topographies of both materials. Moreover, the composition analysis of both HDPE/PP materials, indicated a considerably higher amount of oxygen and silicon at the feed spacer surface, than at the foil surface (see Table 5). Detected Si and O originate probably from the manufacturing impurities or targeted additives. The contamination at the feed spacer surface (see Figure 25 b) can reduce the overall surface accessibility, and influence the effect of performed processes.

4.2 Modification of the polyolefin foils

4.2.1 Plasma treatment with dielectric barrier discharge (DBD) in air

4.2.1.1 Surface chemistry Exposure of a polyolefin surface to plasma allows the incorporation of oxygen functional groups, therefore promotes adhesion and wetting [74]. In order to better understand the chemical modification of the HDPE/PP (80/20 wt%) surfaces in plasma, PP and HDPE foils were examined simultaneously to the blend. An impact of applied plasma intensity on the surface chemistry and morphology of the polyolefin foils was studied. Three different plasma treatment parameters (PL_A , PL_B , and PL_C ; described in detail in Table 3) were applied. The surface elemental compositions (O in at%) and surface free energies of the untreated, as well as exposed to plasma treatment foils are presented in Figures 27 a and b.

Significant incorporation of oxygen was observed for each type of material after exposure to plasma (Figure 27 a). An increase in plasma intensity from PL_A to PL_C resulted in increased oxygen content at the surfaces. No clear tendency in oxygen incorporation between the HDPE, PP, and blend foils could be observed, within the range of tested plasma treatment parameters. The reason is, most probably, the similar dissociation energies of the C–C and C–H bonds in both polyolefins, which hinders the selective modification in plasma (PE backbone: 375 kJ/mol, C–H bond: 396 kJ/mol; tertiary C–H bond in PP: 385 kJ/mol). Moreover, the energy of plasma species exceeds by far the dissociation energies of C–H and C–C bonds. Therefore, selective oxidation is not possible. Consequently, a similar level of functionalization is obtained for the HDPE, PP, and their blend, exposed to plasma [74]. The surfaces treated with the highest intensity plasma (PL_C) possessed an about 0.30 O/C atomic ratio (PP=20.6±1.7 O at%; HDPE=22.5±2.3 O at%, blend=23.1±2.6 O at%).

Taking into consideration the surface free energy investigations (Figure 27 b), the values obtained for the untreated PP (31 mN/m) and HDPE (35 mN/m) are in a good agreement with those reported in the literature (PP=29 mN/m; HDPE=33 mN/m [215]). The contact angle measurements showed a remarkable increase in the surface free energy (SFE) after plasma treatment. There is a tendency in SFE values observed, both before and after plasma treatment: HDPE showed the highest SFE, subsequently blend, and PP. The maximum SFE values obtained for the investigated polyolefin foils after plasma treatment were: 60 mN/m for HDPE, 53 mN/m for blend, while 52 mN/m for PP.

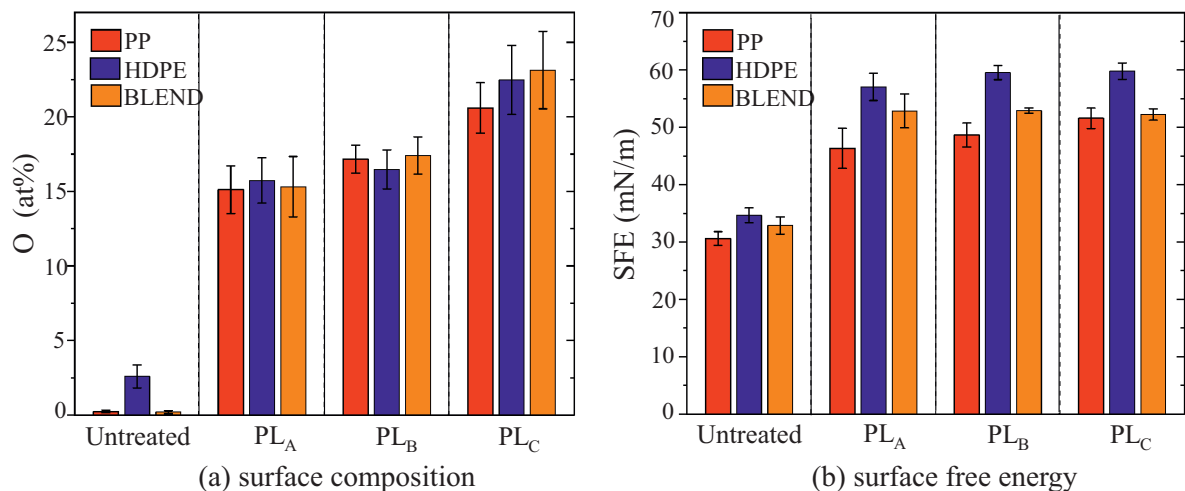


Figure 27: Characterization of the HDPE, PP, and HDPE/PP foils exposed to atmospheric pressure plasma treatment (DBD in air) with different intensities: a–surface composition (O in at%, XPS), b–surface free energy (SFE, contact angle measurements). Plasma intensity increases from PL_A to PL_C, detailed parameters given in Table 3.

Contrary to increased oxygen content with higher plasma intensity, minor changes in the SFE were observed, within applied plasma treatments (Figure 27 b). It has been reported in the literature, that the polar part of the SFE shows a linear dependence on the amount of introduced by plasma treatment oxygen, up to the maximum value (saturation effect), followed by the material degradation, and more in-depth oxidation [74]. It can be concluded, based on this statement, that the steady-state functionalization was possibly reached, already after applying the mildest plasma conditions (PL_A). XPS and contact angle have different sampling depths (XPS up to 10 nm [90], contact angle about 0.5–1 nm [214, 207]). Therefore, deeper penetration of oxygen can be detected by XPS, while more surface sensitive contact angle measurement, does not allow recording the change in material depth. Moreover, the possible presence of the polyolefin degradation products (known as low-molecular-weight oxidized material: LMWOM) on the plasma-treated surfaces can hinder the proper SFE determination. The LMWOMs are degraded polymer fragments, commonly found on the polyolefin surfaces treated with DBD in air [203]. They arise from polymer chains' scission by the high energy plasma species. To identify the possible occurrence of the LMWOM on the plasma-treated surfaces, morphology analysis was performed (see section 4.2.1.2).

ATR-FTIR, with higher analytical information depth, was used as an alternative method to detect oxygen functional groups on the plasma-treated foils. Infrared spectroscopy is useful for the analysis of plasma-treated polymers when the modification depth is at least 100 nm [207]. However, in this case, any absorption bands indicating oxygen functional groups could be assigned when analyzing the blend foil exposed to the highest intensity plasma (PL_C). This result indicates the changes in composition oriented at the surface.

The comparison of obtained compositions and surface free energies of the plasma-treated PP and

HDPE with the literature data is not straightforward. As first, plasma processes are strongly influenced by the plasma generation set-up and treatment parameters, rarely given in detail by authors. Secondly, the effect of plasma exposure on the polymer surface depends among others on material crystallinity [16], sample storage before modification [87], air humidity [59] and analysis conditions, such as the XPS take-off angle [60]. Moreover, nomenclature used in the relevant literature is often confusing due to alternate use of terms corona and dielectric barrier discharge, which are different processes. Nevertheless, some results, considering the atmospheric pressure plasma treatment of PE and PP with dielectric barrier discharge (DBD) in air, are summarized in Table 8, including the data obtained in this work. The focus in this literature review was the threshold amount of oxygen (O/C atomic ratio) and the corresponding SFE/water contact angle (WCA), reported by other authors.

Material	O/C atomic ratio	SFE (mN/m), WCA (°)	Reference
PE	0.24–0.28	45 mN/m	Friedrich [74]
	0.68	52.5°	Borcia et al. [25]
	0.70	40°	Iwata et al. [96]
	0.39	53.3°	Kun et al. [118]
	0.37	52 mN/m, 53.3°	Ren et al. [177]
	0.32	60 mN/m, 45°	this work
PP	0.24–0.28	45 mN/m	Friedrich [74]
	0.13	45 mN/m	O’Hare et al. [160]
	0.16	50 mN/m, 64°	Leroux et al. [132]
	0.42	53.8°	Cui et al. [54]
	0.23	57°	Strobel et al. [203]
	0.28	52 mN/m, 55°	this work

Table 8: Literature review on the threshold O/C atomic ratio and the surface free energy (SFE)/water contact angle (WCA) values for PE and PP treated in atmospheric pressure plasma with DBD in air.

The discrepancy in the literature results on the PE and PP treatment with DBD in air is clearly seen. This is not surprising, since, as already mentioned, the characteristic of generated plasma depends on plenty of factors (e.g., set-up construction, atmospheric conditions). However, apart from some extreme oxidation degrees obtained by Iwata et al. and Borcia et al. for PE [96, 25], as well as reported by Cui et al. for PP [54], both polyolefins show analogous response to the plasma treatment. It is shown especially in the studies of Friedrich, who modified PP and PE under the same conditions [74].

Detection of hydroperoxide groups. Hydroperoxides are found especially favorable among all introduced via plasma treatment functional groups. They can decompose and initiate further grafting onto the surface, as reported elsewhere [96, 230, 43, 208]. The incorporation of hydroperoxides, after applying different plasma treatments (PL_A, PL_B, PL_C) was studied for all

polyolefin foils. Both untreated and plasma-treated samples were simultaneously exposed to SO₂ gas, to derivatize hydroperoxide groups. Their presence at the plasma-treated surfaces was confirmed, via analyzing the sulfur content (procedure given in section 3.2.2). It was concluded, that performed plasma treatment generated hydroperoxides at the investigated surfaces. However, the amount of these functional groups did not varied significantly between tested materials and within applied plasma treatment conditions. An about 0.6 at% of incorporated sulfur was detected by XPS at the plasma-treated specimens, regardless of the treatment parameters. The untreated control samples did not show any sulfur. Assuming the detected amount of sulfur as 0.6 at%, and the total amount of oxygen directly after plasma treatment as 20 at%, it can be estimated that approximately 6% of the entire oxygen originates from hydroperoxide groups. Nevertheless, such mathematical estimation does not consider a variety of functional groups. Some of them have only a single oxygen atom (for instance $-C-OH$, $-C=O$), while the others are at higher oxidation state (e.g., $-O-CO-O$, $-C(O)-O-OH$). Moreover, hydroperoxides can decompose and re-arrange to all kinds of O-containing groups before the derivatization with SO₂ has begun [74]. Therefore, the amount of oxygen in at% cannot be directly used to calculate the density of hydroperoxides. Furthermore, the derivatization reaction applies mainly to the hydroperoxides located at the outermost surface. However, the amount of oxygen detected in XPS considers at least a few nm. Therefore, the percentage of hydroperoxides at the topmost surface can be higher than the estimated 6%.

Despite the difficulty in estimating the number of hydroperoxide groups per surface area, their presence at the surfaces, after plasma treatment, was demonstrated. Consequently, their utilization to initiate the grafting onto the surface is feasible. The obtained hydroperoxide groups' contribution to the overall oxygen content is in good agreement with those found in the literature for PP and PET [102, 170].

4.2.1.2 Surface morphology and topography The surface composition and free energy analyses, performed on the plasma-treated materials, were complemented by an examination of surface morphology and topography. AFM investigations were carried out on the HDPE/PP foil, which served as a model substrate for the feed spacer. The surface morphological characteristics of the blend foil, exposed to plasma with different intensities (PL_A, PL_B and PL_C, treatment details given in Table 3), are summarized in Figures 28 a-c.

The characteristic HDPE and PP crystalline structures, identified on the untreated foil (see Figure 25 a), became less apparent after exposure to plasma. The treatment with the lowest intensity plasma (PL_A) was already found to alter the blend surface (Figure 28 a). The increase in plasma intensity from PL_A to PL_C (Figures 28 a-c) resulted in the progressive coverage of the crystalline structures by an amorphous matter. Generated on the plasma-treated surfaces amorphous islands, are most likely attributed to the low-molecular-weight oxidized material (LMWOM). The LMWOM consists of highly oxidized polymer degradation products (O/C about 0.56 [75]) that originate from the backbone chains' scissions. The LMWOM was often found on the DBD/corona

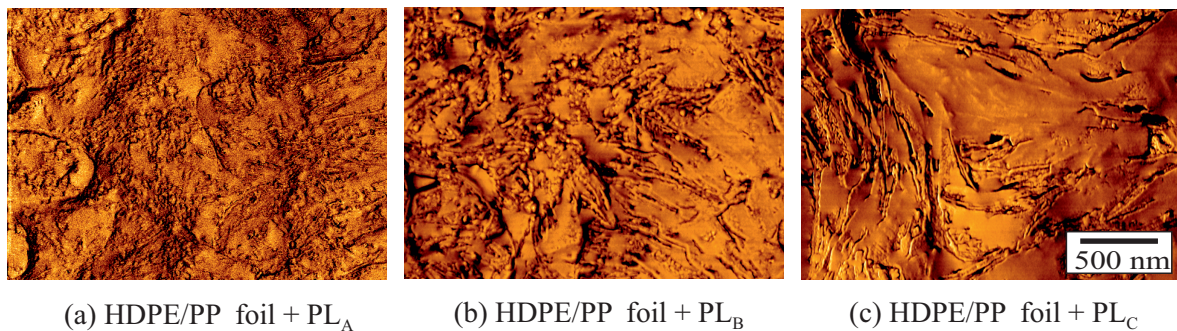


Figure 28: AFM phase imaging of the HDPE/PP foils treated in atmospheric pressure plasma with DBD in air. The intensity of applied plasma increases from PL_A to PL_C , detailed treatment parameters given in Table 3.

treated polyolefins [74]. Similar morphologies are presented, in the numerous publications from Strobel et al., who extensively studied the PP oxidation with DBD in air [204, 203]. Overnay et al., who analyzed the LMWOM on the plasma-treated PP surface, assigned them to melted oxidation products containing oligomers with 16 carbon atoms [166].

The LMWOM layer is highly polar and weakly bonded to the surface. It can be partially dissolved in water and other polar solvents [203]. The presence of the LMWOM on the analyzed surfaces explains, previously reported, only minor SFE differences for the foils exposed to various plasma intensities (see Figure 27 b). Since the LMWOM can dissolve in the contact angle test liquids, the measurements performed on the LMWOM-containing surface, are affected by an experimental error. This was shown by Strobel and coworkers [205].

To confirm, whether observed on the plasma-treated surfaces amorphous matter can be attributed to the LMWOM, further investigations were performed. The PL_C plasma-treated foil (Figure 28 c), the most covered by the amorphous matter, was rinsed in water, and again analyzed by AFM. Obtained morphology after rinsing is depicted in Figure 29 a. It can be clearly seen that the semicrystalline morphology of untreated material is "renewed" after rinsing. This confirms that amorphous matter, presented on the plasma-treated surfaces (see Figures 28 a–c), can be assigned to the water-soluble LMWOM. Schematic representations of the HDPE/PP surface after treatment with PL_C plasma, and after PL_C plasma treatment and subsequent rinsing in water, are given in Figure 29 b. More detailed considerations about the generation of the LMWOM on the exposure to oxygen-containing plasma can be found in the current review [75].

An effect of performed plasma treatments, on the HDPE/PP surface roughness, was studied by AFM height imaging. The R_a and R_z values for the plasma-treated (PL_A , PL_B , PL_C), as well as PL_C plasma treated and rinsed in water (deprived of the LMWOM) blend foils, were determined. Obtained results are summarized in Table 9.

The plasma-treated HDPE/PP surfaces (PL_A , PL_B , PL_C , PL_C +rinsing) demonstrated reduced roughness, in comparison to the untreated foil. No significant differences in the surface rough-

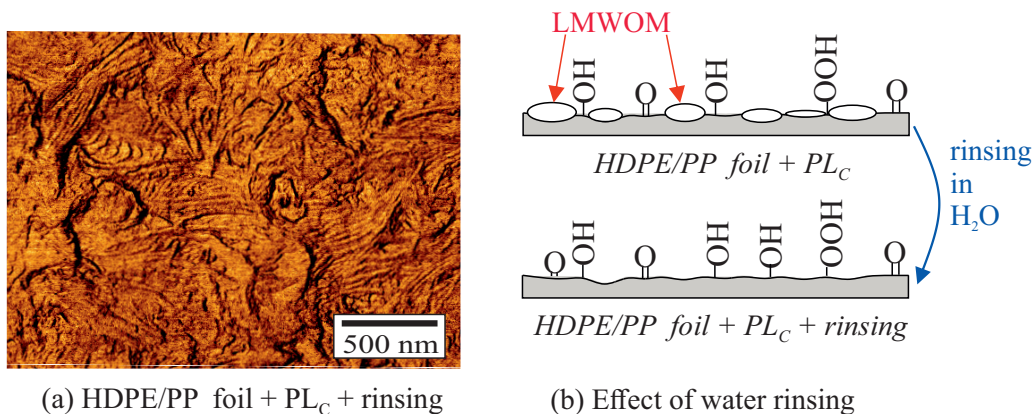


Figure 29: a–AFM phase imaging of the HDPE/PP foil exposed to PL_C plasma and subsequently rinsed in water, b–schematic representation of the HDPE/PP foil directly after treatment with PL_C plasma (above), and after treatment with PL_C plasma and subsequent rinsing in water (below). LMWOM–low-molecular-weight oxidized material. Detailed PL_C plasma treatment parameters are given in Table 3.

Foil sample	R_a (nm)	R_z (nm)
untreated HDPE/PP	8.7 ± 1.1	41.4 ± 5.8
HDPE/PP + PL_A	4.3 ± 0.6	26.3 ± 4.4
HDPE/PP + PL_B	5.2 ± 0.6	32.1 ± 7.9
HDPE/PP + PL_C	5.4 ± 0.8	27.2 ± 4.2
HDPE/PP + PL_C + rinsing	6.2 ± 1.3	33.0 ± 6.6

Table 9: Surface roughness parameters (R_a , R_z ; AFM height imaging) for the untreated, plasma treated (PL_A , PL_B , PL_C), as well as PL_C plasma treated and rinsed in water (PL_C + rinsing), HDPE/PP blend foils (plasma treatment with DBD in air, detailed parameters given in Table 3).

ness, with increasing plasma intensity from PL_A to PL_C , could be concluded. This is most likely influenced by the presence of LMWOM on these surfaces, as observed in AFM phase images (Figures 28). The oxidation by-products accumulate possibly in the material’s valleys, therefore reduce overall surface roughness. Analyzing the roughness after the highest intensity PL_C plasma treatment, and the roughness after PL_C plasma treatment and rinsing in water, a tendentious increase in R_a and R_z values was found. This confirms that the LMWOM might accumulate in the material’s cavities. Therefore, after removing this layer via rinsing, higher surface roughness was shown.

Reduced surface roughness after plasma treatment suggests partial material etching or its slight melting. Morphology of polymer surface can be affected by the temperature generated in plasma. Owing to the low heat conductivity of HDPE and PP, the temperature of these polymer surfaces can be easily raised while exposure to plasma [166]. During a high-frequency DBD treatment of polymer surface, the softening temperature is, quite easily, reached. Consequently, macro-scale deformations of the surface can occur [26]. For example, it was shown that the PP surface,

exposed to DBD treatment, has changed its crystalline level. It was assumed that the polymer surface slightly melts due to discharge heating, therefore became more amorphous [132].

Influence of LMWOM on the surface free energy and composition. To verify how the presence of the LMWOM influences the surface free energy and composition (Figures 27), the highest intensity plasma treated and rinsed (PL_C +rinsing) polyolefins were subjected to XPS and contact angle analyses. Obtained results are summarized in Table 10.

For example, considering the HDPE/PP foil, the SFE was reduced, from 52 mN/m after PL_C plasma treatment (Figure 27 b), to about 41 mN/m after rinsing. This value is still higher than the SFE of untreated blend foil (33 mN/m, Figure 27 b). The oxygen content decreased, from about 23.1 at% (Figure 27 a), to about 5.6 at% (O/C atomic ratio ca. 0.06). All tested surfaces show a similar trend. Moreover, in the literature, the analogous tendency was reported [206]. Presented results confirm that, despite the LMWOM generation, the persistent surface functionalization, is obtained.

Foil sample	O (at%)	SFE (mN/m)
PP + PL_C + rinsing	5.7 ± 1.2	38 ± 2
HDPE + PL_C + rinsing	7.4 ± 1.1	47 ± 2
HDPE/PP + PL_C + rinsing	5.6 ± 1.0	41 ± 3

Table 10: Surface composition (O at%, XPS) and surface free energy (contact angle) of the PL_C plasma treated and rinsed in water PP, HDPE, and HDPE/PP foils. Detailed plasma treatment parameters given in Table 3.

Summary of the polyolefin foils' treatment with DBD in air. Plasma treatment with DBD in the air led to i) successful generation of oxygen functional groups, and ii) higher surface free energy for all tested polymer foils. The presence of hydroperoxide groups, on the plasma-treated surfaces, was demonstrated. This confirms that the proposed grafting mechanism (Figure 10) is feasible. The surface morphology analyses of the DBD-treated blend foil showed the generation of low-molecular-weight oxidized material (LMWOM) after exposure to plasma (Figures 28 a–c). Nevertheless, the durability of DBD modification was confirmed (Table 10).

4.2.2 Sulfobetaine methacrylate (SBMA) coating

4.2.2.1 Surface chemistry The preliminary coating experiments were performed on the PP, HDPE, and HDPE/PP foils. The following parameters were studied: three plasma treatment conditions (PL_A , PL_B , PL_C), two coating temperatures (40°C and 70°C) and three coating durations (30 sec, 15 min, 1 h) [240]. The surface free energy and composition were analyzed for each performed modification, in order to select the most favorable coating parameters. Based on obtained results and literature reports [93, 59, 240, 98], the following parameters for dip coating were selected: PL_C plasma treatment, dip coating time 1 h, and temperature 70°C. Two SBMA molar concentrations were studied: 0.1 mol and 0.5 mol.

The presence of SBMA coating on the surface was verified, analyzing the sulfur atomic concentration (SBMA monomer structure presented in Figure 10) and surface free energy. Sulfur is an only chemical element that could not be incorporated by the preceding plasma treatment (traces of nitrogen were detected on the samples exposed to DBD). Therefore, it was considered as a coating indicator. The surface free energies of coated foils were confronted with the values for untreated materials, as well as with the determined for PL_C plasma treated and rinsed surfaces (PL_C + rinsing, Table 10). The aim was to avoid the dissolution of LMWOM in the test liquid [205]. Obtained composition (sulfur content in at%, XPS) and SFE of the SBMA coated foils, are depicted in Figures 30 a and b.

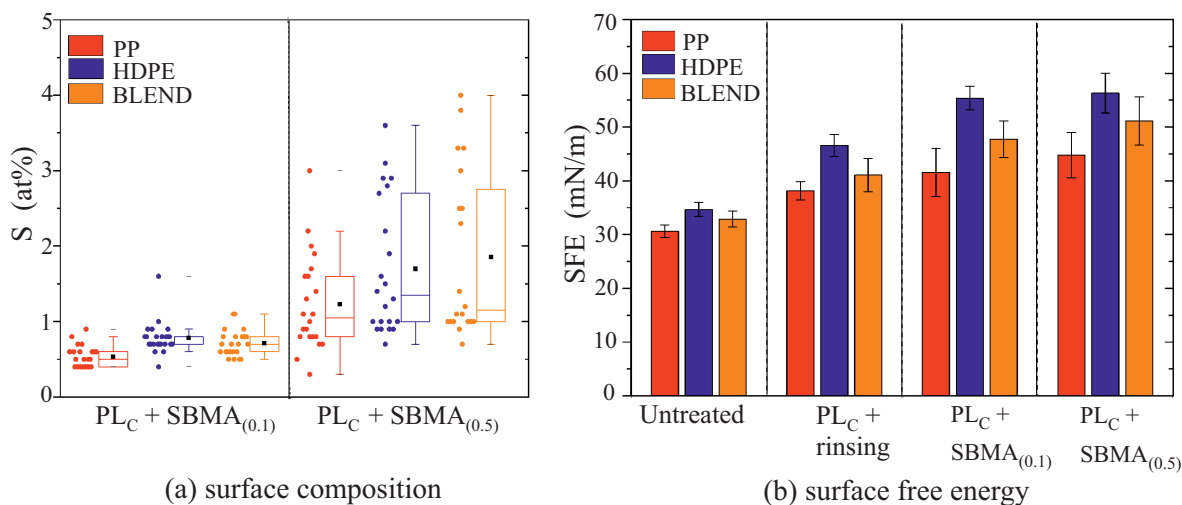


Figure 30: Characterization of the HDPE, PP, and HDPE/PP foils treated in PL_C plasma (detailed parameters given in Table 3) and coated with 0.1 mol and 0.5 mol SBMA (SBMA_(0.1) and SBMA_(0.5), respectively): a–surface composition (S in at%, XPS); b–surface free energy (SFE, contact angle).

Sulfur was detected on all SBMA-coated polyolefins (Figure 30 a). Higher monomer concentration used for coating, resulted in a higher amount of sulfur on the surface. Moreover, significantly higher deviations in sulfur content were found, for the modifications performed with the 0.5 mol SBMA solution. A possible explanation is higher grafting density. With more monomers available, more grafting points can be utilized. Furthermore, probably longer chains are generated, when the coating is conducted in the 0.5 mol SBMA monomer solution. Taking into consideration only one monomer concentration (either 0.1 mol, or 0.5 mol), sulfur concentration detected on three studied foils was not significantly different. Analyzing the PL_C + SBMA_(0.5) modification, the PP foil showed 1.2 ± 0.6 at% S, HDPE 1.7 ± 0.9 at% S, while blend: 1.9 ± 1.1 at% S. Let us consider the chemical composition of SBMA monomer (structure depicted in Figure 10). It can be calculated that the stoichiometric amount of sulfur reaches 5.3 at%, if a surface is fully covered by zwitterionic molecules, and the coating thickness is greater than the XPS information depth (up to 10 nm [29]). Therefore, it is concluded that the generated SBMA coatings show a certain inhomogeneity. This aspect was investigated using surface morphology analyses and presented in the following section (4.2.2.2).

The surface free energy (SFE) analyses of SBMA modified materials indicated the same trend for all studied foils (Figure 30 b). The SBMA coated surfaces had higher SFE, comparing with the untreated materials, as well as exposed to PL_C plasma and rinsed samples. There is also a tendentious increase in SFE with increased SBMA monomer concentration. For instance, considering the HDPE/PP blend, the PL_C plasma-treated surface deprived of LMWOM layer (PL_C + rinsed) had the SFE of about 41 mN/m. The coating with 0.1 mol SBMA monomer solution led to increased SFE value to about 47 mN/m, while the samples modified with 0.5 mol monomer solution had the SFE value of ca. 51 mN/m. Only a tendentious difference in the determined for the modified foil's surface free energies can be possibly attributed to the coating inhomogeneity .

ATR-FTIR with higher information depth was applied as a complementary method to detect SBMA coatings. Two PL_C + SBMA_(0.5) modified blend foils with different sulfur concentrations according to XPS analysis, S=3.8 at% and S=1.1 at%, were studied. The absorption bands, characteristic for SBMA, were found while analyzing the sample with higher sulfur content ($-C=O$: 1730 cm⁻¹, $-SO_3$: 1176 cm⁻¹ and 1035 cm⁻¹ [45]). However, the SBMA coating was not identified by ATR-FTIR on the sample with S=1.1 at%.

According to the proposed coating mechanism (Figure 10), the SBMA graft polymerization should occur onto the polyolefin surface. The following procedure was conducted to verify, if SBMA has built polymer chains on the modified blend foil:

1. Generation of polySBMA gel in the coating solution.
2. Analysis of the prepared polySBMA gel by gel permeation chromatography (GPC) and ATR-FTIR (detailed description of gel's preparation and characterization in section 3.4).
3. Characterization of the SBMA monomer, generated polySBMA gel, and SBMA coated blend foil by ToF-SIMS.

The procedure, carried out to obtain the polySBMA gel, was aimed to prepare a polymer under actual coating conditions. This polymer could be used as a standard for the ToF-SIMS investigations. According to the GPC analysis, the number-average molecular weight (M_n) of generated polySBMA gel was 138,223 g/mol, while the weight-average molecular weight (M_w) was 279,673 g/mol. Therefore, the polydispersity index ($PDI=M_w/M_n$) was 2.02, which is typical for the polymers synthesized by non-living radical polymerization [24].

ATR-FTIR was applied as a complementary method to characterize the polySBMA gel. In this case, to synthesize polySBMA, a conventional free radical polymerization with AIBN initiator, was performed. Next, the IR spectrum of polySBMA was compared with the spectra of polySBMA gel, and SBMA monomer. Figure 31 summarizes obtained results. The presented spectrum of polySBMA synthesized with AIBN initiator, agrees well with literature reports [186].

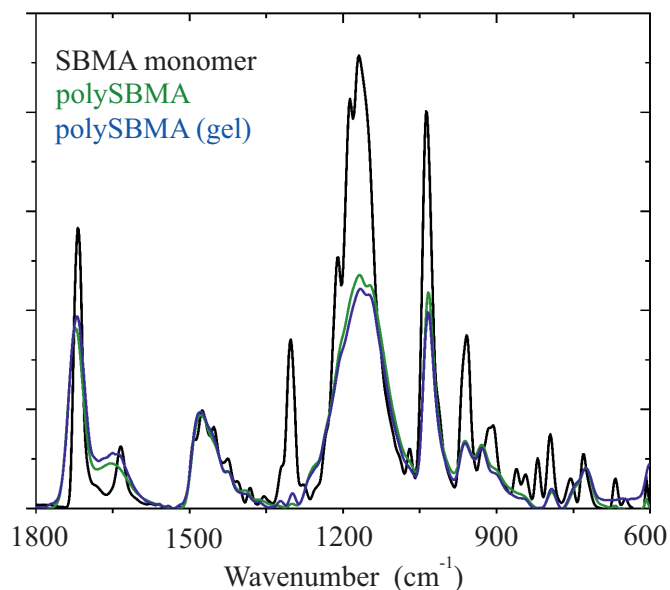


Figure 31: ATR-FTIR spectra of SBMA (sulfobetaine methacrylate) monomer (black), polySBMA synthesized via free radical polymerization (green), and polySBMA gel prepared in the monomer solution (blue).

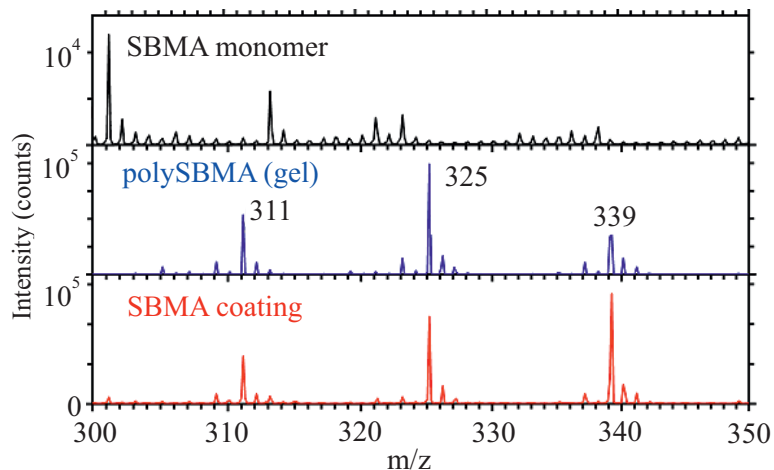


Figure 32: Negative ToF-SIMS spectra of the SBMA monomer (above), prepared polySBMA gel (middle), and SBMA coating (PL_C + SBMA_(0.5), XPS: S=1.4 at%) on the blend foil (below). Spectra were normalized by total intensity, mass range (m/z) 300–350 atomic units.

There is a strong analogy in the spectra obtained for the generated polySBMA gel and the synthesized with AIBN polySBMA. Furthermore, the disappearance of the peak at 819 cm⁻¹ (characteristic for monomer), was observed for both polymers. This absorption band is associated with the C=C bond, which opens during polymerization [52]. Additionally, the peak at 1302 cm⁻¹ could not be assigned for the polySBMA and occurred only with low intensity for the

polySBMA gel. This peak is attributed to the $=\text{CH}_2$ wagging vibration [172], while its vanishing confirms the successful polymerization.

After the characterization of generated polySBMA gel (GPC and ATR-FTIR analyses), ToF-SIMS was performed on the SBMA monomer, polySBMA gel, and SBMA modified blend foil ($\text{PL}_C + \text{SBMA}_{(0.5)}$). The analysis aimed verification, whether the coating has similar characteristics to the gel or the monomer. ToF-SIMS spectra, obtained for the negative polarity secondary ions (mass range 300–350 au), are depicted in Figure 32. Some peaks characteristic for the polySBMA gel, are labeled in the corresponding ToF-SIMS spectrum (311, 325, and 339 au). The SBMA coating shows a similar fingerprint to the polySBMA gel in ToF-SIMS. It is indirect evidence that SBMA indeed exists as a polymer on the modified surface.

Morphology of the HDPE/PP blend foil modified with SBMA, was examined, to better understand the SBMA distribution on the coated surfaces.

4.2.2.2 Surface morphology and topography ToF-SIMS imaging was used to illustrate the coating distribution on a larger area of the blend. The allocation of SO_3^- ions, which are characteristic for SBMA coating, was investigated on the $\text{PL}_C + \text{SBMA}_{(0.5)}$ modified blend foil (sulfur concentration of 1.3 at%, XPS). Images obtained at 3 different positions (a, b and c) are presented in Figures 33 a–c.

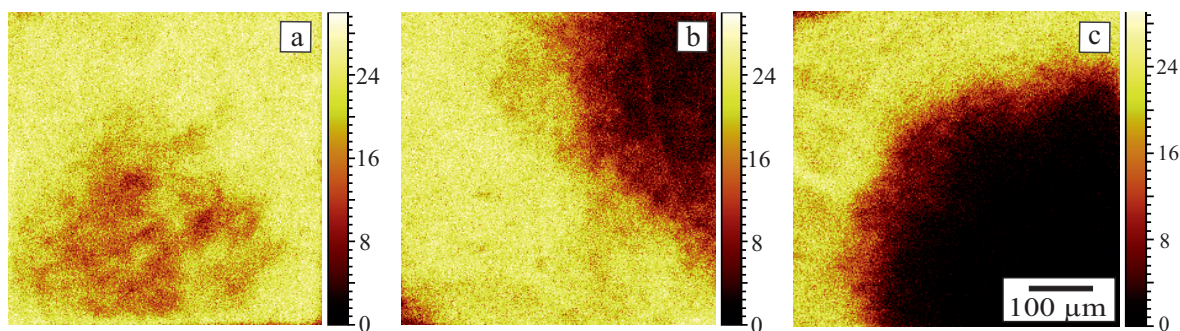


Figure 33: Distribution of SO_3^- ion on the 0.5 mol SBMA coated HDPE/PP foil ($\text{PL}_C + \text{SBMA}_{(0.5)}$, XPS: S=1.3 at%) at three different positions (a, b, c) (negative polarity ToF-SIMS surface imaging, normalized by total intensity). Color scale from black, to red to yellow depending on the SO_3^- ion content.

Inhomogenous signal distribution is clearly seen, which confirms the SBMA coating heterogeneity. The variation in coating thickness (Figure 33 a), as well as an occurrence of pinholes (Figures 33 b and c), were revealed. The overall signal was homogeneously distributed at investigated positions (images not shown). This indicates that the allocation of SBMA characteristic ions does not result from topographic effects.

Alternatively to ToF-SIMS imaging, atomic force microscopy (AFM) was applied to determine the SBMA coating distribution and morphology. The SBMA modified blend foils with various

sulfur concentrations (XPS) were analyzed. Acquired phase images are presented in Figures 34 a and b.

It was observed that the surface morphology of SBMA coated foils is associated with the surface composition determined by XPS. Considering the surface possessing 1.7 at% sulfur (Figure 34 a), amorphous islands (examples highlighted with arrows) can be distinguished. The surface with higher sulfur concentration appeared to be completely covered by the amorphous layer (Figure 34 b).

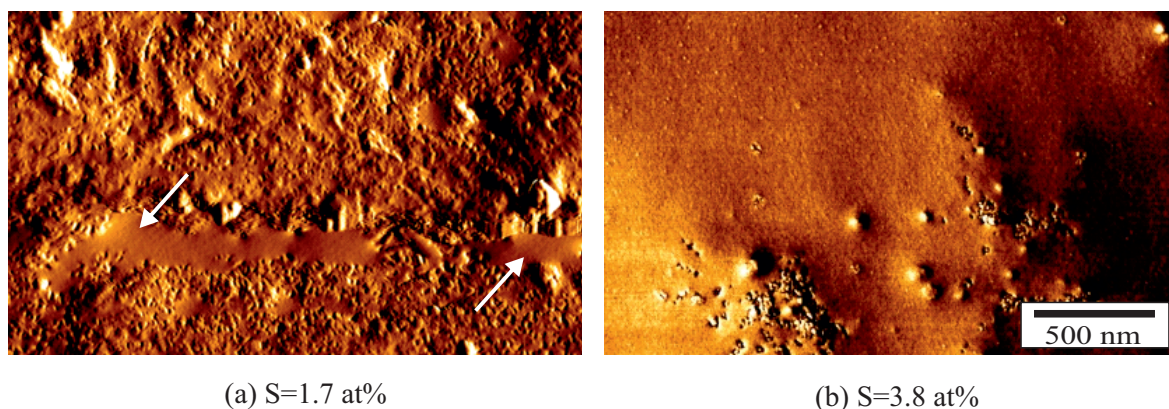


Figure 34: AFM phase imaging of the SBMA coated HDPE/PP foils ($PL_C + SBMA_{(0.5)}$) with different sulfur content (XPS): a–SBMA modified surface with S=1.7 at% (amorphous islands highlighted), b–SBMA modified surface with S=3.8 at%. SBMA–sulfobetaine methacrylate.

To verify, whether the amorphous layer revealed by AFM is indeed attributed to the SBMA coating, surface with the lower sulfur concentration (Figure 34 a) was subjected to the AFM-IR analysis. Figures 35 a and b present the height and deflection images, respectively obtained on the SBMA coated sample with S=1.7 at% (XPS). The coated surface shows heterogeneous topography. An elongated and smooth region with a thickness of about 2 μm , is identified (highlighted with arrows in Figure 35 b). Despite its higher thickness, this area appears analogous to the amorphous island depicted by AFM phase imaging (Figure 34 a).

Figure 35 c depicts IR spectra recorded from regions marked in AFM images (squares in Figures 35 a and b). Considering the smooth sample area (squares red and blue), three additional peaks were identified (1724 cm^{-1} , 1164 cm^{-1} and 1035 cm^{-1}). These peaks did not appear in the spectra recorded from the areas marked as black and violet. They were also not assigned for HDPE or PP. These signals were attributed to the SBMA coating (1724 cm^{-1} : $-\text{C}=\text{O}$ group, 1164 and 1035 cm^{-1} : $-\text{SO}_3$ [45]). They were also found on the sample with higher sulfur concentration (S=3.8 at%), which was subjected to the conventional ATR-FTIR analysis (see chapter 4.2.2.1). This result confirms the assumption that the amorphous area (as highlighted in Figure 34 a) signifies the SBMA coating.

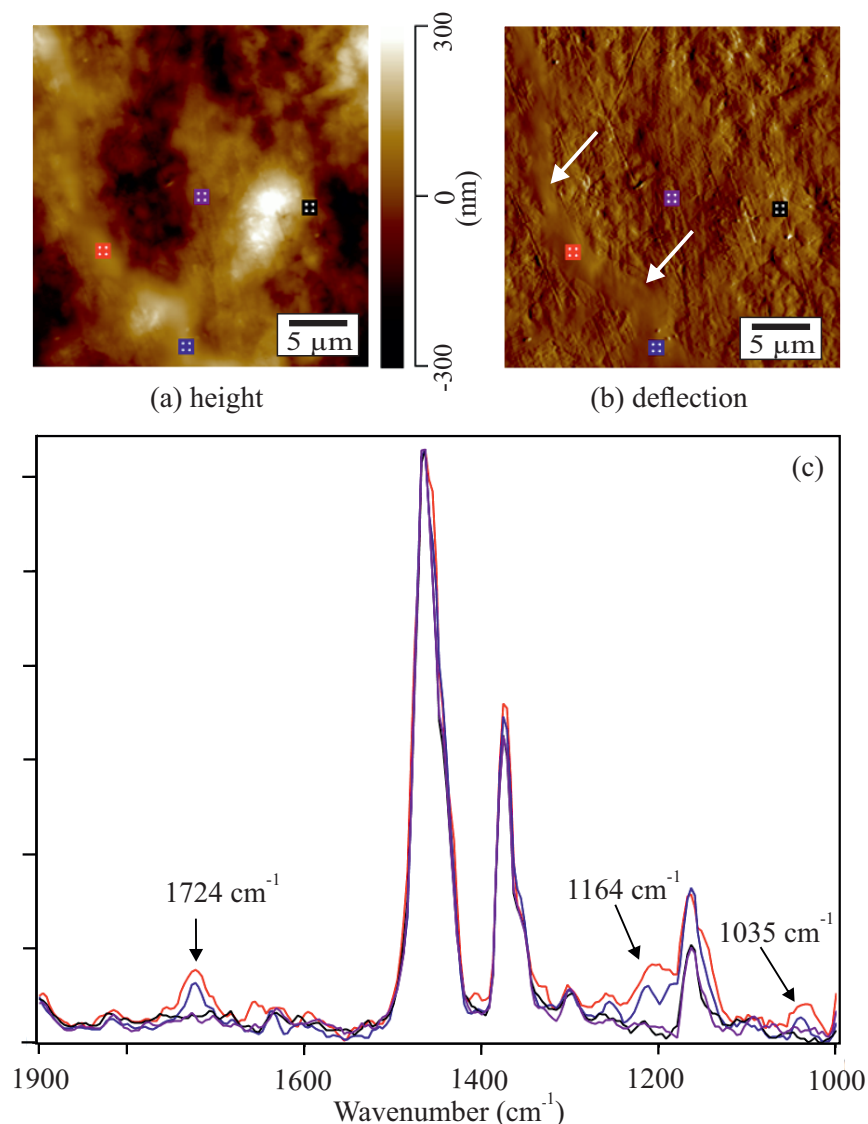


Figure 35: AFM-IR analysis of the SBMA coated HDPE/PP foil ($PL_C + SBMA$) with $S=1.7\text{at}\%$ (XPS): a–AFM height image (height range about 600 nm), b–AFM deflection image (color spots indicate the location of IR spectra, while arrows smooth material region), c–IR spectra recorded from regions marked in AFM images (normalized to 1464cm^{-1}).

4.2.2.3 Coating stability To assess the durability of created SBMA coatings, different washing procedures were performed on the SBMA modified blend foils. The SBMA coated blends were firstly incubated in $\text{NaCl}_{(\text{aq})}$ solution to remove possibly adhered homopolymers. The presence of salt enables side-chain expansion and dissolution of physical zwitterionic hydrogels [239, 142]. This effect could help to extract non-covalently attached SBMA chains. The surface composition was periodically monitored, to justify the possible deterioration of the coating quality. Testing was completed, as soon as the first change in composition was observed.

Furthermore, the oxidation stability at low and high pH was tested. The coated samples were incubated in sodium hydroxide (NaOH) and sulfuric acid (H₂SO₄) solutions, chemicals periodically applied to soak RO membrane modules [131]. Table 11 summarizes obtained results (sulfur concentration, normalized to the value directly after coating) depending on performed washing.

Washing solution/duration	S concentration (norm.,%)
0.1 mol NaCl _(aq) /4 weeks	64±4
NaOH (pH=11)/24 h	13±3
H ₂ SO ₄ (pH=1)/24 h	22±3

Table 11: Sulfur concentration on the SBMA modified blend foil (PL_C + SBMA_(0.5)) after exposure to different washing solutions. Values were normalized to the sulfur concentration directly after coating (XPS analysis).

The SBMA coated surface incubated in NaCl solution showed the first reduction in sulfur concentration after 4 weeks of testing. On the one hand, it can be deduced that about 35% of the initially presented coating originates from strongly adhered SBMA chains. These chains can be washed. At least two adhesion scenarios can be proposed: a) between grafted chains and homopolymers from the solution, or b) homopolymers adhere to the plasma-activated surface. On the other hand, the variation in sulfur concentration over the analyzed sample has to be considered. Performed at regular intervals XPS analyses, represent always a slightly different area of modified material. Considering the heterogenous SBMA distribution on the foils (see section 4.2.2.2), the lower sulfur concentration in some areas is also probable.

The SBMA coatings were more severely affected by performed high and low pH washings. After 24 h exposure to the alkaline solution, sulfur concentration reduced to about 10% of its initial value. Incubation in the H₂SO₄ solution was associated with a reduction of sulfur concentration by approximately 80%. However, in this case, traces of sulfur were detected also on control samples. This indicates that less than 20% of the SBMA coating could withstand this harsh acidic conditions. The hydrolytic degradation of various zwitterionic polymers over a wide pH range was studied. Under strong acidic conditions (pH=0), hydrolysis of the SBMA ester group predominately occurs. The alkaline conditions (pH=14) lead to the accelerated hydrolysis of the ester bonds and Hoffman elimination with the production of vinyl esters [190].

The soaking procedure recommended by the RO manufacturer is usually performed in the pH range from 4 to 10, for a maximum of 8 hours [51]. Therefore, applied pH treatment conditions were much more severe than in a real RO plant operation. Greater durability of the coating can be expected under milder washing conditions. Moreover, chemicals such as NaOH or H₂SO₄ are introduced to the filtration system when there is a high probability of inorganic fouling (scaling) [131]. Therefore, under proper plant operation, the risk of scaling should be significantly reduced, and thus the chemical treatment not required.

Summary of the sulfobetaine methacrylate coating. The SBMA was successfully coated on all polyolefin foils and occurs as a polymer on the surface (Figure 32). The obtained amorphous coatings showed certain heterogeneity (Figures 33 a–c and Figures 34 a and b).

4.2.3 Discussion

Pinhole-free thin coatings can be successfully generated by low-pressure plasma deposition techniques. The major efforts in the plasma-assisted coating technology are currently made to establish deposition processes at atmospheric pressure [26]. In this section, several aspects and limitations of the modification technology proposed will be discussed.

The first modification step was the atmospheric pressure plasma treatment with dielectric barrier discharge (DBD) in air. DBD is characterized by the filamentary operation mode, where plenty of individual discharge filaments are distributed in a gap between two electrodes [101]. This means that the sample is treated punctually with high energy plasma species. The degradative oxidation in plasma dominates over selective non-degradative oxidation. The outermost layer degradation results in generation of the low-molecular-weight oxidized material (LMWOM) [75], which was also confirmed in this work (see Figures 28). The LMWOMs can be formed due to: a) fragmentation, oxidation and re-arrangement of macromolecules, and b) re-deposition of volatile oxidation products on the polyolefin surface. When considering the re-deposited layers on the plasma-treated surfaces, it is also likely that the compounds from ambient air contribute to the LMWOM formation.

The generation of the following oxygen functional groups requires the scission of the polymer backbone: ester, carboxylic acid, aldehyde, primary alcohol, peroxy acid [75]. Therefore, the occurrence of these functionalities within the LMWOM layer is highly probable. The existence of LMWOM can, on the one hand, hinder the adhesion of the coating to the oxidized polyolefin surface. It occurs when the low molecular weight products cannot be distributed or dissolved in the deposited layer. In this case, they became a weak boundary layer at the surface-coating interface. This type of behavior was observed when studied the adhesion of isoprene-styrene block-copolymer to the DBD-treated PP [206]. On the other hand however, if the LMWOM can be distributed in the coating solution, the polymer surface became "free" to interact with monomers. The occurrence of LMWOM can be even beneficial for adhesion. The LMWOM can act as a „coupling agent” between the adhering molecules and the surface. This adhesion-promotion phenomenon was shown for the polyamide ink deposited on the plasma-treated PP [206]. Moreover, it is also likely that the LMWOM layer contains some unsaturated hydrocarbons, which can initiate additional reactions, e.g., cross-linking of the coating. Figures 36 a and b schematically demonstrate the role of LMWOM in adhesion of different coatings to the plasma-treated polyolefin surface. Considering the SBMA coating, the second scenario is more feasible (Figure 36 b). It was demonstrated that the LMWOMs generated on the plasma-treated polyolefins are water-soluble (see Table 10). Therefore, they can dissolve in the SBMA coating solution, since dip coating is performed subsequently after plasma treatment.

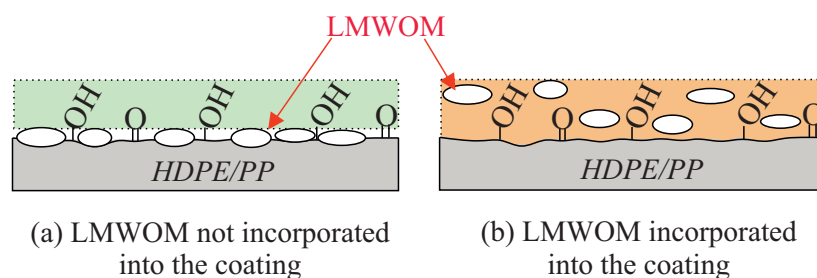


Figure 36: Adhesion between coating and DBD treated HDPE/PP foil in the presence of the LMWOM (schematics): a–LMWOM creates a weak boundary layer (adhesion hindered), b–LMWOM is incorporated into coating structure (good adhesion). LMWOM–low-molecular-weight oxidized material.

The oxidation of polyolefin surface with DBD treatment in air is schematically depicted in Figure 37. The LMWOM formation and its further fragmentation to the volatile products are included. The surface while treatment means the topmost material layer containing the LMWOM (during treatment, or directly after exposure to plasma). The surface without LMWOM (marked in gray) is attributed to the material deprived of the soluble degradation products, for instance, by performed rinsing in water. Both types of surfaces are illustrated in Figure 29 b. The presented scheme also includes the oxidation level of the particular areas according to the XPS analysis. The O/C ratio for the isolated LMWOM is about 50% [75]. The surface covered with the LMWOM shows about 30% O/C (Figure 27 a), while after rinsing the O/C ratio is reduced to about 6% (O=5.6 at% for the blend foil, see Table 10).

An assessment of surface functionalization with DBD by XPS is not easy. The information depth of XPS into polymer materials is about 10 nm [29]. For this reason, determined O/C ratio or O at% concentration is always attributed to the certain material volume. Therefore, the amount of oxygen functional groups at the surface (surface understood as a topmost layer without the LMWOM), which are „available” for the grafting reactions, is not known. The ion sputtering and XPS analysis could be used to investigate the O/C gradient within the material depth. However, the sputtering techniques generate a few artifacts and cause displacement of atoms and groups [202], which impede to draw unambiguous conclusions about surface functionalization.

Free radical graft polymerization onto polyolefin surfaces was proposed, for the generation of SBMA coatings. Such radical polymerization, initiated by the decay of hydroperoxides into alkoxy and hydroxy radicals, has several advantages. The process can be carried out under atmospheric pressure, there is a certain freedom in determining reaction parameters and high tolerance to impurities, beneficial for the industrial processes. Such radical polymerization, initiated by the decay of hydroperoxides into alkoxy and hydroxy radicals, has several advantages. [145]. For this reason, coatings prepared by conventional free radical polymerization have different structures and distributions over the entire modified specimen, as was shown in this work (see Figures 33 and Figures 34 a and b).

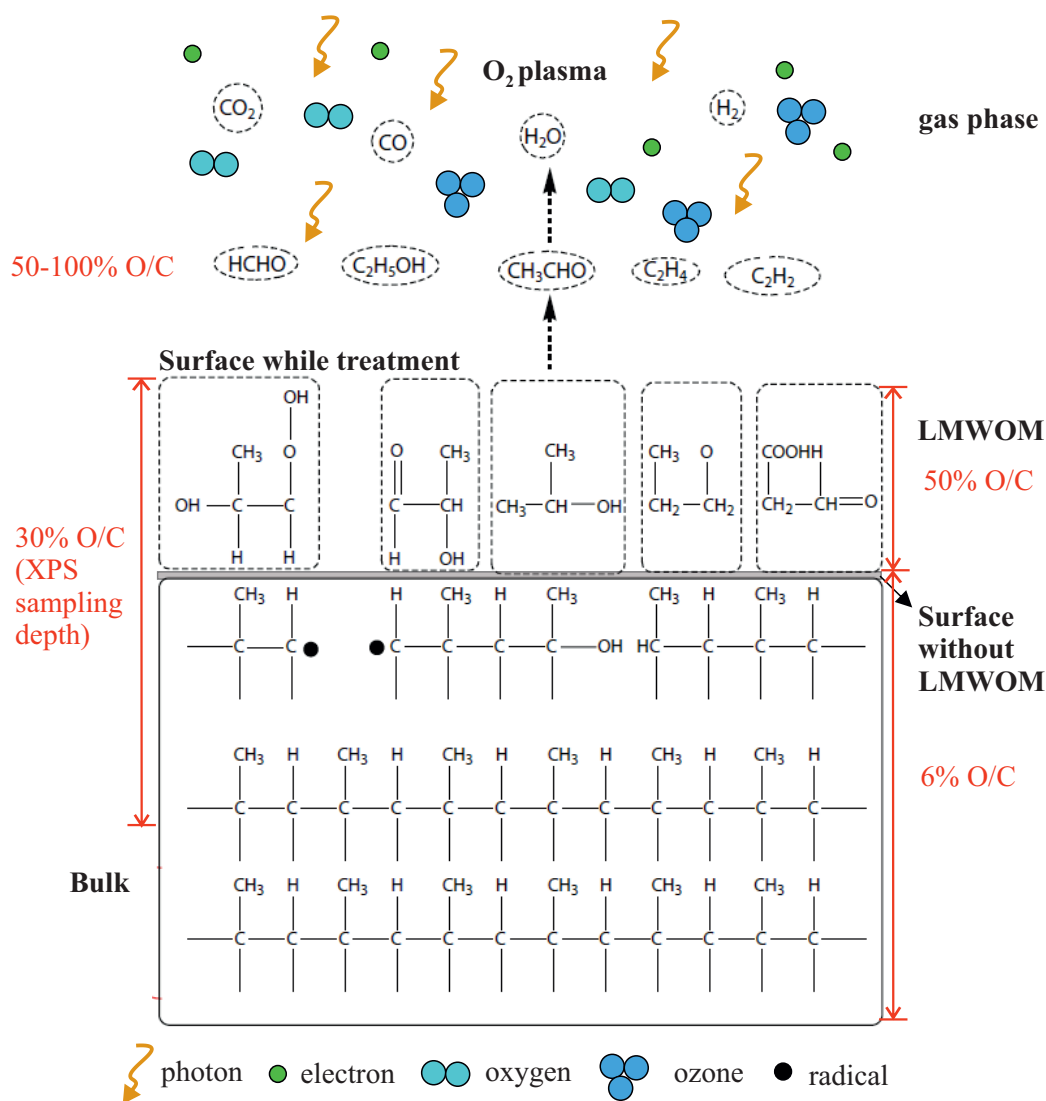


Figure 37: Scheme of the oxidation of polyolefin on exposure to DBD in air. The elemental compositions (O/C in %, XPS) of the particular areas of the foil/near the foil surface, are included. LMWOM—low-molecular-weight oxidized material.

The hydroperoxide groups, able to initiate the grafting reactions, were detected at all plasma-treated polyolefin foils (see section 4.2.1.1). Moreover, it was confirmed that SBMA occurs as a polymer on the modified surfaces (see Figure 32). Therefore, on the one hand, the SBMA polymerization took place, and thus decomposition of hydroperoxides as an initiation mechanism is feasible. However, on the other hand, the presence of polySBMA on the surface does not directly mean its covalent attachment. In the proposed modification process, the competitiveness of favorable graft polymerization and homopolymerization in the solution has to be considered. Decomposing surface hydroperoxide group ($-ROOH$) generates two radicals: $-RO\bullet$ and $\bullet OH$. The surface radical ($-RO\bullet$) initiates grafting, while the $\bullet OH$ radical is involved in, among others, homopolymerization and termination reactions. The extend of homopolymerization in the solution diminishes the number of available monomers, increases the medium viscosity, and thus

slower the diffusion of the monomer to the surface[188]. In this work, the monomer concentration was kept relatively low, to minimize the homopolymerization in the solution, as proposed elsewhere [123]. However, when the SBMA monomer solution was used several times for the coating, visible polySBMA gel was built. This indicates the homopolymerization reaction in the solution. Therefore, it is likely that besides grafting onto the surface, there is a strong adhesion of polySBMA chains to the surface. The partial removal of the coating from the surface was observed after four weeks of immersion in salt water (see Table 11). This confirms the presence of some adhered homopolymers within the coating structure.

The homopolymerization in solution means reducing the quality of the generated SBMA layers when frequently using the same coating mixture. Considering an industrial coating process, the constant monitoring of the solution and coating parameters would be required to ensure sufficient quality. To suppress the formation of homopolymers, an addition of ferrous ammonium sulfate to the coating solution can be proposed [23].

4.3 Modification of the HDPE/PP feed spacer

4.3.1 Surface chemistry

The modification of the feed spacer surface was performed analogously to the polyolefin foils. Based on the preliminary studies (section 4.2.2, [240]), the highest intensity plasma treatment was applied (PL_C), while 0.5 mol SBMA solution was used for the coating preparation.

The surface composition of the HDPE/PP spacer surfaces after performed plasma treatment, as well as after SBMA coating, is presented in Table 12. Example XPS spectra of the untreated, high-intensity plasma-treated (PL_C), and coated feed spacer (0.5 mol SBMA), are shown in Figure 38. The oxygen concentration at the feed spacer surface was significantly enhanced after exposure to DBD in air. The feed spacer surfaces treated with the highest intensity plasma (PL_C) showed about 0.18 O/C atomic ratio (15.0 ± 1.6 O at%). Considering the analogously treated HDPE/PP foil, a greater amount of oxygen at the flat substrate was reported (HDPE/PP foil + $PL_C = 23.1 \pm 2.6$ O at%, see Figure 27 a). This might be related, on the one hand, to the geometry of the feed spacer specimen. The bend strand structure can impede the homogeneous treatment with filamentary DBD discharge. Moreover, high surface irregularity is challenging for the XPS analysis, since the emitted electron yield depends on the surface roughness magnitude [19]. On the other hand, the presence of some extrusion additives or impurities on the spacer surface (see Figure 25 b) could hinder the proper material functionalization in plasma. Furthermore, different crystallinity degrees of the foil and feed spacer surfaces should be considered, as a possible reason for distinct susceptibility towards the plasma treatment [74].

The sulfur concentration detected after SBMA coating agrees well with that obtained for the HDPE/PP foil (see Figure 30 a). Besides characteristic SBMA peaks (C 1s, O 1s, N 1s, S 2p), Si was identified on each analyzed spacer specimen, even up to 5 at%. Silicon content can be

possibly attributed to the manufacturing contaminants (see Figure 25 b).

Spacer sample	O (at%)	S (at%)
Untreated spacer	7.5±2.1	x
Spacer + PL _C	15.0±1.6	x
Spacer + PL _C + SBMA _(0.5)	17.0±1.4	2.1±0.9

Table 12: Surface elemental composition (O and S in at%, XPS) of the untreated, plasma treated (PL_C plasma) and SBMA coated (PL_C + SBMA_(0.5)) spacers (plasma parameter description in Table 3).

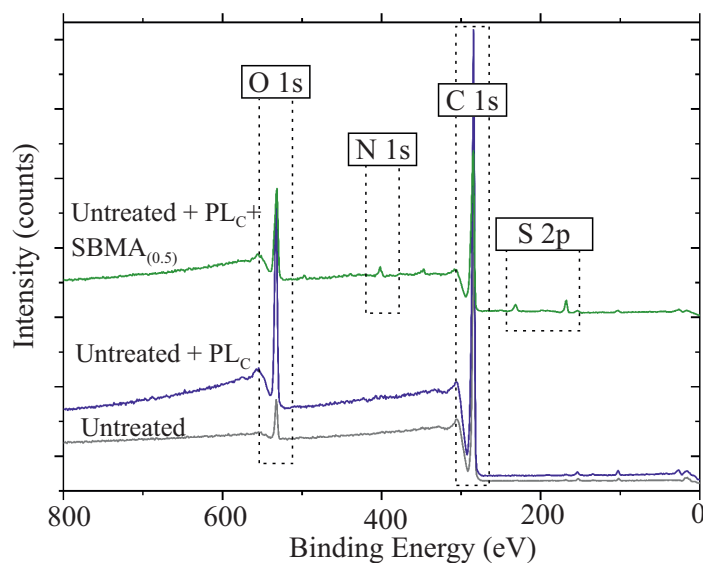


Figure 38: XPS survey spectra of the untreated, high intensity plasma treated (PL_C) and SBMA coated (untreated + PL_C + SBMA_(0.5)) spacers (characteristic peaks highlighted). SBMA–sulfobetaine methacrylate.

The specimen with S=3.5 at% was subjected to ATR-FTIR analysis. The same characteristic SBMA absorption bands, as assigned for the SBMA modified foil (Figure 35 c), were identified ($-\text{C}=\text{O}$: 1730 cm^{-1} , $-\text{SO}_3$: 1176 cm^{-1} and 1035 cm^{-1} [45]).

4.3.2 Surface morphology and topography

The feed spacer morphology was monitored at each modification step by AFM. Obtained phase images after PL_C plasma treatment and SBMA coating (PL_C + SBMA_(0.5)) are presented in Figures 39. The untreated material analyzed by AFM is depicted in Figure 25 b.

The morphology of HDPE/PP feed spacer exposed to the PL_C plasma treatment (Figure 39 a) differs significantly from the blend foil surface modified with PL_C plasma (see Figure 28 c). On the one hand, after exposure to DBD in air, the characteristic HDPE and PP crystalline structures presented on the untreated spacer (see Figure 25 b), could not be any longer revealed. On

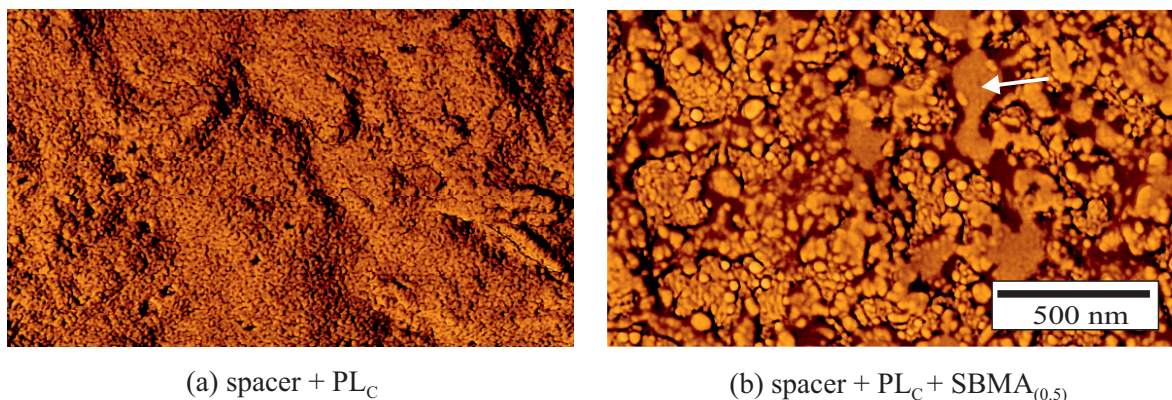


Figure 39: AFM phase imaging of the HDPE/PP feed spacers: a-PL_C plasma treated, b-PL_C plasma treated and 0.5 mol SBMA coated (PL_C + SBMA_(0.5), S=1.7 at%). Example of amorphous island on the coated material marked with arrow.

the other hand, the characteristic amorphous LMWOM layer, observed on the PL_C plasma-treated blend foil (see Figure 28 c), was not found. Rinsing in water, as carried out for the foil surfaces to wash the LMWOM (see Figures 29), did not cause any change in the surface appearance. It is probable that depicted by AFM area represents PP with small nodular crystals. Similar micrographs were presented in the studies on the melt crystallization of semicrystalline isotactic polypropylene [250, 249]. The treated surface could get into closer contact with the plasma generating electrodes, which caused melting due to thermal effect or VUV radiation and re-crystallization on rapid cooling in air [171].

Considering the AFM phase image after plasma treatment and subsequent coating (Figure 39 b), heterogeneous material morphology was observed. Two types of structures were distinguished: amorphous islands (example marked) and granular features. Analyses performed on the SBMA modified films incline towards assigning the coating as an amorphous matter (see Figures 34). Therefore, it was concluded that the area highlighted in Figure 39 b represents the SBMA coating. Granular forms are most probably attributed to the HDPE lamellae damaged by plasma UV. Similar images were assigned as scissions inside lamellae of ultra-high molecular weight PE (Figure 2.58 in [149]). However, these „knobby” like structures can also represent larger nodular PP crystals. Analogous features were shown by Zia et al. [250, 249], O’Hare et al., and Strobel et al., who analyzed the discharge-treated PP [160, 204].

ToF-SIMS imaging was used to illustrate the coating distribution. The SO₃⁻ ion allocation was analyzed, as previously performed for the modified blend foils (see Figures 33). Images obtained at three different positions (a, b, c) for the PL_C + SBMA_(0.5) modified feed spacer are presented in Figures 40 a–c (sample with S=1.7 at%, XPS). Characteristic for the coating signals could be detected at each analyzed position. The shape of islands with higher signal intensity (bright yellow color) corresponds well with the coating characteristic observed by AFM (Figure 39 b). However, the overall signal distributions at investigated positions were, to a certain extend, influenced by material topography.

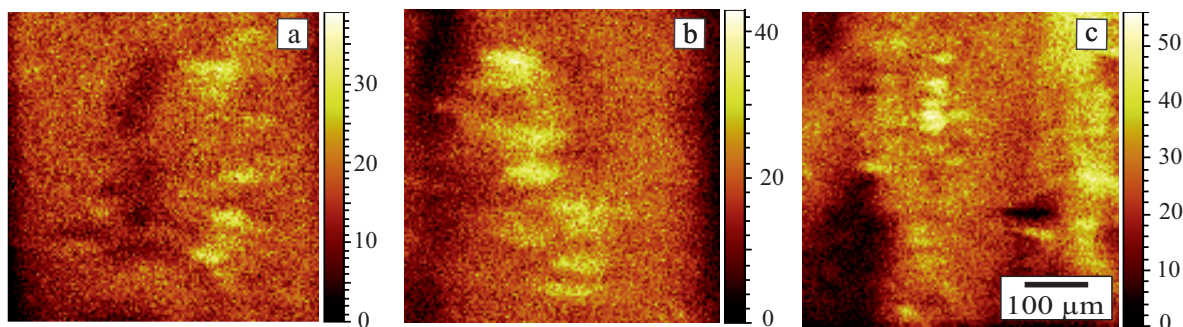


Figure 40: Distribution of SO_3^- ion on the 0.5 mol SBMA coated feed spacer ($\text{PL}_C + \text{SBMA}_{(0.5)}$, XPS: $\text{S}=1.7$ at%) at three different positions (a, b, c) (negative polarity ToF-SIMS surface imaging, normalized by total intensity). Color scale from black, to red, to yellow depending on the SO_3^- ion content.

The PL_C plasma treated and SBMA coated ($\text{PL}_C + \text{SBMA}_{(0.5)}$) feed spacers showed different morphology in comparison to the modified blend foils (see sections 4.2.1.2 and 4.2.2.2). Several reasons may have contributed to the observed effects. On the one hand, heterogeneous morphology of the feed spacer surface, and existing contamination/additives introduced already at the manufacturing stage (see Table 5 and Figure 39 b), have to be considered. On the other hand, the different appearance of crystalline structures on the foil and the spacer surfaces can contribute to various chemical processes on exposure to the plasma treatment. To better understand the occurred phenomena, feed spacer specimens were modified by annealing on the AFM stage (procedure given in section 3.3.2), subsequently, plasma-treated, and SBMA coated.

Surface morphology and topography of the annealed feed spacer. The feed spacer morphology after annealing is depicted in Figure 41 a. The annealing aimed to receive a smoother spacer surface with well revealed semicrystalline morphology. Both blend components can be identified. Thicker lamellae are attributed to the HDPE phase (some examples marked with arrows), while thin lamellae, situated especially in the middle part of the image, represent the PP material (analogous to Figure 2.31 and Figure 2.117 in [149]), respectively. Influence of the PL_C plasma treatment on the annealed feed spacer surface is depicted in Figure 41 b. Analogously to the blend foil (see Figure 28 c), after exposure to the DBD in air, the surface became covered by the amorphous LMWOM layer. These oxidation products could be dissolved in water. After performed rinsing, the pristine lamellae structures were again visible (see Figure 41 c). However, there was also evidence of material's etching.

The SBMA coating structure obtained on the annealed feed spacer is demonstrated in Figure 41 d. It is clearly seen that the SBMA layer is more evenly distributed over the surface, than it was observed for the untreated (reference) spacer (Figure 39 b). Depicted morphology agrees well with determined for the SBMA modified HDPE/PP foil (see Figures 34). Nevertheless, a discontinuous character of the SBMA coating is noticeable. The original material structure can be still identified in some areas of the sample (example marked with arrow in Figure 41 d). This indicates that the coating thickness does not exceed the surface profile depth.

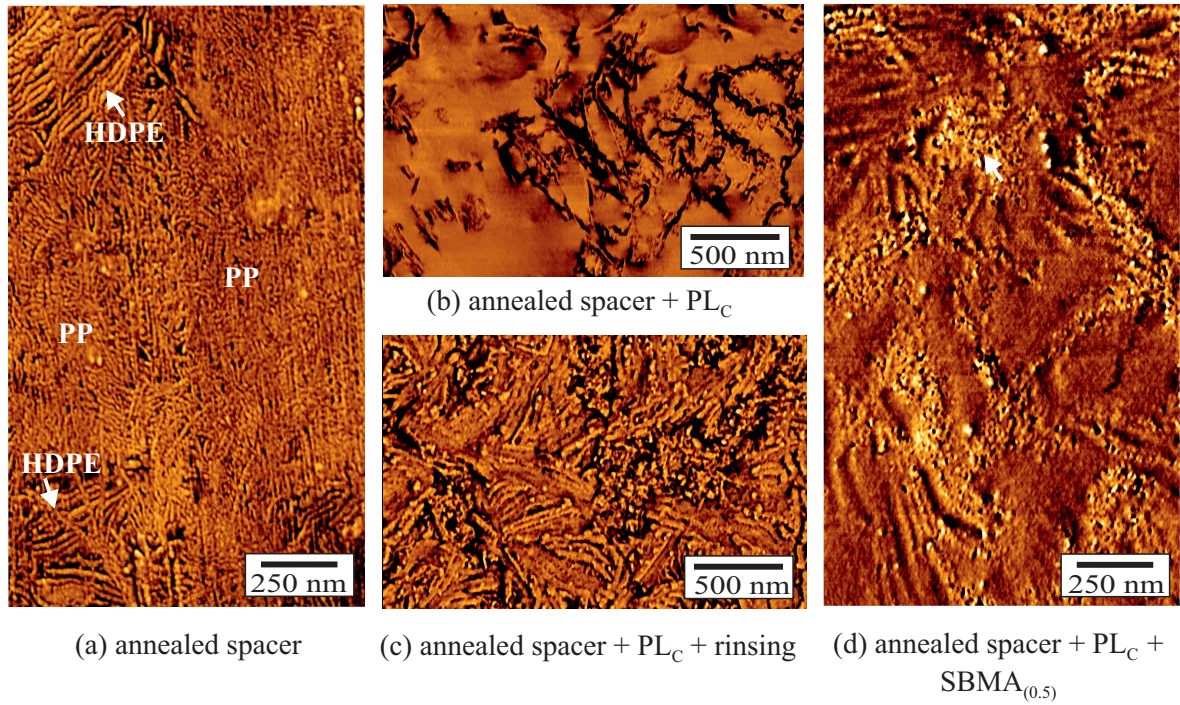


Figure 41: AFM phase imaging of the HDPE/PP feed spacers: a–annealed with marked thicker HDPE lamellae and PP regions, b–annealed and PL_C plasma treated, c–annealed, PL_C plasma treated and subsequently rinsed in water, d–PL_C plasma treated and 0.5 mol SBMA coated (PL_C + SBMA_(0.5)), visible original material structure marked with arrow.

Spacer sample	R _a (nm)	R _z (nm)
untreated spacer	5.1 ± 3.4	28.2 ± 18.8
annealed spacer	0.6 ± 0.1	3.3 ± 0.7
annealed spacer + PL _C	3.8 ± 1.2	17.7 ± 5.9
annealed spacer + PL _C + rinsing	4.2 ± 0.5	8.4 ± 1.1
annealed spacer + PL _C + SBMA _(0.5)	0.9 ± 0.2	5.6 ± 1.2

Table 13: Surface roughness (R_a, R_z, AFM height imaging) for the untreated; annealed; annealed and PL_C plasma treated; annealed, PL_C plasma treated and rinsed in water (PL_C + rinsing); as well as annealed, PL_C plasma treated and 0.5 mol SBMA coated (PL_C + SBMA_(0.5)) feed spacers.

To evaluate an effect of the plasma treatment and SBMA coating on the surface roughness, AFM height imaging was performed on the annealed and subsequently treated spacer specimens. Table 13 summarizes determined R_a and R_z values. As expected, the applied annealing procedure significantly reduced surface roughness. Therefore, the effect of plasma treatment on the surface topography can be better demonstrated. There is a significant increase in surface roughness after exposure to the PL_C plasma, which is attributed to the etching of amorphous material regions, and the presence of LMWOM on the surface [177, 160, 122]. The R_a value after rinsing the sample in water (annealed spacer + PL_C + rinsing) remained in a similar range to the plasma-treated containing the LMWOM (annealed spacer + PL_C). Nevertheless, the R_z was reduced, which indicates a tendentious decrease in the surface roughness.

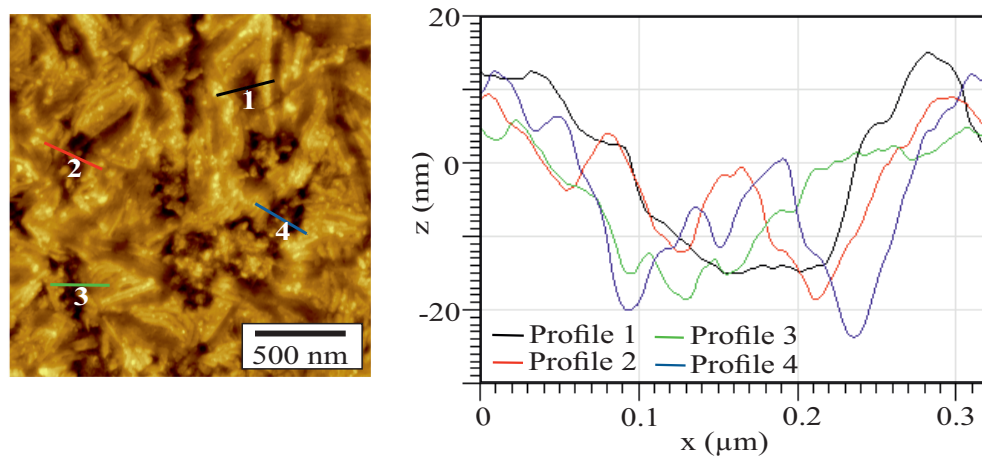
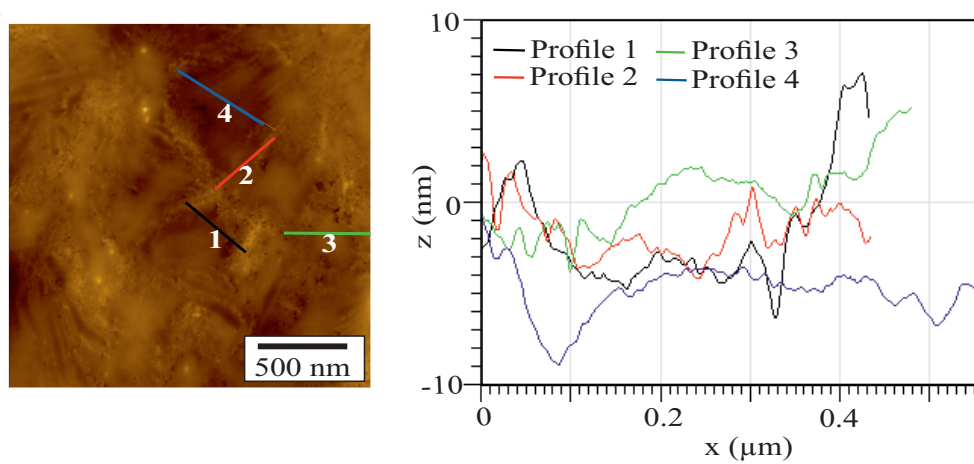
(a) annealed spacer + PL_C + rinsing(b) annealed spacer + PL_C + SBMA_(0.5)

Figure 42: AFM height imaging with extracted surface profiles: a–annealed spacer treated with PL_C plasma and rinsed in water, left: generated profiles across the surface valleys (1–4), right: representation of the extracted profiles (1–4) in the xz -plane, b– annealed spacer treated with PL_C plasma and 0.5 mol SBMA coated, left: generated profiles across the coated areas (1–4), right: representation of the extracted profiles (1–4) in the xz -plane.

The SBMA coating performed on the PL_C plasma-treated surface considerably reduced the roughness. Taking into account depicted coating morphology (Figure 41 d), it can be concluded that SBMA accumulates highly probable in the material cavities. This could explain lower surface roughness after coating and simultaneous identification of the original material structure between coating islands. This was used to estimate the SBMA coating thickness. For this purpose, different surface profiles were extracted and analyzed. Firstly, the PL_C plasma-treated surface after removal of the LMWOM (annealed spacer + PL_C+rinsing) was investigated. During coating, the LMWOM dissolves in the solution and SBMA "replaces" it on the surface. Therefore, material after plasma treatment and removal of the LMWOM is considered as the surface on which SBMA is deposited. Secondly, the PL_C plasma treated and subsequently coated sample was analyzed (annealed spacer + PL_C + SBMA_(0.5)). The results are summarized in Figures 42. For the sample

after PL_C plasma and rinsing (Figure 42 a), the profiles were extracted across the deepest valleys, while for the SBMA coated (Figure 42 b), across the coating islands. Let us discuss the profiles presented in Figure 42 a. If assuming that the coating is situated in the material cavities in such a way to allow detecting of the highest peaks, the thickness of the SBMA layer should not exceed 30 nm (see Profile 4). Analyzing the profiles extracted across the coating islands (Figure 42 b), it is deduced that the coating is situated in the material valleys (about 6 nm in-depth) and does not generate mounds above the surface pattern. Therefore, it is not expected that the thickness of SBMA coating exceeds 25–30 nm, which is estimated maximum surface profile depth for the PL_C plasma treated material deprived of the LMWOM (rinsed in water).

The results from AFM studies on the annealed HDPE/PP feed spacer are schematically depicted in Figures 43 a–c. The scheme represents surface etching after PL_C plasma and formation of the LMWOM layer, including its estimated thickness (Figure 43 b). Figure 43 c illustrates the SBMA coating accumulated in material cavities.

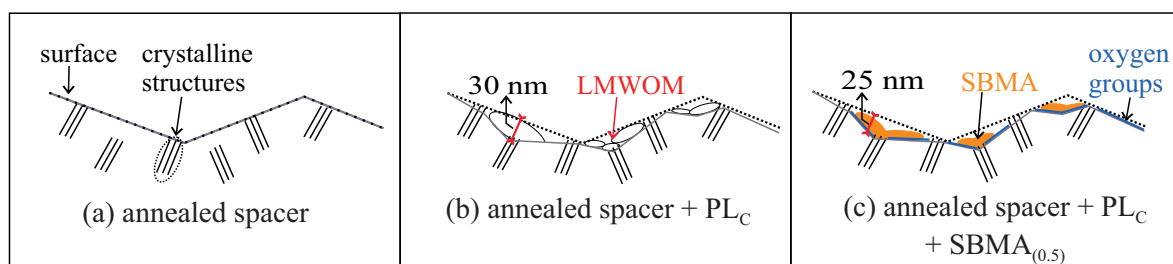


Figure 43: Schematic representation of the HDPE/PP feed spacer cross-section: a–annealed material, b–annealed material treated with PL_C plasma and estimated LMWOM layer thickness, c–annealed material treated with PL_C plasma and coated with 0.5 mol SBMA with estimated coating thickness. Dotted lines represents the surface directly after annealing, while continuous lines show the current surface. LMWOM–low-molecular-weight oxidized material, SBMA–sulfobetaine methacrylate.

Summary of the HDPE/PP feed spacer modification. The feed spacer was successfully coated with SBMA. According to the surface composition studies (XPS), the similar sulfur concentration (characteristic for the coating) was obtained on the feed spacer (Table 12) and on the HDPE/PP foil (Figure 30 a). However, AFM investigations showed different morphologies of the blend materials, after plasma treatment and after coating, respectively (foil: Figure 28 c, Figures 34, and feed spacer: Figure 39 a and Figure 39 b). The treatments performed on annealed spacer surfaces resulted in similar morphologies as revealed for the blend foils (Figures 41 b–d).

4.3.3 Discussion

The HDPE/PP foil and feed spacer extruded from the same raw materials were analogously treated with DBD in air. It was observed that the same treatment affected differently the morphology of both specimens. The exposed to plasma foils, showed the formation of LMWOMs (Figures 28), removed by rinsing in water (Figure 29 a). However, the morphology analysis of plasma-treated feed spacer did not reveal this characteristic amorphous layer containing the polyolefin oxidation products.

To obtain reproducible results from plasma treatment, several requirements have to be fulfilled, e.g., homogeneity of the material and its flatness [91]. Among the material properties which can significantly influence the behavior under exposure to plasma, surface crystallinity is of great importance. Comparing morphologies of the untreated blend foil and spacer (Figures 25 a and b), both surfaces showed the characteristic lamellar structures. Nevertheless, the density and thickness of those crystalline structures are considerably lower on the feed spacer surface. Taking into consideration the manufacturing processes of those materials, lower feed spacer crystallinity is highly probable. The HDPE/PP melt is pressurized and forced through slots in a die plate to generate filers. The fabricated net is directly immersed in a water bath [191]. It is commonly accepted that the cooling conditions influence the crystallization of semicrystalline polymers [150]. Therefore, it is likely that the fast cooling process limits the possibility to develop the large crystalline structures on the feed spacer surface.

Furthermore, oxidation and etching of polymer surface in plasma depends on the material supermolecular structure, which includes crystalline, semi-crystalline, transition zones, and amorphous regions [74]. Consequently, different supermolecular structures of the foil and spacer can result in various responses to the plasma exposure. Assuming lower crystallinity of the feed spacer surface, and considering the preferential oxidation of amorphous material regions in plasma [74], stronger influence of secondary processes (amorphization of topmost layers by cross-linking and VUV [74]), can be expected for the spacer surface.

Moreover, it is possible that different charging effects dominate when modifying feed spacer and foil. The existence of some additives or debris (possibly remains from manufacturing process) on the feed spacer surface (see Figure 25 a) can provoke different response to the charged plasma species. The unusual amorphous islands, identified on the untreated feed spacer, were not found after performed plasma treatment (Figure 39 a). They most probably became oxidized during barrier plasma treatment and affected the processes which took place on the polyolefin surface.

The studies performed on the annealed feed spacer material showed that the surface supermolecular structure influences the obtained effects of plasma treatment. The spacer surface with clearly revealed semicrystalline morphology (see Figure 41 a) behaved analogously to the blend foil. The generation of LMWOM was also observed (foil: Figure 28 c, spacer: Figure 41 b), and the obtained coating structures agreed (foil: Figures 34 a and b, spacer: Figure 41 d). During the annealing process, attention was paid not to affect the spacer standards' configuration. For this reason, the different effects of plasma treatment, observed before and after annealing, can not be attributed to the changed distance to the plasma generating electrodes.

4.4 Examination of antifouling effect

4.4.1 Concept for discontinuous and continuous testing

The potential of SBMA modified blend foils and feed spacers to reduce bacteria adhesion, and thus mitigate biofouling, was initially examined in *Pseudomonas fluorescens* batch culture. A short-term adhesion assay is a common practice to determine the surface susceptibility to biofouling [174, 129] since the initial bacterial adhesion is a prerequisite for biofilm formation [144, 69]. Continuous antifouling studies under real conditions are quite rare in the literature, however crucial to assess long-term coating functionality. In this work, the SBMA modified feed spacers were subjected to continuous antifouling testing in the membrane fouling simulation set-up (MeFoS). The MeFoS was designed to mimic the hydrodynamic conditions in the RO membrane module and to monitor the fouling development over time.

4.4.2 Discontinuous testing with *Pseudomonas fluorescens*

The untreated and SBMA modified (PL_C + SBMA_(0.5)) HDPE/PP foils and feed spacers were simultaneously subjected to bacterial suspension, and generated biofilms investigated. Testing and analysis procedures are given in section 3.5.2.

The blend foils were analyzed by fluorescence microscopy in order to quantify the surface coverage by bacteria. To establish the comparability between performed experiments, the determined surface coverage for each modified sample was normalized to the surface coverage determined for untreated foil in the same experimental set. Bacterial attachment (degree of surface coverage) obtained for the untreated surface was defined as 100%.

SEM was applied to analyze the biofilms formed on the feed spacer surface. However, due to the three-dimensional character of the spacer, it is difficult to provide a definitive statement about biofilm development using microscopic methods. For this reason, the commonly used biological staining with safranin O dye was applied to semi-quantify the biofilms. The stain adsorbed in bacteria cell walls was firstly extracted, followed by UV-Vis absorption measurements (OD₅₃₀), and the calculation of relative biofilm mass on the spacer.

Obtained results from the antifouling studies on the foils and feed spacers are summarized in Figure 44. The *Pseudomonas fluorescens* biofilms on the untreated and SBMA coated foils are depicted in Figures 45 a and b (examples). The SEM micrographs of fouled feed spacers are given in Figures 46 a and b.

A significant reduction in bacterial attachment to both modified with SBMA materials was demonstrated. Regardless applied analytical method (quantitative for foils, or semi-quantitative for spacer), similar degrees of fouling were observed. The 0.5 mol SBMA coated foils showed about 70% reduced bacterial attachment compared to the untreated samples (normalized surface coverage: 30±14%). Results obtained for the analogously modified feed spacer indicated the

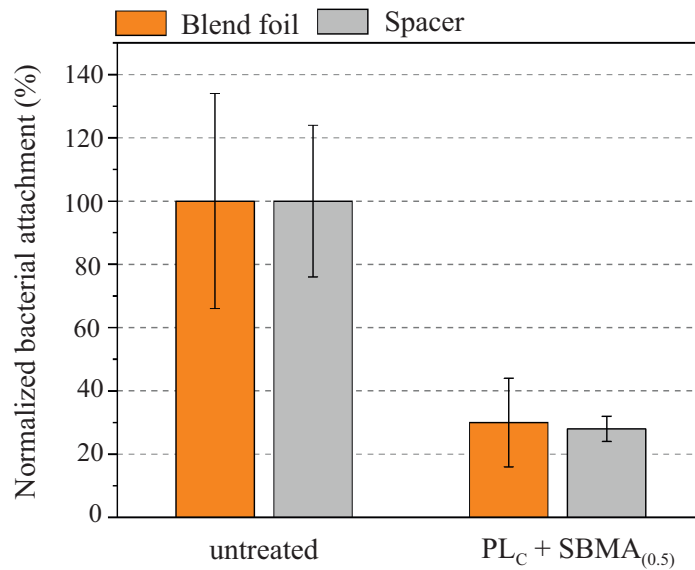
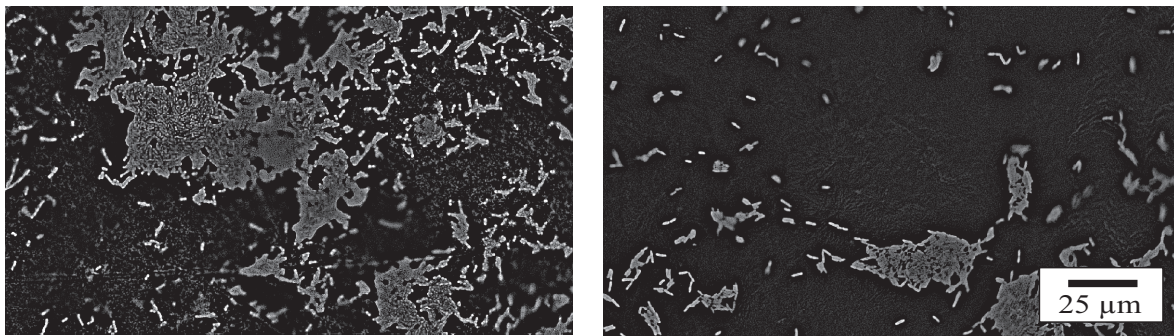


Figure 44: Normalized bacterial attachment to the untreated and SBMA coated (PL_C + SBMA_(0.5)) HDPE/PP foils and feed spacers (*Pseudomonas fluorescens* bacteria, discontinuous experiments).



(a) untreated HDPE/PP foil

(b) HDPE/PP foil + PL_C + SBMA_(0.5)

Figure 45: Fluorescence microscopy imaging of the *Pseudomonas fluorescens* biofilms on the HDPE/PP foils (discontinuous experiments): a–untreated surface, b– SBMA coated surface (PL_C + SBMA_(0.5)). Bacteria presented in white.

bacterial attachment of $28 \pm 4\%$. The comparable anti-adhesion effect regardless of the specimen geometry suggests, either good transferability of the proposed modification technology from the flat foil to the 3D feed spacer or steady antifouling characteristics of the generated SBMA layers irrespective surface topography. Comparing individual experiments, there was some deviation in biofilm development on the untreated materials. As presented in Figure 44, the surface coverage by bacteria varied by about 30%. One of the possible explanations can be the quality of untreated surfaces. These are industrially manufactured materials, therefore burden with surface defects such as scratches or grooves. Those surface irregularities are attractive for bacteria to adhere and to build biofilms.

Considering obtained SEM images of the untreated and SBMA coated spacers (Figure 46 a) and

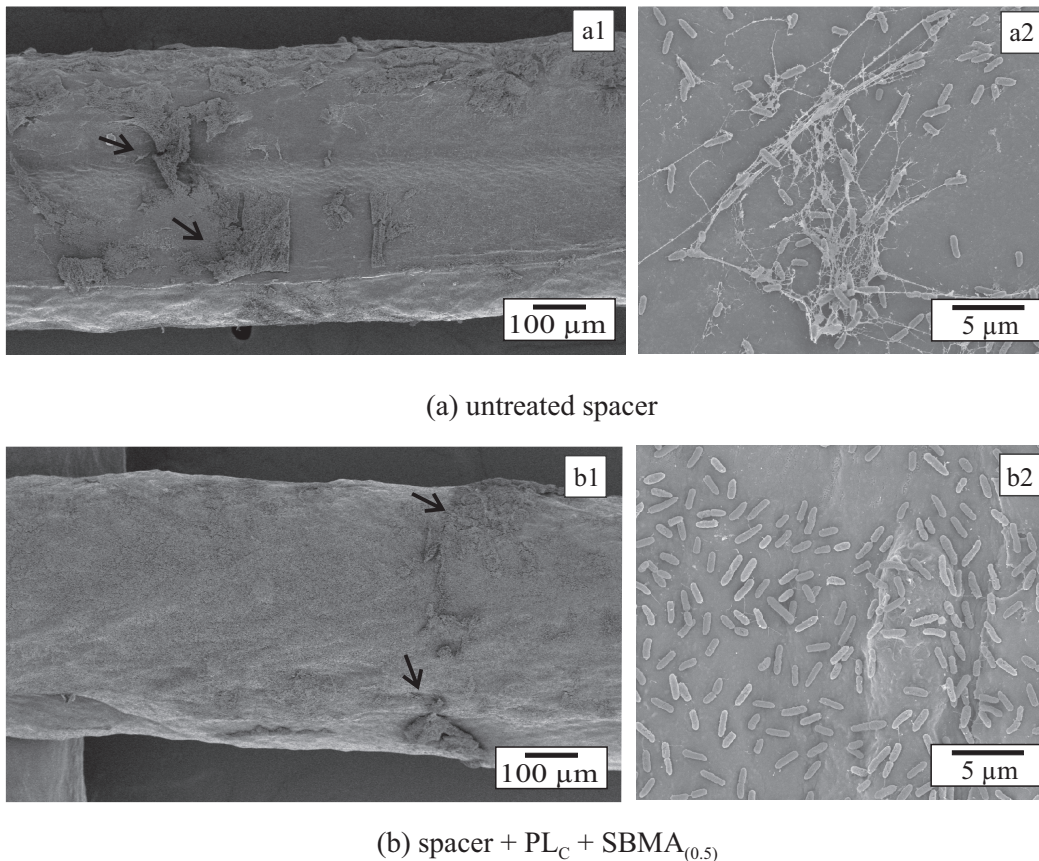


Figure 46: SEM imaging of the *Pseudomonas fluorescens* biofilms on the HDPE/PP feed spacers (overview of the filament (left) and enlargement on the biofilm structure (right)): a–untreated, b–PL_C plasma treated and 0.5 mol SBMA coated surface (both 24 h incubation in batch).

Figure 46 b1, respectively), large biofilm agglomerates were identified on both investigated samples (examples marked with arrows). Nevertheless, the SBMA coated spacer was noticeably less affected by biofouling. Additionally, the detailed images of the spacer surfaces (Figures 46 a2 and b2) demonstrated reduced EPS (extracellular polymeric substance) production on the SBMA coated samples at the early stage of biofouling. In general, EPS is created by bacteria to improve adhesion to the surface, as well as cohesion in the biofilm [71, 201]. Fewer EPS indicates weaker bacteria-surface interactions, therefore possibly easier detachment of bacteria under applied stress, e.g., turbulent flow near the surface.

In the performed short-term batch experiments, the SBMA coated substrates showed good anti-adhesion properties. On the one hand, there are plenty of examples in the literature confirming the antifouling effect of thin SBMA coatings [94, 42, 114]. On the other hand, coating homogeneity plays a crucial role in providing the desired antifouling capability, while irregular surfaces supposed to be more prone to bacterial adhesion [146, 147, 35]. Therefore, the anti-adhesion property of proposed SBMA coatings might be attributed only to steric hindrance and reduction of van der Waals attractive forces between a bacterium and the substrate surface. This hypothesis would mean that, regardless of what kind of coating is on the surface, it can generate the barrier

for bacteria to settle. Another important point to consider is the possible contribution of plasma treatment to the biofouling reduction on the SBMA modified surfaces. The exposure to plasma increased the surface free energy and hydrophilicity. Therefore, the plasma-activated surfaces might be already less prone to microorganisms adhesion than the untreated materials. There are some reports on the improved antifouling property of plasma-treated surfaces [241, 242]. Nevertheless, some contradictory results were published as well [173].

In order to better understand the origin of reduced bacterial adhesion to the SBMA modified HDPE/PP surfaces, a series of experiments on the blend foils were performed. Obtained results and conclusions are presented in the following section.

4.4.3 Study of the anti-adhesion effect of SBMA coatings

The following hypotheses regarding the generated SBMA coatings were made:

- *Hypothesis 1:* since the generated SBMA coatings are heterogeneous (see e.g., Figure 33 and Figure 40), the reduced bacterial adhesion might be due to applied plasma treatment. To verify this hypothesis, the surface properties such as surface free energy (SE), composition, and roughness were compared for the PL_C plasma treated and the PL_C plasma treated and 0.5 mol SBMA coated blend foils. Subsequently, batch experiments with *Pseudomonas fluorescens* were performed, to evaluate the potential anti-adhesion property of PL_C plasma treated HDPE/PP foils.
- *Hypothesis 2:* steric hindrance is responsible for the anti-adhesion property of SBMA modified materials. The coating is beneficial due to an excluded volume effect (entropy penalty), therefore prevents potential foulants from approaching the surface [189]. To verify this statement, an alternative coating agent: 2-(Dimethylamino)ethyl methacrylate (DMAEMA), was proposed (structure depicted in Figure 47). Firstly, DMAEMA polymerizes easily by free radical mechanism [200]. Secondly, it does not have a zwitterionic structure. Therefore, the effect of surface chemistry on biofouling mitigation can be better assessed when comparing the SBMA and DMAEMA coatings. Following the surface properties analyses, batch experiments with *Pseudomonas fluorescens* were accomplished to test the anti-adhesion potential of DMAEMA modified blend foils.

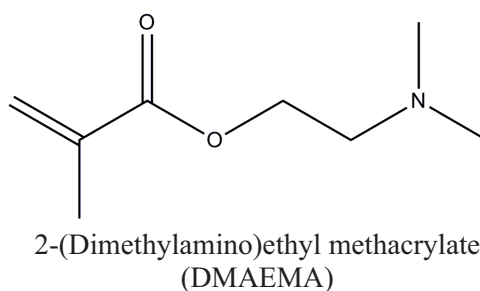


Figure 47: Chemical structure of 2-(Dimethylamino)ethyl methacrylate (DMAEMA).

Study on hypothesis 1. The HDPE/PP surface exposed to the PL_C plasma treatment became covered by the water-soluble LMWOM (see Figure 28 c). This indicates that in case of heterogeneous distribution of the SBMA coating, non-covered areas would have similar characteristics to the PL_C plasma treated and rinsed specimen (PL_C + rinsing, Figure 29 a). Therefore, there is a necessity to analyze the PL_C plasma treated and rinsed surfaces as well. The selected parameters of the HDPE/PP surface at each stage of modification (untreated, plasma-treated, coated), as well as the PL_C plasma-treated surface without LMWOM (PL_C + rinsing), are summarized in Table 14.

Parameter	HDPE/PP foil untreated	HDPE/PP foil + PL _C	HDPE/PP foil + PL _C + rinsing	HDPE/PP foil + PL _C + SBMA _(0.5)
SFE (mN/m)	33.0±1.0	52.0±1.0	41.0±3.0	51.0±5.0
O (at%)	0.2±0.1	23.1±2.6	5.6±1.0	16.4±0.8
R _a (nm)	8.7±1.1	5.4±0.8	6.2±1.3	4.2±2.8
Bacterial attachment (norm., %)	100±34	x	82±28	30±14

Table 14: Surface properties of the untreated, PL_C plasma treated, PL_C plasma treated and rinsed in water, as well as PL_C plasma treated and 0.5 mol SBMA coated HDPE/PP foils. SFE—surface free energy (contact angle), O at %—oxygen concentrations at the surface (XPS), R_a—surface roughness (AFM height imaging).

The effect of PL_C plasma treatment on the surface characteristic was already analyzed in section 4.2.1. Currently, the focus is placed on the following scenario: the PL_C plasma-treated surface is subjected to SBMA coating in a 0.5 mol monomer solution. The LMWOM generated after exposure to DBD dissolves in the coating solution. The SBMA coated surface is heterogeneous, partially covered by the coating, while some areas appear as the PL_C plasma-treated deprived of LMWOM. The question is, whether these non-coated material regions can be responsible for the observed anti-adhesion effect.

The SBMA modified foil has higher surface free energy and tendentially lower roughness than the PL_C plasma-treated and rinsed surface (R_z showed the same tendency as given R_a). Observed higher SFE and roughness deviations for the SBMA coated foils comparing with other analyzed specimens, is most probably attributed to the heterogeneous distribution of SBMA on the surface. From the results obtained on the annealed feed spacer surface (Figures 41 and 42) can be deduced that the coating accumulates mostly in the material cavities. This explains the tendency of reduced surface roughness after coating.

The performed discontinuous tests with *Pseudomonas fluorescens* did not show significantly reduced susceptibility to fouling of the PL_C plasma treated and rinsed samples. Referring to the first hypothesis, applied plasma treatment is not sufficient to ensure the anti-adhesion properties. Therefore, the SBMA coating is necessary in order to noticeably minimize biofouling. The observed anti-adhesion properties of SBMA modified foils are attributed to surface chemistry

(higher SFE) and topography (lower roughness). It is known that hydrophilic and smooth surfaces weaken the bacterial-surface interactions and minimize the bacterial adhesion [148, 72, 50].

Study on hypothesis 2. For the investigation it was assumed that DMAEMA coating creates a morphology similar to the observed for the SBMA modified foils. In this case, surface chemistry and steric hindrance effects could be discussed.

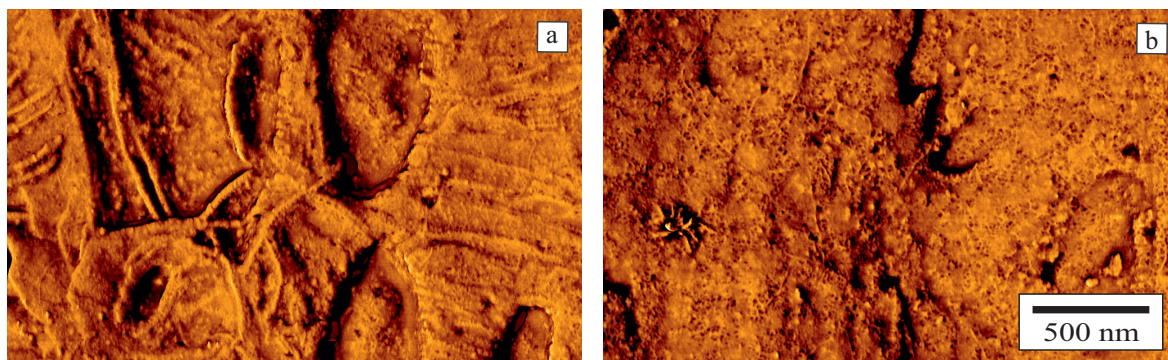
There are several studies that compare the antifouling potential of DMAEMA and SBMA materials. For instance, experiments performed on the SBMA-DMAEMA hydrogels showed more severe biofouling with an increase of DMAEMA contribution in the hydrogel structure. These results were consistent regardless of the applied microorganism [217]. The biofouling resistance of polySBMA and polyDMAEMA brushes with the same thickness was also studied. The polySBMA coatings showed significantly better antifouling performance against various proteins, marine bacterium *Cobetia marina*, as well as algae [231]. These reports clearly indicate enhanced biofouling resistance of the zwitterionic surfaces in comparison to the functionalized with DMAEMA. Therefore, if the anti-adhesion effect of generated SBMA coatings is attributed only to steric hindrance, similar biofilm development should be demonstrated on the SBMA and DMAEMA coated blend foils.

The characteristic of analogously prepared SBMA and DMAEMA coatings is summarized in Table 15. Nitrogen concentration was chosen to compare the surface compositions (both monomers contain one nitrogen atom, structures presented in Figures 47 and 10).

Parameter	SBMA coated HDPE/PP foil	DMAEMA coated HDPP/PP foil
SFE (mN/m)	51.0±5.0	46.0±4.0
N (at%)	2.1±0.6 (N* = 5.3)	3.3±0.3 (N* = 9.1)
R _a (nm)	4.2±2.8	6.8±1.9
R _z (nm)	22.8±15	32.5±10
Bacterial attachment (norm., %)	30±14	116±40

Table 15: Surface properties of the SBMA and DMAEMA coated blend foils. SFE–surface free energy (contact angle), N at%–nitrogen concentrations at the surface (XPS), R_a–surface roughness (AFM height imaging). Data marked with * are calculated values for a corresponding complete surface coverage with the coating thickness at least the XPS information depth.

The DMAEMA modified surface showed lower surface free energy comparing with the SBMA coated, however, the difference cannot be considered as significant. Analyzing nitrogen concentration, in both cases about 40% surface coverage by the coating can be estimated (considering the stoichiometric composition, and assuming the coating thickness at least the XPS information depth). Considering topography analysis, the DMAEMA modified blend has similar roughness to the PL_C plasma treated and rinsed foil (see Table 14). This is tendentiously higher than the



HDPE/PP foil + PL_C + DMAEMA_(0.5)

Figure 48: AFM phase imaging of the HDPE/PP foil modified with DMAEMA at two different positions (PL_C plasma treatment with subsequent coating in 0.5 mol DMAEMA monomer solution).

roughness determined for SBMA coated surface. However, performed antifouling testing indicated that the DMAEMA modified foils were significantly more prone to fouling than the SBMA coated. Moreover, the DMAEMA modification performed worst than the simultaneously studied untreated foils (for this reason the normalized bacterial attachment >100%). This inclines towards the morphology analysis of the DMAEMA coated surface. The corresponding AFM phase images obtained at two different positions are given in Figures 48 a and b.

The analyzed by AFM surface areas appear to be completely covered by the DMAEMA coating. However, surface morphology is significantly different from that observed for the SBMA coating (Figures 34). While the amorphous SBMA coating tends to accumulate in the material valleys, the DMAEMA coating exhibits high heterogeneity. This DMAEMA coating structure resulted most probably in the high susceptibility to bacterial adhesion. Furthermore, coating thickness is an important parameter affecting bacterial adhesion [48, 235]. For instance, a strong correlation between film thickness and the antifouling property was shown for the poly(hydroxy-functional methacrylates) deposited on the gold substrate (SI-ATRP method). Too thin or too thick brushes led to high protein adsorption, while the optimum coating thickness was about 20–45 nm [246]. The DMAEMA coating is likely significantly thicker than the SBMA coating, therefore it shows a different response to bacterial adhesion.

The second hypothesis attributed the anti-adhesion property of SBMA coatings only to the steric hindrance effect. To verify this statement, the coatings which different chemical composition were prepared. It was assumed that analogously performed modification with DMAEMA can lead to comparable surface morphology. In this particular case, the effect of surface chemical composition on the anti-adhesion property could be studied. However, it was shown that the SBMA and DMAEMA coatings have significantly different morphologies. Therefore, any unequivocal conclusion, regarding the importance of the surface composition on the anti-adhesion property, cannot be drawn. Nevertheless, it was demonstrated that steric hindrance does not provide any anti-adhesion effect, and the coating structure plays a significant role.

4.4.4 Continuous testing with fouling simulation set-up

Determination of testing conditions. The SBMA coated foils and feed spacers showed reduced susceptibility to biofouling in the short-term batch experiments. In order to verify the antifouling potential of SBMA modified spacers under practical flow conditions, continuous testing in a fouling simulation set-up (MeFoS) was conducted (set-up and experimental details given in section 3.5.3). The feed channel pressure drop (FCPD) increase over time was indicating the biofilm building. For the better comparison between individual tests, the FCPD values were normalized to the initial feed channel pressure drop (day 0): $FCPD_{t=0}$. There was severe biofouling identified, once the normalized FCPD reached 300%.

Initially performed fouling simulation experiments were aimed to establish the most suitable testing procedure. The primary studies were performed with the untreated feed spacers. Without additional nutrient dosage, no FCPD increase was observed within 90 days. To promote biofouling within a reasonable laboratory test duration, the substrate solution was dosed to the feed water. Three different substrate dosage rates were tested, to choose the most favorable nutrient load for the utilized tap water. The feed channel pressure drop evolution for the untreated HDPE/PP feed spacers depending on the substrate dosage rate is presented in Figure 49.

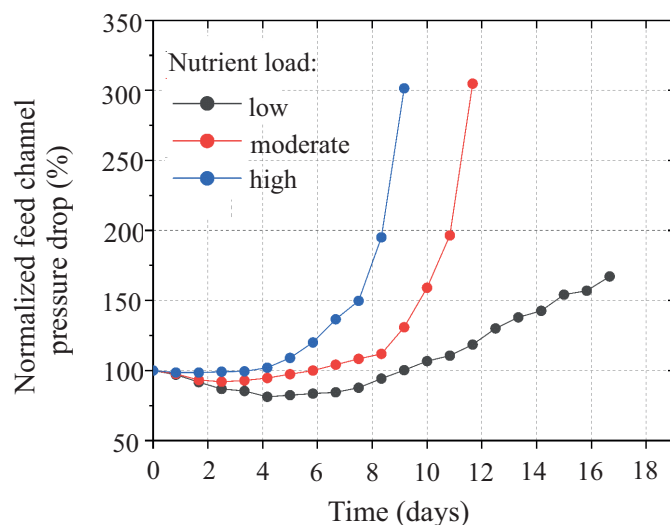


Figure 49: Normalized feed channel pressure drop (FCPD) over time for the untreated HDPE/PP feed spacer in dependence on the nutrient load (low– $0.015 \text{ L}\cdot\text{h}^{-1}$, middle– $0.03 \text{ L}\cdot\text{h}^{-1}$, high– $0.045 \text{ L}\cdot\text{h}^{-1}$).

As expected, fouling evolution was dependent on the nutrient load. Looking at the experiments performed at the high and moderate substrate dosage flow rates, a typical exponential FCPD increase, characteristic for a log-phase of bacterial growth, was observed. In case of high nutrient availability, severe biofouling was observed already after 9 days testing, while the moderate dosage required about 12 days. Analyzing the experiment with the lowest nutrient load, a more linear FCPD increase was reported. After 17 days of testing, the normalized FCPD reached only about 170%. It is possible that under this nutrient condition, microorganisms were not able to rapidly proliferate. A slight decrease in the normalized FCPD at the initial stage of experiments

can be attributed to some variation of the inlet pressure in the system. Some time is usually required to stabilize the system.

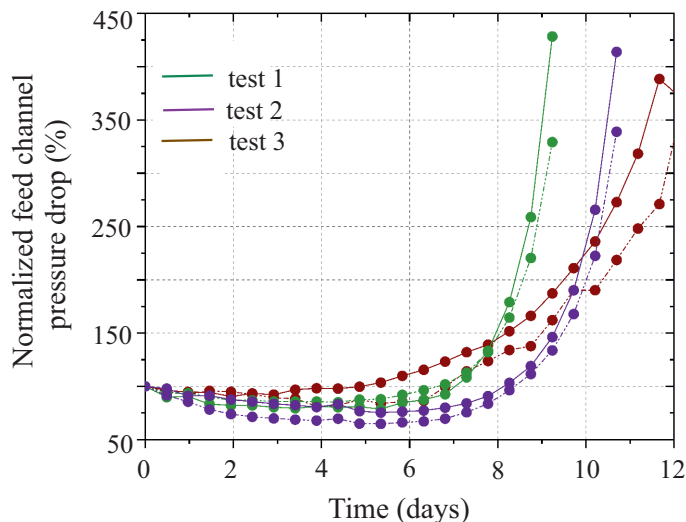


Figure 50: Normalized feed channel pressure drop (FCPD) over time for two untreated HDPE/PP feed spacers tested in parallel (nutrient load of $0.03 \text{ L}\cdot\text{h}^{-1}$). Continuous and dotted lines of the same color represent one experiment. Three independent experiments were conducted (test 1, test 2, test 3).

To better mimic the feed water conditions in the full-size RO modules, and at the same time ensure the reasonable testing time, the moderate nutrient load was chosen for subsequent experiments. The comparable conditions were applied in other publications on the continuous antifouling testing of the modified spacers [151, 9].

After establishing the nutrient dosage conditions, experiments were conducted to demonstrate the set-up reliability. For this purpose, two untreated feed spacers were simultaneously tested under the same conditions to confirm, whether a similar FCPD development is obtained for both of them. Only in this case, the comparison between the untreated and SBMA modified feed spacer could be made. Three independent experiments were carried out (test 1–test 3), in each of them two untreated feed spacers were studied. The results are summarized in Figure 50.

Considering the three performed tests, in each case slightly different experimental duration was required to observe severe biofouling. Test 1 was completed after 9 days of monitoring, while test 3 took about 11 days to observe the normalized FCPD over 300%. This is most likely attributed to the microbial load in tap water. The bacterial colonies in tap determined for 6 days were $175 \pm 116 \text{ CFU}/100\text{g}$ (see chapter 3.5.3). High standard deviation confirms a strong variation of the microbial load from day to day. Nevertheless, the feed channel pressure drop increase showed a similar trend for all performed experiments. There is also a good agreement of the results when comparing two untreated feed spacers tested in parallel in one test. The maximum time difference necessary for severe biofouling to occur (normalized FCPD $> 300\%$) on both tested in parallel specimens was about 15 h (test 3). Therefore, while testing the untreated and SBMA coated spacers, longer biofouling postpone should be observed to conclude a significant

improvement in the antifouling properties of the modified sample.

Coating stability under experimental conditions. The coating stability under experimental conditions was evaluated before performing the long-term fouling tests. Table 16 summarizes surface elemental compositions of the untreated and SBMA coated feed spacers and PA membranes before testing ($t=0$), and after 3 weeks parallel testing in the MeFoS ($t=3w$). No additional nutrient dosage was applied in this study. Therefore no FCPD increase was observed within experiment duration.

Taking into consideration the PA membrane surface after testing ($t=3w$), additional chemical elements, not presented on the reference membrane (PA membrane at $t=0$), were detected. The presence of Si, Mg and Ca can indicate slight inorganic or colloidal fouling [100]. No significant difference in the composition was observed for the PA membrane samples tested in FS1 (fouling simulation cell 1 with the untreated spacer) and FS2 (fouling simulation cell 2 with the SBMA coated spacer). Analyzing the changes in the composition of the untreated feed spacer specimen, higher amounts of O, N and Si concentrations were detected after completing the 3 weeks trial ($S_{t=3w}$, FS1). Higher oxygen and nitrogen contents can be attributed to the presence of some organic substances on the surface. Moreover, Mg and Ca were found on the spacer surface after completing the 3 weeks experiment with tap water. This corresponds well with the membrane analyses and can indicate the deposition of inorganics. Considering the SBMA coated spacer (S-SBMA), only slightly reduced sulfur content after 3 weeks of continuous testing was reported (sulfur was chosen as SBMA indicator). Since no sulfur was detected on the untreated spacer studied in parallel, a maximum 20% deterioration of the coating quality can be expected while testing ($S\text{-SBMA}_{t=0}=1\text{ at\%}$, $S\text{-SBMA}_{t=3w}=0.8\text{ at\%}$). Furthermore, the SBMA modified feed spacer showed noticeably higher O, N, Na, Cl and Si concentrations, while lower C after the study. Additionally, Mg, Ca and Al were identified, not presented on the newly coated surface. These results incline toward the conclusion that the SBMA coating can attract inorganic compounds. Calcium, aluminum, and magnesium appeared in the significantly higher concentration on the SBMA coated spacer than on the untreated spacer tested in the same trial. Therefore, there is a possible interaction between the SBMA modified surface and the ions in water. The zwitterionic polymers are known from their „anti-polyelectrolyte” effect. The presence of salt in the water-polymer solution improves solubility and influences the conformation of polyzwitterionic chains. This is possible due to electrostatic interactions between the sulfonate/quaternized ammonium groups and ions of the opposite charge [142].

The presence of calcium on the surface can indicate among others calcium carbonate or sulfate, which are one of the most common scalants [100]. If CaSO_4 is the source of identified calcium, the sulfur detected on SBMA modified spacer can denote not only the coating, but also inorganic material. However, since the occurrence of Ca and Mg was especially prominent on the SBMA coated surface, it can be assumed that the coating was present, and therefore interacted with those ions. There was a similar stability experiment performed with distilled water as a feed. Even if calcium was not identified on the SBMA modified surface, sulfur was

Sample	Elemental composition									
	C (at%)	O (at%)	N (at%)	S (at%)	Na (at%)	Cl (at%)	Si (at%)	Mg (at%)	Ca (at%)	Al (at%)
	before testing (t=0)									
S _{t=0}	89.8±4.1	7.5±2.1	x	x	x	x	2.6±2.2	x	x	x
S-SBMA _{t=0}	79.5±1.5	16.8±0.7	0.9±0.4	1.0±0.4	0.2±0.1	0.1±0.1	1.6±0.2	x	x	x
M _{t=0}	69.5±0.2	17.5±0.1	8.2±0.2	3.4±0.1	0.3±0.0	1.1±0.0	x	x	x	x
	after 3 weeks testing (t=3w) FS1-untreated spacer									
S _{t=3w} (FS1)	76.9±2.2	16.4±1.5	2.0±0.5	x	x	x	4.3±1.0	0.2±0.2	0.1±0.1	x
M _{t=3w} (FS1)	70.0±0.4	16.7±0.2	10.2±0.1	0.7±0.1	0.1±0.1	1.3±0.1	0.5±0.3	0.1±0.0	0.4±0.0	x
	after 3 weeks testing (t=3w) FS2-SBMA coated spacer									
S-SBMA _{t=3w} (FS2)	63.8±1.8	22.6±1.2	3.1±0.4	0.8±0.1	1.2±0.2	0.9±0.1	2.5±0.7	3.5±0.7	1.0±0.2	0.7±0.1
M _{t=3w} (FS2)	68.9±0.7	17.0±0.5	10.0±0.1	0.5±0.0	0.9±0.3	2.2±0.3	0.3±0.4	x	0.2±0.2	x

Table 16: Surface elemental composition (XPS) of the untreated (S) and SBMA coated (S-SBMA; PL_C+SBMA_(0.5)) feed spacers and corresponding PA membranes (M) prior (t=0) and after 3 weeks (t=3w) continuous testing in the MeFoS (tap water, no additional nutrient dosage). FS1-fouling simulation cell 1, FS2-fouling simulation cell 2.

detected after one week of testing. Therefore, the SBMA coating can most probably withstand the flow conditions in simulation trials.

Antifouling testing of the SBMA modified feed spacers. The SBMA modified feed spacers ($PL_C + SBMA_{(0.5)}$) were subjected to continuous testing in the MeFoS. Two fouling simulation cells (FS1, FS2) operated in parallel under the same conditions to compare the fouling susceptibility of untreated and SBMA modified feed spacers. Five independent experiments were performed, two representative results are presented in Figure 51.

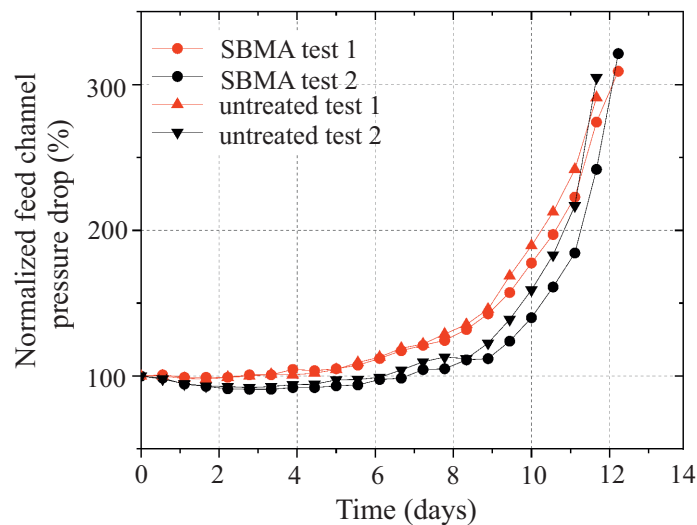


Figure 51: Normalized feed channel pressure drop (FCPD) over time for the untreated and SBMA modified ($PL_C + SBMA_{(0.5)}$) HDPE/PP feed spacers tested in parallel (nutrient load of $0.03 \text{ L}\cdot\text{h}^{-1}$). Lines of the same color represent one experiment (red—test 1, black—test 2).

The fouling simulations on unmodified and SBMA modified spacers receiving nutrients, showed similar increases in feed channel pressure drop over the 12-days study. This result was confirmed in five independent trials. Each experiment was considered individually, without calculating the middle values from all performed trials. The reason is the variation of tap water quality, and thus actual testing conditions. Nevertheless, parallel analyses of the unmodified and modified feed spacer are sufficient to compare their behavior, as shown elsewhere [193, 151, 9].

Similar conclusions about the coating behavior were drawn, for instance, by Miller et al., who studied polydopamine and polydopamine-g-poly(ethylene glycol) feed spacer coatings under analogous, relevant to module operation, conditions [151]. Different antifouling behavior of the SBMA modified surfaces, in the short-term batch, and in the long-term continuous studies, will be discussed in the following section.

Summary of the antifouling studies on the HDPE/PP foils and feed spacers. The SBMA coatings on HDPE/PP substrates were able to reduce *Pseudomonas fluorescens* biofouling by about 70% in 24 h batch experiments. The anti-adhesion property of generated coatings was attributed to the chemistry and structure of the SBMA layer. The SBMA modified feed spacers

could not significantly mitigate biofouling in the long-term fouling simulation experiments.

4.4.5 Discussion

The initial bacterial adhesion was recognized as a critical step in biofilm formation [144, 69]. Therefore, short-term batch experiments are commonly used to test antifouling potential. In this work, the SBMA coated spacers showed satisfactory anti-adhesion properties in the short-term batch experiments. However, there was no significant biofouling postpone observed while testing under conditions adequate for practice. A similar conclusion was already drawn by other authors who studied the long-term antifouling resistance of the chemically conditioned feed spacers [9, 151, 231]. Plenty of factors contribute to different results from the short-term static and long-term dynamic examinations. The effects, most important to consider, were divided into two categories: testing conditions and coating behavior. They are schematically depicted in Figure 52

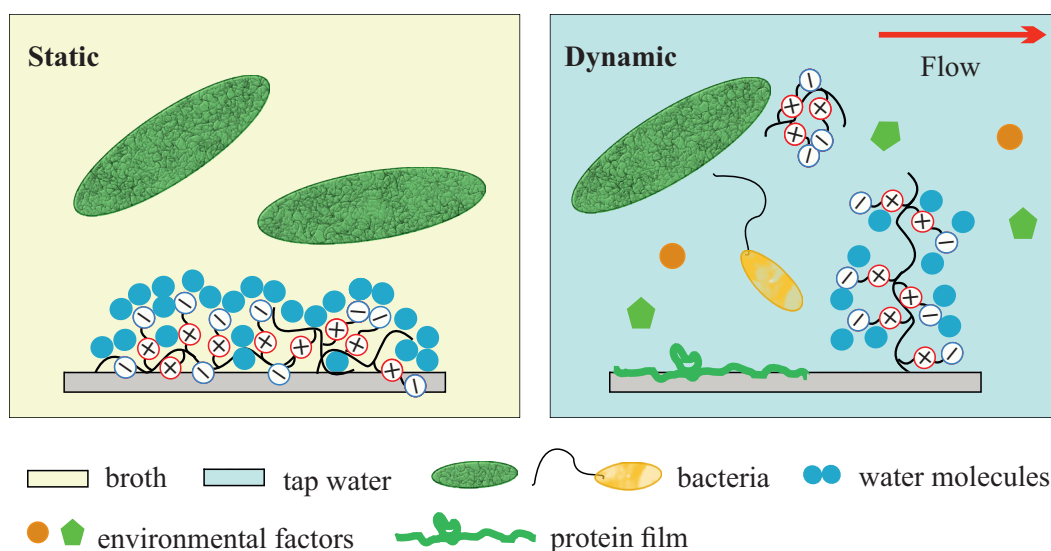


Figure 52: Schematic representation of the static (batch) and dynamic (fouling simulation) antifouling testing of SBMA modified surfaces.

Testing conditions. To begin with, tap water used in fouling simulation (dynamic) trials is a more complex solution than the model bacterial culture in a standard broth solution. Firstly, a mixed bacterial culture is more resistant to dynamic environmental conditions [110]. Secondly, interactions between different organisms in tap water and a variety of their surface characteristics, cannot be mimicked in batch experiments [72]. Under the shear stress conditions, the microorganism's selection occurs. Therefore, the species able to build mechanically stable biofilms become dominant [69]. Moreover, the presence of additional components in tap water, such as proteins, has to be considered. They might lead to the initial organic fouling or surface conditioning [35], which can influence bacterial adhesion. Dissolved inorganics are known to affect the microorganisms' adhesion to the surface [228, 80]. The coating stability tests with tap water showed significant amount of Ca and Mg on the SBMA modified feed spacer (see Table 16). These

divalent ions are possibly attracted to the zwitterionic groups. Subsequently, they can act as a bridging agent between the microorganisms in water and the modified surface. According to literature reports, calcium ions can promote interactions between proteins and the bacterium cell surface. They also influence the way how bacterial cells interact with different substrata [80]. For instance, Cao et al. studied the resistance of different polysaccharide coatings to microorganisms' adhesion. The complexation of calcium ions facilitated the adhesion of hematopoietic cells. Worse antifouling resistance was caused by changing the mechanical and entropic properties of polysaccharide films after the binding of calcium [36]. There was a similar observation obtained during the investigation of *Pseudomonas aeruginosa* biofilms on alginate films. Divalent cations were affecting the properties of the bacterium's cell wall and the coating characteristics [58]. Considering these results, the presence of calcium or magnesium cations in the feed water may have changed the antifouling performance of SBMA coatings. Therefore, future antifouling studies on the SBMA coatings should include continuous experiments with deionized water as a feed, to exclude the possible influence of dissolved ions.

Nutrient type and availability are also of great importance for the biofilm establishment and growth. The biofilm-associated bacteria can sense the current nutrient conditions and accurately react via adapting structure, EPS production, etc. Rapid biofilm growth dominates under high nutrient concentration. Under low substrate availability, efficient proliferation is preferred [67]. The short-term biofouling experiments are to provide an appropriate amount of nutrients to accelerate biofilm development within a short time. The bacteria in a log-phase growth are commonly used for maximum attachment. On the other hand, however, due to the limited duration of the batch experiments, microorganisms are not able to proliferate to a significant extent. Therefore, mainly the initial bacterial adhesion is analyzed in these short-term studies. Even if the bacterial attachment is noticeably postponed, it is only a matter of time until a few adhered microorganisms will generate a biofilm. Furthermore, during fouling simulation, a considerable biofilm thickness is necessary to record the FCPD increase, which is a biofouling indicator. This means that in a single fouling simulation trial the several biofilm development cycles take place: from the initial attachment, growth, and detachment with the colonization of new areas.

Coating behavior. Another factor that plays a significant role in the long-term antifouling property is the coating quality. Performed in this work coating stability tests under static and dynamic conditions (section 4.2.2.3 and Table 16, respectively) showed partial leaching of the SBMA coating over time (within 30%). Therefore, the coating's anti-adhesion properties can worsen while long exposure to foulants. Furthermore, the feed spacer junctions become fouled as first [211, 223]. However, there is a lack of appropriate analytical methods to study the coating properties at these troublesome areas. Moreover, different SBMA coating structures under static and dynamic conditions can be expected [30]. In batch experiments, the SBMA-grafted chains might adhere to the surface and generate a physical hydrogel structure (see Figure 52). A laminar water film is built on the top of such conformation. This water film can postpone the initial bacterial adhesion. Under the flow conditions, however, the shear forces might overcome the adhesion forces between the SBMA chains and the surface. Therefore, the grafted zwitteri-

onic chains become stretched and oriented perpendicular to the surface. In this case, there is no protecting water film and the surface becomes exposed to the microorganisms' adhesion.

The feed channel pressure drop (FCPD) increase is the membrane performance parameter most sensitive to fouling [223]. Consequently, the fouling simulator set-up became a commonly accepted tool to investigate membrane fouling [151, 9, 193, 222]. The apparatus is universal to study new feed spacer geometries. In this case, the focus is placed on improved mixing in the feed channel and reduced concentration polarization near the membrane surface. Therefore, the feed water composition is a secondary matter. However, testing of the feed spacer coatings is much more complex. For instance, improved fouling resistance of the feed spacer may facilitate the microorganisms' colonization on the membrane surface. Biofouling on the membrane would affect the filtration parameters such as flux and rejection. This cannot be monitored by the current fouling simulation set-up. Therefore, in order to receive comprehensive information about the antifouling properties of coated spacers, consideration of all RO membrane performance indicators (FCPD, flux, rejection) is necessary.

The SBMA coated spacers could not significantly mitigate biofouling under conditions applied in the fouling simulation trials. Nevertheless, it does not necessarily mean that the proposed modification will not show satisfactory performance in a different water system. Moreover, the SBMA coating on the feed spacer may facilitate biofouling removal from the feed channel. Greater susceptibility to cleaning would be beneficial to improve a performance recovery of the already fouled membrane element. Follow-up experiments should include a two-phase flow cleaning on the fouled feed spacers, for instance, by applying nitrogen gas to the system.

5 Summary and conclusions

The aim of this work was the development, implementation, and testing of non-toxic antifouling coatings for feed spacer materials. The particular focus was placed on the possibility to transfer the proposed modification technology to the industrial-scale process. Feed spacers have a grid-like structure. They are applied in the reverse osmosis (RO) membrane modules for water desalination to separate the membrane sheets and create a channel for water flow. Therefore, they are an essential part of the RO modules. However, they are also prone to bacterial adhesion and biofouling.

As antifouling coating material, zwitterionic sulfobetaine methacrylate ([2-(Methacryloyloxy)ethyl]dimethyl-(3-sulfopropyl)ammonium hydroxide), SBMA) was selected. The coatings were deposited onto the feed spacer materials using atmospheric pressure plasma treatment followed by wet chemical coating. Considering difficult feed spacer structure, the modifications were performed not only on the 3D HDPE/PP (80/20 wt%) spacer material, but also on the flat HDPE, PP, and HDPE/PP (80/20 wt%) foils manufactured from the same raw materials. The created coatings were subjected to chemical, morphological and topographical analyses. The antifouling properties were investigated in batch, and continuously in a fouling simulator (MeFoS).

Plasma treatment and wet coating. In the proposed two-stage procedure for the chemical conditioning of the feed spacer surface, the first modification step was the atmospheric pressure plasma treatment with dielectric barrier discharge (DBD) in air. This treatment aimed to increase surface hydrophilicity and introduce oxygen functional groups. There is a relationship between applied plasma treatment parameters and the amount of oxygen at the examined surfaces. The hydroperoxide groups, able to initiate grafting, were identified at the surfaces exposed to plasma. However, their concentration did not vary significantly within applied plasma treatment conditions. The DBD treatment in air led to the generation of the low-molecular-weight oxidize material (LMWOM) on the polyolefin surfaces. The LMWOM was found water-soluble, and its occurrence did not exclude the surface functionalization with oxygen functional groups.

In the second modification step, the plasma-treated materials were subjected to wet coating in the SBMA monomer solution. It was demonstrated that polySBMA was successfully deposited on the modified materials. The amorphous SBMA coating was heterogeneously distributed on the surfaces. Studies on the annealed, and thus smooth, feed spacer surface showed that the

SBMA coating most probably accumulates in the material cavities and its thickness does not exceed 30 nm. The coating stability tests indicated that the original coating structure contains some loosely bonded SBMA chains. These chains were partially removed during incubation in salt water.

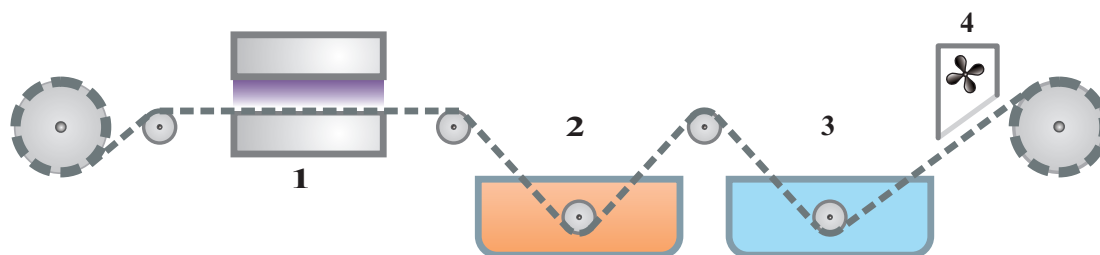
The HDPE/PP foil and feed spacer subjected to the analogous plasma treatment and coating conditions demonstrated significantly different morphologies. This effect was most probably attributed either to various supermolecular structures of both surfaces, or the feed spacer contamination as a leftover from the manufacturing process.

Antifouling testing. The susceptibility of SBMA coated materials to reduce bacterial adhesion was firstly studied in batch experiments with the Gram-negative *Pseudomonas fluorescens*. Despite its heterogeneous distribution on the surface, the SBMA coating reduced the bacterial adhesion more than threefold in comparison to the reference materials. The SBMA modified foils and spacers showed analogous antifouling performance. Based on the comparative experiments performed with 2-(Dimethylamino)ethyl methacrylate (DMAEMA), which did not reduce biofouling, the anti-adhesion property of SBMA coating was attributed to its favorable morphology and chemistry.

The SBMA modified spacers were additionally subjected to continuous antifouling testing in the fouling simulator. The feed channel pressure drop (FCPD) increase, which is an indicator of biofouling, was simultaneously monitored for the untreated and SBMA modified spacers. The SBMA coating on the feed spacer could not significantly mitigate biofouling under applied experimental conditions. The coating stability tests performed without nutrient dosage showed the occurrence of calcium and magnesium on the SBMA modified spacer. The zwitterionic coating was assumed to attract calcium and magnesium ions, which could influence its antifouling behavior.

Potential for industrial application. The proposed concept for a two-stage antifouling modification of the feed spacer surface can be transferred to an industrial roll-to-roll process. A concept of such an industrial coating line is given in Figure 53. After surface treatment in plasma with DBD in air (1st modification step), and coating with sulfobetaine methacrylate (2nd modification step), the rinsing procedure can be applied to remove unreacted monomers, followed by drying (e.g., infrared, hot air). The suggested procedure can be also used to modify other polyolefin surfaces, e.g., polyethylene terephthalate (PET) or polystyrene (PS). Furthermore, a wide range of different hydrophilic monomers with antifouling properties, such as 2-Hydroxyethyl methacrylate (HEMA) or 2-Methacryloyloxyethyl phosphorylcholine (MPC), can be used as coating agents.

The proposed modification employs the free radical polymerization reaction. Therefore, besides SBMA grafting onto the surface, the homopolymerization in the coating solution has to be considered. In order to ensure the appropriate coating quality in continuous processing, the viscosity of the solution should be constantly monitored. Moreover, there are homopolymerization inhibitors



1. DBD in air (step 1) 2. Wet chemical treatment (step 2) 3. Rinsing 4. Drying

Figure 53: Modification of the feed spacer in a continuous process. DBD—dielectric barrier discharge.

recommended in the coating mixture.

Future studies. It is likely that feed water components, such as dissolved organics or ions, interact with the SBMA coating and influence its antifouling properties. For this reason, the feed water with different compositions should be used in the future fouling simulation experiments. For instance, water pretreatment with ion exchange could help to remove calcium and magnesium from the feed. In this case, the possible interactions coating-ions-bacteria would be excluded, and the anti-biofouling properties of the coating better evaluated.

The microorganisms will be always present in the industrial membrane systems. According to Hans-Curt Flemming, one of the well-known experts in the field of biofouling: "the basic idea is to live with biofilms and try to avoid the threshold when the biofouling takes place" [69]. Therefore, antifouling surface modification is beneficial, not only when the bacterial adhesion is reduced, but also if the biofilm cleaning is facilitated. It is possible that the hydrophilic SBMA coating promotes biofilm removal. Future studies should consider two-stage testing: (1) a *fouling stage*; where the feed channel pressure drop increase is monitored; and (2) a *cleaning stage*; where the biofilm is removed, for instance by introducing pressurized air to the system. This procedure would enable an assessment, whether the SBMA coating enhances biofilm detachment.

In the follow-up study, attempts should be made to improve coating homogeneity. For this purpose, the co-polymerization of SBMA with hydrophilic poly(ethylene glycol) diacrylate (PEGDA) can be proposed. The first experiments with SBMA/PEGDA coating mixtures have been already performed. The surface composition and morphology analyses indicated that the co-polymerization is a promising approach to increase surface coverage by the coating.

General summary. This thesis is another step forward in the chemical conditioning of the feed spacer surface for the antifouling purpose. The importance of continuous antifouling testing, under conditions representative for practice, has been shown. However, the question, whether the feed spacer coating is the most suitable antifouling strategy for the RO membrane module, remains still open and should be further explored.

References

- [1] H. S. Abid, D. J. Johnson, R. Hashaikeh, and N. Hilal. A review of efforts to reduce membrane fouling by control of feed spacer characteristics. *Desalination*, 420:384–402, 2017.
- [2] H. S. Abid, B. S. Lalia, P. Bertoncello, R. Hashaikeh, B. Clifford, D. T. Gethin, and N. Hilal. Electrically conductive spacers for self-cleaning membrane surfaces via periodic electrolysis. *Desalination*, 416:16 – 23, 2017.
- [3] LANXESS AG. Principles of Reverse Osmosis Membrane Separation- brochure, 2013.
- [4] LANXESS AG. Novel feed spacer technology towards enhanced RO element performance-brochure, 2016.
- [5] A. Allen, A. Semiao, O. Habimana, R. Heffernan, A. Safari, and E. Casey. Nanofiltration and reverse osmosis surface topographical heterogeneities: Do they matter for initial bacterial adhesion? *Journal of Membrane Science*, 486:10–20, 2015.
- [6] Z. Amjad. *Reverse osmosis: membrane technology, water chemistry and industrial applications*. New York: Van Nostrand Reinhold, 1993.
- [7] K. Andes, C. R. Bartels, E. Liu, and N. Sheehy. Methods for enhanced cleaning of fouled ro elements. In *The International Desalination Association World Congress on Desalination and Water Reuse*, 2013.
- [8] P.A. Araujo, J.C. Kruithof, M.C.M. Van Loosdrecht, and J.S. Vrouwenvelder. The potential of standard and modified feed spacers for biofouling control. *Journal of Membrane Science*, 403-404:58–70, 2012.
- [9] P.A. Araujo, D.J. Miller, P.B. Correia, M.C.M. van Loosdrecht, J.C. Kruithof, B.D. Freeman, D.R. Paul, and J.S. Vrouwenvelder. Impact of feed spacer and membrane modification by hydrophilic, bactericidal and biocidal coating on biofouling control. *Desalination*, 295:1–10, 2012.
- [10] A. N. Bach. On the role of peroxides in the processes of slow oxidation. *Zh Russ Phys-Chem Soc*, 29:373–395, 1987.
- [11] R. E. Baier. Surface behaviour of biomaterials: The theta surface for biocompatibility. *Journal of Materials Science: Materials in Medicine*, 17(11):1057–1062, 2006.
- [12] J. Baker, T. Stephenson, S. Dard, and P. Cote. Characterisation of fouling of nanofiltration membranes used to treat surface waters. *Environmental Technology*, 16(10):977–985, 1995.
- [13] J.S. Baker and L.Y. Dudley. Biofouling in membrane systems — a review. *Desalination*, 118(1):81 – 89, 1998.
- [14] R. W. Baker. *Membrane Technology and Applications*. John Wiley and Sons Ltd, 2012.

- [15] C.H. Bamford and J.C. Ward. The effect of the high-frequency discharge on the surfaces of solids. i—the production of surface radicals on polymers. *Polymer*, 2:277 – 293, 1961.
- [16] I. Banik, K. S.Kim, Y. I. Yun, D. H. Kim, C. M. Ryu, C. S. Park, G. S. Sur, and C. E. Park. A closer look into the behavior of oxygen plasma-treated high-density polyethylene. *Polymer*, 44(4):1163 – 1170, 2003.
- [17] G.; Briggs D. Beamson. *High Resolution XPS of Organic Polymers The Scienta ESCA300 Database*. John Wiley and Sons Ltd, 1992.
- [18] J.K. Beasley. The evaluation and selection of polymeric materials for reverse osmosis membranes. *Desalination*, 22(1):181–189, 1977.
- [19] L. S. De Bernardez, J. Ferrón, E. C Goldberg, and R. H. Buitrago. The effect of surface roughness on xps and aes. *Surface Science*, 139(2):541–548, 1984.
- [20] C. Berne, C. Ellison, A. Ducret, and Y. Brun. Bacterial adhesion at the single-cell level. *Nature Reviews Microbiology*, 16:616–627, 2018.
- [21] F. Beyer. Isolation and characterization of microorganism involved in membrane biofouling. Technical report, Wetsus, <https://www.wur.nl/en/show/Isolation-and-characterization-of-microorganism-involved-in-membrane-biofouling-1.htm>, 2019.
- [22] A. Bhattacharya and B.N. Misra. Grafting: a versatile means to modify polymers: Techniques, factors and applications. *Progress in Polymer Science*, 29(8):767 – 814, 2004.
- [23] S.N. Bhattacharyya and D. Maldas. Graft copolymerization onto cellulose. *Progress in Polymer Science*, 10(2):171 – 270, 1984.
- [24] H. S. Bisht and A. K. Chatterjee. Living free-radical polymerization —a review. *Journal of Macromolecular Science, Part C*, 41(3):139–173, 2001.
- [25] G. Borcia, C. A. Anderson, and N. M. D. Brown. The surface oxidation of selected polymers using an atmospheric pressure air dielectric barrier discharge. part i. *Applied Surface Science*, 221(1):203 – 214, 2004.
- [26] J. P. Borra, A. Valt, F. Arefi-Khonsari, and M. Tatoulian. Polymer surface processing by atmospheric pressure dbd for post-discharge grafting of washing-resistant functional coatings. In *THERMEC 2009*, volume 638 of *Materials Science Forum*, 2010.
- [27] R. Bos, H. C. van der Mei, and H. J. Busscher. Physicochemistry of initial microbial adhesive interactions-its mechanisms and methods for study. *FEMS Microbiology Reviews*, 23(2):179–230, 1999.
- [28] R. Brandenburg. Dielectric barrier discharges: progress on plasma sources and on the understanding of regimes and single filaments. *Plasma Sources Science and Technology*, 26(5):053001, 2017.
- [29] D. Briggs. *Surface Analysis of Polymers by XPS and Static SIMS*. Cambridge University Press, 1989.
- [30] A. M. Brzozowska, E. Spruijt, A. de Keizer, M. A. Cohen Stuart, and W. Norde. On the stability of the polymer brushes formed by adsorption of ionomer complexes on hydrophilic and hydrophobic surfaces. *Journal of Colloid and Interface Science*, 353(2):380 – 391, 2011.
- [31] H. J Busscher and A. H. Weerkamp. Specific and nonspecific interactions in bacterial adhesion to solid substrata. *FEMS Microbiology Review*, 46(2):165–173, 1987.

- [32] G. Buyle, J. Schneider, M. Walker, Y. Akishev, A. Napartovich, and M. Perucca. Plasma systems for surface treatment. In M. Perucca H. Rauscher and G. Buyle, editors, *Plasma Technology for Hyperfunctional Surfaces: Food, Biomedical, and Textile Applications*, chapter 2, pages 33–61. John Wiley & Sons, Ltd, 2010.
- [33] J. E. Cadotte. Interfacially synthesized reverse osmosis membrane, patent us4277344 a, July 1981.
- [34] J. E. Cadotte. Evolution of composite reverse osmosis membranes. *Materials Science of Synthetic Membranes*, (269):273–294, 1985.
- [35] D. Campoccia, L. Montanaro, and C. R. Arciola. A review of the biomaterials technologies for infection-resistant surfaces. *Biomaterials*, 34(34):8533 – 8554, 2013.
- [36] X. Cao, M. E. Pettit, S. L. Conlan, W. Wagner, A. D. Ho, A. S. Clare, J. A. Callow, M. E. Callow, M. Grunze, and A. Rosenhahn. Resistance of polysaccharide coatings to proteins, hematopoietic cells, and marine organisms. *Biomacromolecules*, 10(4):907–915, 2009.
- [37] M. Chaimberg and Y. Cohen. Kinetic modeling of free-radical graft polymerization. *AIChE Journal*, 40(2):294–311, 1994.
- [38] C.-M.; Weng L.-T Chan. Applications of x-ray photoelectron spectroscopy and static secondary ion mass spectrometry in surface characterization of copolymers and blends. *Reviews in Chemical Engineering*, 16(4):341–408, 2011.
- [39] C.-M.; Weng L.-T Chan. Surface characterization of polymer blends by xps and tof-sims. *Materials (Basel)*, 9(8):655–674, 2016.
- [40] Y. Chang, W. Chang, Y. J. Shih, T. C. Wei, and G.H. Hsiue. Zwitterionic sulfobetaine-grafted poly(vinylidene fluoride) membrane with highly effective blood compatibility via atmospheric plasma-induced surface copolymerization. *ACS applied materials & interfaces*, 3:1228–1237, 2011.
- [41] Y. Chang, S. Chen, Z. Zhang, and S. Jiang. Highly protein-resistant coatings from well-defined diblock copolymers containing sulfobetaines. *Langmuir*, 22(5):2222–2226, 2006.
- [42] Y. Chang, S.-C. Liao, A. Higuchi, R.-C. Ruaan, C.-W. Chu, and W.-Y. Chen. A highly stable nonbiofouling surface with well-packed grafted zwitterionic polysulfobetaine for plasma protein repulsion. *Langmuir*, 24(10):5453–5458, 2008.
- [43] Y. Chang, Y.-J. Shih, R.-C. Ruaan, A. Higuchi, W.-Y. Chen, and J.-Y. Lai. Preparation of poly(vinylidene fluoride) microfiltration membrane with uniform surface-copolymerized poly(ethylene glycol) methacrylate and improvement of blood compatibility. *Journal of Membrane Science*, 309(1):165 – 174, 2008.
- [44] Y. Chang, S.-H. Shu, Y.-J. Shih, C.-W. Chu, R.-C. Ruaan, and W.-Y. Chen. Hemocompatible mixed-charge copolymer brushes of pseudozwitterionic surfaces resistant to nonspecific plasma protein fouling. *Langmuir*, 26(5):3522–3530, 2010.
- [45] S. Chen, X. Lu, Y. Hu, and Q. Lu. Biomimetic honeycomb-patterned surface as the tunable cell adhesion scaffold. *Biomater. Sci.*, 3:85–93, 2015.
- [46] S. Chen, J. Zheng, L. Li, and S. Jiang. Strong resistance of phosphorylcholine self-assembled monolayers to protein adsorption. Insights into nonfouling properties of zwitterionic materials. *Journal of the American Chemical Society*, 127(41):14473–14478, 2005.

- [47] S.-H. Chen, Y. Chang, R. Lee, T.-C. Wei, A. Higuchi, F.-M. Ho, C.-C. Tsou, H.-T. Ho, and J.-Y. Lai. Hemocompatible control of sulfobetaine-grafted polypropylene fibrous membranes in human whole blood via plasma-induced surface zwitterionization. *Langmuir*, 28:17733–17742, 2012.
- [48] G. Cheng, Z. Zhang, S. Chen, J. D. Bryers, and S. Jiang. Inhibition of bacterial adhesion and biofilm formation on zwitterionic surfaces. *Biomaterials*, 28(29):4192–4199, 2007.
- [49] Y.-N. Chou, F. Sun, H.-C. Hung, P. Jain, A. Sinclair, P. Zhang, T. Bai, Y. Chang, T.-C. Wen, Q. Yu, and S. Jiang. Ultra-low fouling and high antibody loading zwitterionic hydrogel coatings for sensing and detection in complex media. *Acta Biomaterialia*, 40:31–37, 2016.
- [50] R. R. Choudhury, J. M. Gohil, S. Mohanty, and S. K. Nayak. Antifouling, fouling release and antimicrobial materials for surface modification of reverse osmosis and nanofiltration membranes. *J. Mater. Chem. A*, 6:313–333, 2018.
- [51] Hydranautics Nitto Group Company. Foulants and cleaning procedures for composite polyamide ro membrane elements. Technical Service Bulletin 107.24, Hydranautics, 401 Jones Rd. Oceanside, CA 92058, 2014.
- [52] C. Coury and A. M. Dillner. A method to quantify organic functional groups and inorganic compounds in ambient aerosols using attenuated total reflectance ftir spectroscopy and multivariate chemometric techniques. *Atmospheric Environment*, 42(23):5923–5932, 2008.
- [53] S.A. Creber, J.S. Vrouwenvelder, M.C.M. van Loosdrecht, and M.L. Johns. Chemical cleaning of biofouling in reverse osmosis membranes evaluated using magnetic resonance imaging. *Journal of Membrane Science*, 362(1):202–210, 2010.
- [54] N.-Y. Cui and N. M.D. Brown. Modification of the surface properties of a polypropylene (pp) film using an air dielectric barrier discharge plasma. *Applied Surface Science*, 189(1):31–38, 2002.
- [55] J. Dabrowski and H.-J. Muessig. *Silicon Surfaces and Formation of Interfaces*. WORLD SCIENTIFIC, 2000.
- [56] S. Daer, J. Kharraz, A. Giwa, and S. W. Hasan. Recent applications of nanomaterials in water desalination: A critical review and future opportunities. *Desalination*, 367:37–48, 2015.
- [57] A. Dazzi, R. Prazeres, F. Glotin, and J. M. Ortega. Local infrared microspectroscopy with subwavelength spatial resolution with an atomic force microscope tip used as a photothermal sensor. *Optics Letters*, 30(18):2388–2390, 2005.
- [58] A. J. de Kerchove and M. Elimelech. Calcium and magnesium cations enhance the adhesion of motile and nonmotile pseudomonas aeruginosa on alginate film. *Langmuir*, 24(7):3392–3399, 2008.
- [59] Rajesh Dorai and Mark J Kushner. A model for plasma modification of polypropylene using atmospheric pressure discharges. *Journal of Physics D: Applied Physics*, 36(6):666–685, 2003.
- [60] T. Dufour, J. Minnebo, S. Abou Rich, E. C. Neyts, A. Bogaerts, and F. Reniers. Understanding polyethylene surface functionalization by an atmospheric he/o₂ plasma through combined experiments and simulations. *Journal of Physics D: Applied Physics*, 47(22):224007–224019, 2014.

- [61] D. J. Dyer, J. Feng, C. Fivelson, R. Paul, R. Schmidt, and T. Zhao. Photoinitiated polymerization from self-assembled monolayers. In *Polymer Brushes: Synthesis, Characterization, Applications*, chapter 7, pages 129–150. John Wiley & Sons, Ltd, 2005.
- [62] M. Elimelech and W. Phillip. The future of seawater desalination: Energy, technology, and the environment. *Science*, 333:712–717, 2011.
- [63] M. Elimelech, X. Zhu, A. E. Childress, and S. Hong. Role of membrane surface morphology in colloidal fouling of cellulose acetate and composite aromatic polyamide reverse osmosis membranes. *Journal of Membrane Science*, 127(1):101–109, 1997.
- [64] C. Engler and W. Wild. Über die sogenannte, «aktivierung» des sauerstoffs und über superoxydbildung. *Berichte der deutschen chemischen Gesellschaft*, 30(2):1669–1681, 1897.
- [65] I. Eshet, V. Freger, R. Kasher, M. Herzberg, J. Lei, and M. Ulbricht. Chemical and physical factors in design of antibiofouling polymer coatings. *Biomacromolecules*, 12(7):2681–2685, 2011.
- [66] D. W. Fakes, J. M. Newton, J. F. Watts, and M. Edgell. Surface modification of a contact lens co-polymer by plasma-discharge treatments. *Surface and Interface Analysis*, 10(8):416–423, 1987.
- [67] N. M. Farhat, L. Javier, M. C. M. van Loosdrecht, J. C. Kruithof, and J. S. Vrouwenvelder. Role of feed water biodegradable substrate concentration on biofouling: Biofilm characteristics, membrane performance and cleanability. *Water Research*, 150:1 – 11, 2019.
- [68] H. C Flemming. Reverse osmosis membrane biofouling. *Experimental Thermal and Fluid Science*, pages 382–391, 1997.
- [69] H. C. Flemming. Biofouling in water systems – cases, causes and countermeasures. *Applied Microbiology and Biotechnology*, 59:629–640, 2002.
- [70] H. C. Flemming and J. Wingender. Biofilme — die bevorzugte lebensform der bakterien: Flocken, filme und schlämme. *Biologie in unserer Zeit*, 31:169–180, 2001.
- [71] H. C. Flemming and J. Wingender. The biofilm matrix. *Nature Reviews Microbiology*, 8:623–633, 2010.
- [72] M. Fletcher and G. I. Loeb. Influence of substratum characteristics on the attachment of marine pseudomonad to solid surfaces. *Applied and Environmental Microbiology*, 37(1):67–72, 1979.
- [73] Internation Organization for Standardization. Iso 4288:1996 Geometrical product specifications (gps) - Surface texture: Profile method- Rules and procedures for the assessment of surface texture. Technical report.
- [74] J. Friedrich. *The Plasma Chemistry of Polymer Surfaces*. Wiley-VCH Verlag GmbH & Co. KGaA, 2012.
- [75] J. Friedrich, M. Jabłońska, and G. Hidde. Plasma oxidation of polyolefins - course of o/c ratio from unmodified bulk to surface and finally to co₂ in the gas phase: A critical review. *Reviews of Adhesion and Adhesives*, 7(3):233–257, 2019.
- [76] J. Friedrich, S. Wettmarshausen, and M. Hennecke. Haloform plasma modification of polyolefin surfaces. *Surface and Coatings Technology*, 203(23):3647 – 3655, 2009.
- [77] C. Fritzmann, J. Löwenberg, T. Wintgens, and T. Melin. State-of-the-art of reverse osmosis desalination. *Desalination*, 216(1):1–76, 2007.

- [78] T. Furukawa, H. Sato, Y. Kita, K. Matsukawa, H. Yamaguchi, S. Ochiai, H. Siesler, and Y. Ozaki. Molecular structure, crystallinity and morphology of polyethylene/polypropylene blends studied by raman mapping, scanning electron microscopy, wide angle x-ray diffraction, and differential scanning calorimetry. *Polymer Journal*, 38:1127–1136, 2006.
- [79] K. E. Geckeler, R. Gebhardt, and H. Grünwald. Surface modification of polyethylene by plasma grafting with styrene for enhanced biocompatibility. *Naturwissenschaften*, 84:150–151, 1997.
- [80] G. Geesey, B. Wigglesworth-Cooksey, and K. Cooksey. Influence of calcium and other cations on surface adhesion of bacteria and diatoms: A review. *Biofouling*, 15(1-3):195–205, 2000.
- [81] A. Giwa, N. Akther, V. Dufour, and S. W. Hasan. A critical review on recent polymeric and nano-enhanced membranes for reverse osmosis. *RSC Adv.*, 6:8134–8163, 2016.
- [82] J. Glater, M.R. Zachariah, S.B. McCray, and J.W. McCutchan. Reverse osmosis membrane sensitivity to ozone and halogen disinfectants. *Desalination*, 48(1):1–16, 1983.
- [83] P.S. Goh, T. Matsuura, A.F. Ismail, and N. Hilal. Recent trends in membranes and membrane processes for desalination. *Desalination*, 391:43–60, 2016. Advances in Membrane Des: Keynotes from MEMDES 2-Singapore.
- [84] C. S. Gudipati, J. A. Finlay, J. A. Callow, M. E. Callow, and K. L. Wooley. The antifouling and fouling-release performance of hyperbranched fluoropolymer-poly(ethylene glycol) composite coatings evaluated by adsorption of biomacromolecules and the green fouling Alga Ulva. *Langmuir*, 21(7):3044–3053, 2005.
- [85] C. S. Gudipati, C. M. Greenlief, J. A. Johnson, P. Prayongpan, and K. L. Wooley. Hyperbranched fluoropolymer and linear poly(ethylene glycol) based amphiphilic crosslinked networks as efficient antifouling coatings. An insight into the surface compositions, topographies, and morphologies. *Journal of Polymer Science Part A: Polymer Chemistry*, 42(24):6193–6208, 2004.
- [86] G. Guillen and E. M. V. Hoek. Modeling the impacts of feed spacer geometry on reverse osmosis and nanofiltration processes. *Chemical Engineering Journal*, 149:221–231, 2009.
- [87] S. Guimond and M. R. Wertheimer. Surface degradation and hydrophobic recovery of polyolefins treated by air corona and nitrogen atmospheric pressure glow discharge. *Journal of Applied Polymer Science*, 94:1291–1303, 2004.
- [88] S. Guo, D. Jańczewski, X. Zhu, R. Quintana, T. He, and K. G. Neoh. Surface charge control for zwitterionic polymer brushes: Tailoring surface properties to antifouling applications. *Journal of Colloid and Interface Science*, 452:43 – 53, 2015.
- [89] M. He, K. Gao, L. Zhou, Z. Jiao, M. Wu, J. Cao, X. You, Z. Cai, Y. Su, and Z. Jiang. Zwitterionic materials for antifouling membrane surface construction. *Acta Biomaterialia*, 40:142 – 152, 2016.
- [90] H. Hillborg and U.W. Gedde. Hydrophobicity recovery of polydimethylsiloxane after exposure to corona discharges. *Polymer*, 39(10):1991 – 1998, 1998.
- [91] R. Hippler, H. Kersten, M. Schmidt, and K. H. Schoenbach. *Low temperature plasmas. Fundamentals, technologies, and techniques*, volume 2. Wiley-VCH Verlag GmbH & Co. KGaA, 2008.

- [92] T. Hirotsu. Graft polymerized membranes of methacrylic acid by plasma for water-ethanol permseparation. *Industrial & Engineering Chemistry Research*, 26(7):1287–1290, 1987.
- [93] T. Hirotsu. Effects of oxygen exposure on plasma graft polymerization of some hydrophilic monomers onto polypropylene films. *Journal of Macromolecular Science, Part A*, 33(11):1663–1674, 1996.
- [94] U. Hirsch, M. Rühl, N. Teuscher, and A. Heilmann. Antifouling coatings via plasma polymerization and atom transfer radical polymerization on thin film composite membranes for reverse osmosis. *Applied Surface Science*, 436:207 – 216, 2018.
- [95] A. A. Ismail, F. R. van de Voort, and J. Sedman. Fourier transform infrared spectroscopy: Principles and applications. In J.R.J. Paré and J.M.R. Bélanger, editors, *Instrumental Methods in Food Analysis*, volume 18 of *Techniques and Instrumentation in Analytical Chemistry*, chapter 4. Elsevier, 1997.
- [96] H. Iwata, A. Kishida, M. Suzuki, Y. Hata, and Y. Ikada. Oxidation of polyethylene surface by corona discharge and the subsequent graft polymerization. *Journal of Polymer Science: Part A: Polymer Chemistry*, 26:3309–3322, 1988.
- [97] M. Jabłońska, S. Reißaus, S. Henning, M. Menzel, A. Hähnel, J. Klehm, U. Hirsch, and A. Heilmann. From the surface to the bulk: a comparison of methods for the microanalysis of an immiscible polymer blend. *Micron*, 124:102685–102693, 2019.
- [98] M. Jabłońska, M. Menzel, U. Hirsch, and A. Heilmann. Assessment of anti-adhesion and anti-biofouling potential of plasma-mediated sulfobetaine methacrylate coatings of feed spacer. Submitted to *Desalination* (DES-2020-709).
- [99] J.-F. Jhong, A. Venault, C.-C. Hou, S.-H. Chen, T.-C. Wei, J. Zheng, J. Huang, and Y. Chang. Surface zwitterionization of expanded poly(tetrafluoroethylene) membranes via atmospheric plasma-induced polymerization for enhanced skin wound healing. *ACS Applied Materials & Interfaces*, 5(14):6732–6742, 2013.
- [100] S. Jiang, Y. Li, and B. P. Ladewig. A review of reverse osmosis membrane fouling and control strategies. *Science of The Total Environment*, 595:567–583, 2017.
- [101] N. Jidenko, M. Petit, and J.-P. Borra. Electrical characterization of microdischarges produced by dielectric barrier discharge in dry air at atmospheric pressure. *Journal of Physics D: Applied Physics*, 39:281–293, 2006.
- [102] R. Joshi, J. Friedrich, and M. Wagner. Role of hydrogen peroxide in selective oh group functionalization of polypropylene surfaces using underwater capillary discharge. *Journal of Adhesion Science and Technology*, 25:283–305, 2011.
- [103] M. R. Jung, F. D. Horgen, S. V. Orski, V. Rodriguez, K. L. Beers, G. H. Balazs, T. T. Jones, T. M. Work, K. C. Brignac, S.-J. Royer, K. D. Hyrenbach, B. A. Jensen, and J. M. Lynch. Validation of atr ft-ir to identify polymers of plastic marine debris, including those ingested by marine organisms. *Marine Pollution Bulletin*, 127:704 – 716, 2018.
- [104] A. J. Karabelas and D. C. Sioutopoulos. New insights into organic gel fouling of reverse osmosis desalination membranes. *Desalination*, 368:114–126, 2015.
- [105] K. Kato, E. Uchida, E.-T. Kang, Y. Uyama, and Y. Ikada. Polymer surface with graft chains. *Progress in Polymer Science*, 28(2):209 – 259, 2003.

- [106] M. T. Khan, M. Busch, V. G. Molina, A.-H. Emwas, C. Aubry, and J.-P. Croué. How different is the composition of the fouling layer of wastewater reuse and seawater desalination membranes? *Water Research*, 59:271–282, 2014.
- [107] M. T. Khan, C.-L. de Manes, C. Aubry, and J.-P. Croué. Source water quality shaping different fouling scenarios in a full-scale desalination plant at the red sea. *Water Research*, 47(2):558–568, 2013.
- [108] Y. C. Kim and M. Elimelech. Adverse impact of feed channel spacers on the performance of pressure retarded osmosis. *Environmental Science and Technology*, 46:4673–4681, 2012.
- [109] T. Klämpfl. *Cold atmospheric plasma decontamination against nosocomial bacteria*. PhD thesis, Technische Universität München, 2014.
- [110] R. Kleerebezem and M. C. M. van Loosdrecht. Mixed culture biotechnology for bioenergy production. *Current Opinion in Biotechnology*, 18(3):207 – 212, 2007.
- [111] V. Kochkodan and N. Hila. A comprehensive review on surface modified polymer membranes for biofouling mitigation. *Desalination*, 356:187–207, 2015.
- [112] U. Kogelschatz, B. Eliasson, and W. Egli. Dielectric-barrier discharges. principle and applications. *J. Phys. IV France*, 07:C4–47–C4–66, 1997.
- [113] R.-Q. Kou, Z.-K. Xu, H.-T. Deng, Z.-M. Liu, P. Seta, and Y. Xu. Surface modification of microporous polypropylene membranes by plasma-induced graft polymerization of alfa-allyl glucoside. *Langmuir*, 19(17):6869–6875, 2003.
- [114] J. Koubková, H. Macková, V. Proks, M. Trchová, J. Brus, and D. Horák. Raft of sulfobetaine for modifying poly(glycidyl methacrylate) microspheres to reduce nonspecific protein adsorption. *Journal of Polymer Science Part A: Polymer Chemistry*, 53(19):2273–2284, 2015.
- [115] K. Košutić, L. Kaštelan-Kunst, and B. Kunst. Porosity of some commercial reverse osmosis and nanofiltration polyamide thin-film composite membranes. *Journal of Membrane Science*, 168(1):101–108, 2000.
- [116] J. Kucera. *Reverse Osmosis Industrial Processes and Applications*. John Wiley & Sons, 2015.
- [117] G. Kühn, St. Weidner, R. Decker, A. Ghode, and J. Friedrich. Selective surface functionalization of polyolefins by plasma treatment followed by chemical reduction. *Surface and Coatings Technology*, 116-119:796 – 801, 1999.
- [118] W. Kun, L. Jian, R. Chunsheng, W. Dezhen, and W. Younian. Surface modification of polyethylene (PE) films using dielectric barrier discharge plasma at atmospheric pressure. *Plasma Science and Technology*, 10(4):433–437, 2008.
- [119] M. Kuzuya, S. Kondo, M. Sugito, and T. Yamashiro. Peroxy radical formation from plasma-induced surface radicals of polyethylene as studied by electron spin resonance. *Macromolecules*, 31(10):3230–3234, 1998.
- [120] M. Kuzuya, A. Noguchi, M. Ishikawa, A. Koide, K. Sawada, A. Ito, and N. Noda. Electron spin resonance study of free-radical formation and its decay of plasma-irradiated poly(methacrylic acid) and its esters. *The Journal of Physical Chemistry*, 95(6):2398–2403, 1991.

- [121] D.Y. Kwok and A.W. Neumann. Contact angle measurement and contact angle interpretation. *Advances in Colloid and Interface Science*, 81(3):167 – 249, 1999.
- [122] O.-J. Kwon, S. Tang, S.-W. Myung, N. Lu, and H.-S. Choi. Surface characteristics of polypropylene film treated by an atmospheric pressure plasma. *Surface and Coatings Technology*, 192(1):1 – 10, 2005.
- [123] M. Kyomoto, T. Moro, F. Miyaji, M. Hashimoto, H. Kawaguchi, Y. Takatori, K. Nakamura, and K. Ishihara. Effect of 2-methacryloyloxyethyl phosphorylcholine concentration on photoinduced graft polymerization of polyethylene in reducing the wear of orthopedic bearing surface. *Journal of Biomedical Materials Research Part A*, 86A(2):439–447, 2008.
- [124] R. Lalani and L. Liu. Synthesis, characterization, and electrospinning of zwitterionic poly(sulfobetaine methacrylate). *Polymer*, 52(23):5344 – 5354, 2011.
- [125] S. C. Lange, E. van Andel, M. M. J. Smulders, and H. Zuilhof. Efficient and tunable three-dimensional functionalization of fully zwitterionic antifouling surface coatings. *Langmuir*, 32(40):10199–10205, 2016.
- [126] W. Langenbeck and W. Pritzkow. Untersuchungen über den mechanismus der paraffinoxydation, 1. teil. *Fette, Seifen, Anstrichmittel*, 55(7):435–440, 1953.
- [127] I. Langmuir. Oscillations in ionized gases. *Proceedings of the National Academy of Sciences*, 14(8):627–637, 1928.
- [128] K. P. Lee, T. C. Arnot, and D. Mattia. A review of reverse osmosis membrane materials for desalination—development to date and future potential. *Journal of Membrane Science*, 370(1):1–22, 2011.
- [129] W. Lee, C. H. Ahn, S. Hong, S. Kim, S. Lee, Y. Baek, and J. Yoon. Evaluation of surface properties of reverse osmosis membranes on the initial biofouling stages under no filtration condition. *Journal of Membrane Science*, 351(1):112 – 122, 2010.
- [130] J. Lei and X. Liao. Surface graft copolymerization of acrylic acid onto ldpe film through corona discharge. *European Polymer Journal*, 37(4):771 – 779, 2011.
- [131] Lenntech. Chemical pretreatment for ro and nf. Technical Application Bulletin 111, Hydranautics Group, 2013.
- [132] F. Leroux, C. Campagne, A. Perwuelz, and L. Gengembre. Polypropylene film chemical and physical modifications by dielectric barrier discharge plasma treatment at atmospheric pressure. *Journal of Colloid and Interface Science*, 328(2):412 – 420, 2008.
- [133] S. C. Leterme, C. L. Lan, D. A. Hemraj, and A. V. Ellis. The impact of diatoms on the biofouling of seawater reverse osmosis membranes in a model cross-flow system. *Desalination*, 392:8–13, 2016.
- [134] J. A. Lichter, M. T. Thompson, M. Delgadillo, T. Nishikawa, M. F. Rubner, and K. J. van Vliet. Substrata mechanical stiffness can regulate adhesion of viable bacteria. *Biomacromolecules*, 9(6):1571–1578, 2008.
- [135] J.-H. Lin, Y.-J. Pan, C.-F. Liu, C.-L. Huang, C.-T. Hsieh, C.-K. Chen, Z.-I. Lin, and C.-W. Lou. Preparation and compatibility evaluation of polypropylene/high density polyethylene polyblends. *Materials*, 8(12):8850–8859, 2015.
- [136] S. Loeb and S. Sourirajan. Sea water demineralization by means of an osmotic membrane. *Advances in Chemistry*, 38:117–132, 1963.

- [137] D. López, H. Vlamakis, and R. Kotler. Biofilms. *Cold Spring Harbor Perspectives in Biology*, pages 1–11, 2010.
- [138] A. B. Lowe and C. L. McCormick. Synthesis and solution properties of zwitterionic polymers. *Chemical Reviews*, 102(11):4177–4190, 2002.
- [139] J. R. MacCallum and C. T. Rankin. A novel method for modifying surfaces. *Journal of Polymer Science Part B: Polymer Letters*, 9(10):751–752, 1971.
- [140] K.-E. Magnusson. Physicochemical properties of bacterial surface. *Biochemical Society Transactions*, 17(3):454–458, 1989.
- [141] K.C. Marshall, R. Stout, and R. Mitchell. Mechanism of the initial events in the sorption of marine bacteria to surfaces. *Journal of General Microbiology*, 68:337–348, 1971.
- [142] P. Mary, D. D. Bendejacq, M.-P. Labeau, and P. Dupuis. Reconciling low- and high-salt solution behavior of sulfobetaine polyzwitterions. *The Journal of Physical Chemistry B*, 111(27):7767–7777, 2007.
- [143] F. Massines, G. Gouda, Nicolas Gherardi, M. Duran, and E. Croquesel. The role of dielectric barrier discharge atmosphere and physics on polypropylene surface treatment. *Plasmas and Polymers*, 6:35–49, 2001.
- [144] A. Matin, Z. Khan, S. M. J. Zaidi, and M. C. Boyce. Biofouling in reverse osmosis membranes for seawater desalination: Phenomena and prevention. *Desalination*, 281:1–16, 2011.
- [145] K. Matyjaszewski and J. Spanswick. Controlled/living radical polymerization. *Materials Today*, 8(3):26 – 33, 2005.
- [146] E. W. McAllister, L. C. Carey, P. G. Brady, R. Heller, and S. G. Kovacs. The role of polymeric surface smoothness of biliary stents in bacterial adherence, biofilm deposition, and stent occlusion. *Gastrointestinal Endoscopy*, 39(3):422–425, 1993.
- [147] L. Mei, H. J. Busscher, H.C. van der Mei, and Y. Ren. Influence of surface roughness on streptococcal adhesion forces to composite resins. *Dental Materials*, 27(8):770–778, 2011.
- [148] L. Mi and S. Jiang. Integrated antimicrobial and nonfouling zwitterionic polymers. *Angewandte Chemie International Edition*, 53:1746–1754, 2014.
- [149] G. H. Michler. *Atlas of Polymer Structures: Morphology, Deformation and Fracture Structures*. Carl Hanser Carl Hanser Verlag, 2016.
- [150] D. Mileva, D. Tranchida, and M. Gahleitner. Designing polymer crystallinity: An industrial perspective. *Polymer Crystallization*, 1(2), 2018.
- [151] D. J. Miller, P. A. Araújo, P. B. Correia, M. M. Ramsey, J. C. Kruithof, M. C. M. van Loosdrecht, B. D. Freeman, D. R. Paul, M. Whiteley, and J. S. Vrouwenvelder. Short-term adhesion and long-term biofouling testing of polydopamine and poly(ethylene glycol) surface modifications of membranes and feed spacers for biofouling control. *Water Research*, 46(12):3737 – 3753, 2012.
- [152] T. Miyasaka, T. Ikemoto, and T. Kohno. Tof-sims imaging of pe/pp polymer using multivariate analysis. *Applied Surface Science*, 255(4):1576 – 1579, 2008.
- [153] S. Morsch, Y. Liu, S. B. Lyon, and S. R. Gibbon. Insights into epoxy network nanostructural heterogeneity using afm-ir. *ACS Applied Materials & Interfaces*, 8(1):959–966, 2016.

- [154] P. Munk and T. M. Aminabhavi. *Introduction to macromolecular science*. - 2nd ed. John Wiley & Sons, Inc., 2002.
- [155] O. Nedela, P. Slepicka, and V. Svorcik. Surface modification of polymer substrates for biomedical applications. *Materials*, 10:1115, 2017.
- [156] H. Y. Ng and M. Elimelech. Influence of colloidal fouling on rejection of trace organic contaminants by reverse osmosis. *Journal of Membrane Science*, 244(1):215–226, 2004.
- [157] H.-Y. Nie. Negative hydrocarbon species C₂nH⁻: How useful can they be? *Journal of Vacuum Science & Technology B*, 34(3):030603, 2016.
- [158] E. R. Nightingale. Phenomenological theory of ion solvation. effective radii of hydrated ions. *The Journal of Physical Chemistry*, 63(9):1381–1387, 1959.
- [159] A. G. Nurioglu, A. C. Esteves, and G. With. Non-toxic, non-biocide-release antifouling coatings based on molecular structure design for marine applications. *J. Mater. Chem. B*, 3:6547–6570, 2015.
- [160] L.-A. O’Hare, S. Leadley, and B. Parbhoo. Surface physicochemistry of corona discharge treated polypropylene film. *Surface and Interface Analysis*, 33:335–342, 2002.
- [161] R. H. Olley, A. M. Hodge, and D. C. Bassett. A permanganic etchant for polyolefines. *Journal of Polymer Science: Polymer Physics Edition*, 17:627–643, 1979.
- [162] P. Ommen, N. Zobek, and R. L. Meyer. Quantification of biofilm biomass by staining: Non-toxic safranin can replace the popular crystal violet. *Journal of Microbiological Methods*, 141:87 – 89, 2017.
- [163] World Health Organization and United Nations Childrens’ Fund. Progress on drinking water, sanitation and hygiene: 2017 update and SDG baselines. Technical report, 2017.
- [164] E. Ostuni, R. G. Chapman, M. N. Liang, G. Meluleni, G. Pier, D. E. Ingber, and G. M. Whitesides. Self-assembled monolayers that resist the adsorption of proteins and the adhesion of bacterial and mammalian cells. *Langmuir*, 17(20):6336–6343, 2001.
- [165] T. Ougizawa and T. Inoue. Morphology of polymer blends. In L. A. Utracki and C. A. Wilkie, editors, *Polymer Blends Handbook*, pages 875–918. Springer Netherlands, 2014.
- [166] R. M. Overney, R. Luthi, H. Haefke, J. Frommer, E. Meyer, H. J. Guntherodt, S. Hild, and J. Fuhrmann. An atomic force microscopy study of corona-treated polypropylene films. *Applied Surface Science*, 64:197–203, 1993.
- [167] G. K. Pang, K. Z. Baba-Kishi, and A. Patel. Topographic and phase-contrast imaging in atomic force microscop. *Ultramicroscopy*, 81(2):35 – 40, 2000.
- [168] M. Pasmore, P. Todd, B. Pfeifer, M. Rhodes, and C. N. Bowman. Effect of polymer surface properties on the reversibility of attachment of pseudomonas aeruginosa in the early stages of biofilm development. *Biofouling*, 18(1):65–71, 2002.
- [169] M. Perucca. Introduction to plasma and plasma technology. In H. Rauscher, M. Perucca, and G. Buyle, editors, *Plasma Technology for Hyperfunctional Surfaces: Food, Biomedical, and Textile Applications*, pages 1–32. John Wiley & Sons, Ltd, 2010.
- [170] J. M. Pochan, L. J. Gerenser, and J. F. Elman. An e.s.c.a. study of the gas-phase derivatization of poly(ethylene terephthalate) treated by dry-air and dry-nitrogen corona discharge. *Polymer*, 27(7):1058 – 1062, 1986.

- [171] F. Poncin-Epaillard, J. C. Brosse, and T. Falher. Cold plasma treatment: surface or bulk modification of oolymer films? *Macromolecules*, 30(15):4415–4420, 1997.
- [172] S. G. Prasad, A. De, and U. De. Structural and optical investigations of radiation damage in transparent pet polymer films. *International Journal of Spectroscopy*, 2011:1–7, 2011.
- [173] N. Recek, M. Jaganjac, M. Kolar, L. Milkovic, M. Mozetič, K. Stana-Kleinschek, and A. Vesel. Protein adsorption on various plasma-treated polyethylene terephthalate substrates. *Molecules*, 18(10):12441–12463, 2013.
- [174] J. A. Redman, S. L. Walker, and M. Elimelech. Bacterial Adhesion and Transport in Porous Media: Role of the Secondary Energy Minimum. *Environmental Science & Technology*, 38(6):1777–1785, 2004.
- [175] C. E. Reid and E. J. Breton. Water and ion flow across cellulosic membranes. *Journal of Applied Polymer Science*, 1:133–143, 1959.
- [176] K. Reid, M. Dixon, C. Pelekani, K. Jarvis, M. Willis, and Y. Yu. Biofouling control by hydrophilic surface modification of polypropylene feed spacers by plasma polymerisation. *Desalination*, 335(1):108–118, 2014.
- [177] C.-S. Ren, K. Wang, Q.-Y. Nie, D.-Z. Wang, and S.-H. Guo. Surface modification of pe film by dbd plasma in air. *Applied Surface Science*, 255(5):3421 – 3425, 2008.
- [178] H. Richard. *Development of low-biofouling polypropylene feed spacers for reverse osmosis*. PhD thesis, The University of Toledo, 2011.
- [179] S. Richter. *Korrelationen von Plasma- und Materialparametern zur Kontrolle des industriellen Atmosphärendruck-Plasmaprozesses*. PhD thesis, Martin-Luther-Universität Halle-Wittenberg, 2014.
- [180] A. Ronen, R. Semiat, and C. G. Dosoretz. Impact of zno embedded feed spacer on biofilm development in membrane systems. *Water Research*, 47(17):6628 – 6638, 2013.
- [181] D. Ryklin and T. Silich. Investigation of fibres migration in cotton/polypropylene blended yarn. *Materials Science*, 20(3):301–305, 2014.
- [182] J. E. Sader, J. W. M. Chon, and P. Mulvaney. Calibration of rectangular atomic force microscope cantilevers. *Review of Scientific Instruments*, 70(10):3967–3969, 1999.
- [183] J. J. Sadhwani and J. M. Veza. Cleaning tests for seawater reverse osmosis membranes. *Desalination*, 139(1):177–182, 2001.
- [184] N. Saha, C. Monge, V. Dulong, C. Picart, and K. Glinel. Influence of polyelectrolyte film stiffness on bacterial growth. *Biomacromolecules*, 14(2):520–528, 2013.
- [185] H. Sano, T. Usami, and H. Nakagawa. Lamellar morphologies of melt-crystallized polyethylene, isotactic polypropylene and ethylene-propylene copolymers by the ruo4 staining technique. *Polymer*, 27(10):1497 – 1504, 1986.
- [186] M. G. Santonicola, M. Memesa, A. Meszyńska, Y. Ma, and G. J. Vancso. Surface-grafted zwitterionic polymers as platforms for functional supported phospholipid membranes. *Soft Matter*, 8:1556–1562, 2012.
- [187] A. Savitzky and M. J. E. Golay. Smoothing and differentiation of data by simplified least squares procedures. *Analytical Chemistry*, 36(8):1627–1639, 1964.

- [188] S. Saxena, A. Ray, and B. Gupta. Graft polymerization of acrylic acid onto polypropylene monofilament by rf plasma. *Journal of Applied Polymer Science*, 116:2884 – 2892, 2010.
- [189] J. B. Schlenoff. Zwitteration: coating surfaces with zwitterionic functionality to reduce nonspecific adsorption. *Langmuir*, 30(32):9625–9636, 2014.
- [190] E. Schönemann, A. Laschewsky, and A. Rosenhahn. Exploring the long-term hydrolytic behavior of zwitterionic polymethacrylates and polymethacrylamides. *Polymers*, 10(6):639–661, 2018.
- [191] Inc. Schweitzer-Mauduit International (SWM). Swm portfolio. Technical report, Schweitzer-Mauduit International, Inc., 2017.
- [192] S. S. Shenvi, A. M. Isloor, and A.F. Ismail. A review on ro membrane technology: Developments and challenges. *Desalination*, 368:10–26, 2015.
- [193] A. Siddiqui, S. Lehmann, S. S. Bucs, M. Fresquet, L. Fel, E. I.E. C. Prest, J. Ogier, C. Schellenberg, M. C. M. van Loosdrecht, J. C. Kruithof, and J. S. Vrouwenvelder. Predicting the impact of feed spacer modification on biofouling by hydraulic characterization and biofouling studies in membrane fouling simulators. *Water Research*, 110:281 – 287, 2017.
- [194] N. Siebrath, N. Farhat, W. Ding, J. Kruithof, and J. S. Vrouwenvelder. Impact of membrane biofouling in the sequential development of performance indicators: Feed channel pressure drop, permeability, and salt rejection. *Journal of Membrane Science*, 585:199–207, 2019.
- [195] W. V. Siemens. Ozone production in an atmospheric-pressure dielectric barrier discharge. *Annalen der Chemie und Physik*, 102(66), 1857.
- [196] M. Šimor and Y. Creighton. Treatment of polymer surfaces with surface dielectric barrier discharge plasmas. In M. Thomas and K. Mittal, editors, *Atmospheric Pressure Plasma Treatment of Polymers*, pages 27–81. John Wiley & Sons, Ltd, 2013.
- [197] M.-C. Sin, Y.-M. Sun, and Y. Chang. Zwitterionic-based stainless steel with well-defined polysulfobetaine brushes for general bioadhesive control. *ACS Applied Materials & Interfaces*, 6(2):861–873, 2014.
- [198] F. Song, H. Koo, and D. Ren. Effects of material properties on bacterial adhesion and biofilm formation. *Journal of Dental Research*, 94(8):1027–1034, 2015.
- [199] F. Song and D. Ren. Stiffness of cross-linked poly(dimethylsiloxane) affects bacterial adhesion and antibiotic susceptibility of attached cells. *Langmuir*, 30(34):10354–10362, 2014.
- [200] T. A. Sonia and C. P. Sharma. Polymers in oral insulin delivery. In *Oral Delivery of Insulin*, pages 257–310. Woodhead Publishing, 2014.
- [201] P. Stoodley, K. Sauer, D. G. Davies, and J. W. Costerton. Biofilm as complex differentiated communities. *Annual Review of Microbiology*, pages 187– 206, 2002.
- [202] S. Storp. Radiation damage during surface analysis. *Spectrochimica Acta Part B: Atomic Spectroscopy*, 40(5):745 – 756, 1985.
- [203] M. Strobel, C. Dunatov, J. M. Strobel, C. S. Lyons, S. J. Perron, and M. C. Morgen. Low-molecular-weight materials on corona-treated polypropylene. *Journal of Adhesion Science and Technology*, 3(1):321–335, 1989.

- [204] M. Strobel, V. Jones, C. Lyons, M. Ulsh, M. Kushner, R. Dorai, and M. Branch. A comparison of corona-treated and flame-treated polypropylene films. *Plasmas and Polymers*, 8(1):61–95, 2003.
- [205] M. Strobel, S. M. Kirk, L. Heinzen, E. Mischke, C. S. Lyons, J. Endle, D. Poirier, and G. Dillingham. Contact angle measurements on oxidized polymer surfaces containing water-soluble species. *Journal of Adhesion Science and Technology*, 29(14):1483–1507, 2015.
- [206] M. Strobel and C. S. Lyons. The role of low-molecular-weight oxidized materials in the adhesion properties of corona-treated polypropylene film. *Journal of Adhesion Science and Technology*, 17(1):15–23, 2003.
- [207] M. Strobel, M. J. Walzak, J. M. Hill, A. Lin, E. Karbasheski, and C. S. Lyons. A comparison of gas-phase methods of modifying polymer surfaces. *Journal of Adhesion Science and Technology*, 9(3):365–383, 1995.
- [208] M. Suzuki, A. Kishida, H. Iwata, and Y. Ikada. Graft copolymerization of acrylamide onto a polyethylene surface pretreated with glow discharge. *Macromolecules*, 19(7):1804–1808, 1986.
- [209] R. L. Taylor, J. Verran, G. C. Lees, and A. J. P. Ward. The influence of substratum topography on bacterial adhesion to polymethyl methacrylate. *Journal of Materials Science: Materials in Medicine*, 9(1):17–22, 1998.
- [210] C. Tendero, C. Tixier, P. Tristant, J. Desmaison, and P. Leprince. Atmospheric pressure plasmas: A review. *Spectrochimica Acta Part B: Atomic Spectroscopy*, 61(1):2 – 30, 2006.
- [211] T. Tran, B. Bolto, S. Gray, M. Hoang, and E. Ostarcevic. An autopsy study of a fouled reverse osmosis membrane element used in a brackish water treatment plant. *Water Research*, 41(17):3915 – 3923, 2007.
- [212] H. H. Tuson and D. B. Weibel. Bacteria–surface interactions. *Soft Matter*, 9:4368–4380, 2013.
- [213] M. Ulbricht. Advanced functional polymer membranes. *Polymer*, 47(7):2217 – 2262, 2006.
- [214] Y. Uyama, H. Inoue, K. Ito, A. Kishida, and Y. Ikada. Comparison of different methods for contact angle measurement. *Journal of Colloid and Interface Science*, 141(1):275 – 279, 1991.
- [215] D. W. van Krevelen. *Properties of Polymers, Their Correlation with Chemical Structure; their Numerical Estimation and Prediction from Additive Groups Contributions*, 4th edition. Elsevier Science, 2009.
- [216] J. A.M. van Paassen, J. C. Kruithof, S. M. Bakker, and F. S. Kegel. Integrated multi-objective membrane systems for surface water treatment: pre-treatment of nanofiltration by riverbank filtration and conventional ground water treatment. *Desalination*, 118(1):239 – 248, 1998.
- [217] A. Venault, C.-W. Huang, J. Zheng, A. Chinnathambi, S. A. Alharbi, Y. Chang, and Y. Chang. Hemocompatible biomaterials of zwitterionic sulfobetaine hydrogels regulated with ph-responsive dmaema random sequences. *International Journal of Polymeric Materials and Polymeric Biomaterials*, 65(2):65–74, 2016.
- [218] M. C. M. von Loosdrecht. *Bacterial Adhesion*. PhD thesis, Agricultural University Wageningen, Netherlands, 1988.

- [219] J. S. Vrouwenvelder. *Biofouling of spiral wound membrane systems*. PhD thesis, Del University of Technology, 2009.
- [220] J. S. Vrouwenvelder, C. Hinrichs, W. G. J. van der Meer, M. C. M. van Loosdrecht, and J. C. Kruithof. Pressure drop increase by biofilm accumulation in spiral wound ro and nf membrane systems: role of substrate concentration, flow velocity, substrate load and flow direction. *Biofouling*, 25(6):543–555, 2009.
- [221] J. S. Vrouwenvelder, J. A. M. van Paassen, J. C. Kruithof, and M. C. M. van Loosdrecht. Sensitive pressure drop measurements of individual lead membrane elements for accurate early biofouling detection. *Journal of Membrane Science*, 338(1):92 – 99, 2009.
- [222] J. S. Vrouwenvelder, J. A. M. van Paassen, L. P. Wessels, A. F. van Dam, and S. M. Bakker. The membrane fouling simulator: A practical tool for fouling prediction and control. *Journal of Membrane Science*, 281(1):316 – 324, 2006.
- [223] J. S. Vrouwenvelder, D. A. Graf von der Schulenburg, J. Kruithof, M. Johns, and M. C. M. van Loosdrecht. Biofouling of spiral-wound nanofiltration and reverse osmosis membranes: a feed spacer problem. *Water Research*, 43:583–594, 2009.
- [224] J. Wang, X. Liu, and H.-S. Choi. Graft copolymerization kinetics of acrylic acid onto the poly(ethylene terephthalate) surface by atmospheric pressure plasma inducement. *Journal of Polymer Science Part B: Polymer Physics*, 46(15):1594–1601, 2008.
- [225] P. E. West. *Introduction to Atomic Force Microscopy. Theory, Practice, Applications*. P. West, 2006.
- [226] Y. Wibisono, W. Yandi, M. Golabi, R. Nugraha, E. Cornelissen, A. Kemperman, T. Ederth, and K. Nijmeijer. Hydrogel-coated feed spacers in two-phase flow cleaning in spiral wound membrane elements: A novel platform for eco-friendly biofouling mitigation. *Water Research*, 71:171 – 186, 2015.
- [227] G. Wietzel. Herstellung synthetischer fettsäuren durch oxydation von paraffinischen kohlenwasserstoffen mit kolekularem sauerstoff. *Chemical Engineering Science*, 3:17–30, 1954.
- [228] M. C. Willbert. Enhancement of membrane fouling resistance through surface modification. water treatment technology program report no. 22. Technical report, UNITED STATES DEPARTMENT OF THE INTERIOR, 1997.
- [229] J. Wu, W. Lin, Z. Wang, S. Chen, and Y. Chang. Investigation of the hydration of non-fouling material poly(sulfobetaine methacrylate) by low-field nuclear magnetic resonance. *Langmuir*, 28(19):7436–7441, 2012.
- [230] L. Xu, Z. Fang, P. Song, and M. Peng. Surface-initiated graft polymerization on multiwalled carbon nanotubes pretreated by corona discharge at atmospheric pressure. *Nanoscale*, 2:389–393, 2010.
- [231] W. Yandi, S. Mieszkin, A. di Fino, P. M. Tanchereau, M. E. Callow, J. A. Callow, L. Tyson, A. S. Clare, and T. Ederth. Charged hydrophilic polymer brushes and their relevance for understanding marine biofouling. *Biofouling*, 32(6):609–625, 2016.
- [232] H.-L. Yang, J. C.-T. Lin, and C. Huang. Application of nanosilver surface modification to ro membrane and spacer for mitigating biofouling in seawater desalination. *Water Research*, 43(15):3777 – 3786, 2009.

- [233] L.-S.; Xu; Z.-K. Yang, Y.-F.; Wan. Surface engineering of microporous polypropylene membrane for antifouling: A mini-review. *Journal of Adhesion Science and Technology*, 25(1-3):245–260, 2011.
- [234] R. Yang, E. Goktekin, and K. K. Gleason. Zwitterionic antifouling coatings for the purification of high-salinity shale gas produced water. *Langmuir*, 31(43):11895–11903, 2015.
- [235] W. Yang, S. Chen, G. Cheng, H. Vaisocherová, H. Xue, W. Li, J. Zhang, and S. Jiang. Film thickness dependence of protein adsorption from blood serum and plasma onto poly(sulfobetaine)-grafted surfaces. *Langmuir*, 24(17):9211–9214, 2008.
- [236] Y.-F. Yang, Y. Li, Q.-L. Li, L.-S. Wan, and Z.-K. Xu. Surface hydrophilization of microporous polypropylene membrane by grafting zwitterionic polymer for anti-biofouling. *Journal of Membrane Science*, 362(1):255 – 264, 2010.
- [237] Z. Yang, D. Saeki, and H. Matsuyama. Zwitterionic polymer modification of polyamide reverse-osmosis membranes via surface amination and atom transfer radical polymerization for anti-biofouling. *Journal of Membrane Science*, 550:332 – 339, 2018.
- [238] T. Yasuda, T. Okuno, K. Yoshida, and H. Yasuda. A study of surface dynamics of polymers. ii. investigation by plasma surface implantation of fluorine-containing moieties. *Journal of Polymer Science Part B: Polymer Physics*, 26(8):1781–1794, 1988.
- [239] L. Ye, Y. Zhang, Q. Wang, X. Zhou, B. Yang, F. Ji, D. Dong, L. Gao, Y. Cui, and F. Yao. Physical cross-linking starch-based zwitterionic hydrogel exhibiting excellent biocompatibility, protein resistance, and biodegradability. *ACS Applied Materials & Interfaces*, 8(24):15710–15723, 2016.
- [240] H. E. Yener. Antifouling coating of polymer films combining plasma treatment and wet chemical methods. Master’s thesis, Martin Luther University of Halle-Wittenberg, Faculty of Natural Science II, 2017.
- [241] H.-Y. Yu, L.-Q. Liu, Z.-Q. Tang, M.-G. Yan, J.-S. Gu, and X.-W. Wei. Surface modification of polypropylene microporous membrane to improve its antifouling characteristics in an smbr: Air plasma treatment. *Journal of Membrane Science*, 311(1):216 – 224, 2008.
- [242] Y. Yuan, M. P. Hays, R. Hardwidge, and J. Kim. Surface characteristics influencing bacterial adhesion to polymeric substrates. *RSC Advances*, 7:14254–14261, 2017.
- [243] R. Zhang, Y. Liu, M. He, Y. Su, X. Zhao, M. Elimelech, and Z. Jiang. Antifouling membranes for sustainable water purification: strategies and mechanisms. *Chem. Soc. Rev.*, 45:5888–5924, 2016.
- [244] X. Zhang, L. Wang, and E. Levanen. Superhydrophobic surfaces for the reduction of bacterial adhesion. *RSC Advances*, 3:12003–12020, 2013.
- [245] Z. Zhang, T. Chao, L. Liu, G. Cheng, B. D. Ratner, and S. Jiang. Zwitterionic hydrogels: an in vivo implantation study. *Journal of Biomaterials Science, Polymer Edition*, 20(13):1845–1859, 2009.
- [246] C. Zhao, L. Li, Q. Wang, Q. Yu, and J. Zheng. Effect of film thickness on the antifouling performance of poly(hydroxy-functional methacrylates) grafted surfaces. *Langmuir*, 27(8):4906–4913, 2011.
- [247] K. Zheng, R. Liu, and Y. Huang. A two-dimensional ir correlation spectroscopic study of the conformational changes in syndiotactic polypropylene during crystallization. *Polymer Journal*, 42:81–85, 2010.

- [248] H. Zhou and G.L. Wilkes. Comparison of lamellar thickness and its distribution determined from d.s.c., saxs, tem and afm for high-density polyethylene films having a stacked lamellar morphology. *Polymer*, 38(23):5735 – 5747, 1997.
- [249] Q. Zia and R. Androsch. Effect of atomic force microscope tip geometry on the evaluation of the crystal size of semicrystalline polymers. *Measurement Science and Technology*, 20(9):097003, 2009.
- [250] Q. Zia, D. Mileva, and R. Androsch. Rigid amorphous fraction in isotactic polypropylene. *Macromolecules*, 41(21):8095–8102, 2008.

Abbreviations

AFM	atomic force microscopy
AIBN	2,2'-Azobis(2-methylpropionitrile)
ATD	anti-telescoping devices
ATR	attenuated total reflectance
au	atomic units
BV	ball valve
BVC	check valve
CA	cellulose acetate
CCD	charge-coupled device
CFU	colony-forming unit
DBD	dielectric barrier discharge
DMAEMA	2-(Dimethylamino)ethyl methacrylate
DMSO	dimethyl sulfoxide
DSC	differential scanning calorimetry
E	elastic modulus
e.g.	exempli gratia, for example
EPS	extracellular polymeric substance
et. al	et alia, and others
FCPD	feed channel pressure drop
FRP	free radical polymerization
FS	fouling simulation cell
FTIR	Fourier-transform infrared spectroscopy
gfp	green fluorescent protein
GPC	gel permeation chromatography
HAVB	hyaluronic acid derivative grafted with vinylbenzyl groups
HBFP	hyperbranched fluoropolymer
HDPE	high-density polyethylene
HEMA	2-Hydroxyethyl methacrylate
IR	infrared
LMWOM	low-molecular-weight oxidized material
M_n	number-average molecular weight
M_w	weight-average molecular weight
MeFoS	membrane fouling simulator
MFI	melt flow index

MPC	2-Methacryloyloxyethyl phosphorylcholine
mPDA	m-Phenylenediamine
NMR	nuclear magnetic resonance
non-LTE	non-local-thermodynamic equilibrium
OD	optical density
PA	polyamide
PAA	poly(acrylic acid)
PAH	poly(allylamine hydrochloride)
PDA	polydopamine
PDI	polydispersity index
PDMS	polydimethylsiloxane
PE	polyethylene
PEG	poly(ethylene glycol)
PEGDA	poly(ethylene glycol) diacrylate
PET	polyethylene terephthalate
PL	plasma treatment with dielectric barrier discharge in air; A, B, C indicate different energy dose
PLL	poly(L-lysine)
PMMA	poly(methyl methacrylate)
PP	polypropylene
PS	polysulfone
PP	polypropylene
PTFE	poly(tetrafluoroethylene)
PVC	polyvinyl chloride
PVDF	polyvinylidene fluoride
R _a	roughness average, arithmetic mean deviation of the profile over the sampling length
R _z	ten-point average roughness, average value of the five highest peaks and the five deepest valleys over the sampling length
RI	refractive index
RO	reverse osmosis
SBMA	sulfobetaine methacrylate, [2-(Methacryloyloxy)ethyl]dimethyl-(3-sulfopropyl)ammonium hydroxide
SDBD	surface dielectric barrier discharge
SDBS	sodium dodecylbenzene sulfonate
SEM	scanning electron microscopy

SFE	surface free energy
SI-ATRP	surface-initiated atom transfer radical polymerization
SPMA	3-Sulfopropyl methacrylate potassium salt
TEM	transmission electron microscopy
TFC	thin-film composite
TMC	1,3,5-Benzenetricarbonyl trichloride
ToF-SIMS	time-of-flight secondary ion mass spectrometry
UV-Vis	ultraviolet-visible
VDBD	volume dielectric barrier discharge
VOC	volatile organic compound
VUV	vacuum ultraviolet
WCA	water contact angle
WHO	World Health Organization
XPS	X-ray photoelectron spectroscopy

List of chemicals

Plasma treatment

<u>Chemical</u>	<u>CAS-Nr.</u>	<u>Supplier</u>
acetone	67-63-0	Sigma-Aldrich Chemie GmbH
sulfur dioxide (SO ₂)	10114005	Air Liquide

Wet coating

<u>Chemical</u>	<u>CAS-Nr.</u>	<u>Supplier</u>
[2-(Methacryloyloxy)ethyl dimethyl-(3-sulfopropyl) ammonium hydroxide	3637-26-1	Sigma-Aldrich Chemie GmbH
2-(Dimethylamino)ethyl methacrylate	2867-47-2	Sigma-Aldrich Chemie GmbH
poly(ethylene glycol) diacrylate (M _n =575)	26570-48-9	Sigma-Aldrich Chemie GmbH
sodium chloride (NaCl)	231-598-3	Carl Roth GmbH + Co. KG
sodium hydroxide (NaOH)	215-185-5	Carl Roth GmbH + Co. KG
sulfuric acid (H ₂ SO ₄)	7664-93-9	VWR International GmbH

Biofouling tests

<u>Chemical</u>	<u>CAS-Nr.</u>	<u>Supplier</u>
isopropanol	67-63-0	VWR International GmbH
CASO	459290265	Carl Roth GmbH + Co. KG
sodium phosphate monobasic (NaH ₂ PO ₄)	7558-80-7	Sigma-Aldrich Chemie GmbH
sodium nitrate (NaNO ₃)	7631-99-4	Sigma-Aldrich Chemie GmbH
sodium acetate (CH ₃ COONa)	127-09-3	Sigma-Aldrich Chemie GmbH
ethanol	64-17-5	VWR International GmbH
safranin O	477-73-6	ACROS Organics- Thermo Fisher Scientific Inc.
glutaraldehyde	111-13-8	Carl Roth GmbH + Co. KG
phosphate-buffered saline	-	BioWest SAS

Others

<u>Chemical</u>	<u>CAS-Nr.</u>	<u>Supplier</u>
potassium permanganate (KMnO ₄)	7722-64-7	Carl Roth GmbH + Co. KG

ruthenium tetroxide (RuO ₄)	12036-10-1	ACROS Organics- Thermo Fisher Scientific Inc.
diiodomethane (CH ₂ I ₂)	75-11-6	Alfa Aesar, Thermo Fisher GmbH
dimethyl sulfoxide ((CH ₃) ₂ SO)	67-68-5	Carl Roth GmbH + Co. KG
2,2'-Azobis(2- methylpropionitrile)	78-67-1	Sigma-Aldrich Chemie GmbH
sodium azide (NaN ₃)	26628-22-8	Sigma-Aldrich Chemie GmbH
sodium nitrate (NaNO ₃)	7631-99-4	Sigma-Aldrich Chemie GmbH

Declaration under Oath

I declare under penalty of perjury that this thesis is my own work entirely and has been written without any help from other people. I used only the sources mentioned and included all the citations correctly both in word or content.

Halle (Saale), 05.05.2020

Magdalena Jabłońska

Resume

Magdalena Jabłońska

M. Sc., Chemical Engineering

born on July 14, 1990 in Brzesko (Poland)

Nationality: Polish

Marital status: single

Education

- 06/2009 Nicolaus Copernicus High School in Brzesko (Poland)
- 10/2009 Tadeusz Kościuszko Cracow University of Technology
Faculty of Chemical Engineering and Technology
Subject area: Chemical and Process Engineering (Bachelor)
- 07-09/2012 Bachelor thesis in cooperation with Lurgi S.A in Cracow,
topic: „Future outlook to sustainable transportation fuel
production”: the fuel and energy market analysis".
- 02/2012 Engineer degree in "Chemical and Process Engineering"
- 02/2013 Tadeusz Kościuszko Cracow University of Technology
Faculty of Chemical Engineering and Technology
and Fachhochschule Münster
Faculty of Chemical Engineering
german-polish master degree course Chemical Processing
- 03/2014 Master thesis in cooperation with IAB Ionenaustauscher GmbH
in Bitterfeld, topic: "Influence of polysulfone layer thickness on
the performance and durability of high flux brackish reverse
osmosis membranes"
- 09/2014 Master of Science Chemical Engineering (overall grade 1.4)
- since 08/2015 PhD student at Martin Luther University Halle-Wittenberg,
Zentrum für Ingenieurwissenschaften

Work experience

- since 10/2014 Research assistant in Fraunhofer Institute for Microstructure of
Materials and Systems IMWS in Halle,
Business Unit Biological and Macromolecular Materials

Publications and awards

Peer-reviewed articles

M. Jabłońska, M. Menzel, U. Hirsch, A. Heilmann: Assessment of anti-adhesion and anti-biofouling potential of plasma-mediated sulfobetaine methacrylate coatings of feed spacer. In: Desalination (submitted, DES_2020_709)

J. Friedrich, M. Jabłońska, G. Hidde: Plasma Oxidation of Polyolefins - Course of O/C Ratio from Unmodified Bulk to Surface and Finally to CO₂ in the Gas Phase: A Critical Review. In: Rev. Adhesion Adhesives, 7 (2019) 233-257

M. Jabłońska, S. Reißaus, S. Henning, M. Menzel, A. Hähnel, J. Klehm, U. Hirsch, A. Heilmann: From the surface to the bulk: A comparison of methods for the microanalysis of an immiscible polymer blend. In: Micron 124 (2019) 102685

Conference contributions

M. Jabłońska, M. Rühl, M. Menzel, U. Hirsch, A. Heilmann: Anti-adhesion and Biofouling Studies of Zwitterionic Coatings of Feed Spacer for Biofouling Mitigation; 4th International Conference on Desalination using Membrane Technology, MEMDES, Perth, 01.-04.12.2019 (Presentation)

M. Jabłońska, T. Kürbitz, N. Teuscher, S. Richter, S. Schulze, A. Heilmann: Plasma-Funktionalisierung und Modifizierung von Nettings mit Antifouling-Beschichtung für die Anwendung in Reversosmose-Modulen zur Wasseraufbereitung; 12. Aachener Tagung Wassertechnologie, Aachen, 24.-25.10.2017 (Presentation)

M. Jabłońska, U. Hirsch, S. Richter, S. Schulze, A. Heilmann: Antifouling Modification of Reverse Osmosis Membrane by Coatings on Feed Spacer; 3rd International Conference on Desalination using Membrane Technology, MEMDES, Gran Canaria, 02.-05.04.2017 (Poster)

M. Jabłońska, U. Hirsch, N. Teuscher, M. Rühl, A. Heilmann: Biofouling Prevention by Functional Coatings on Feed Spacers in Membrane Modules for Water Desalination; PERMEA MELPRO 2016, Prag, 15.-19.05.2016 (Poster)

Awards

Hugo-Junkers-Preis für Forschung und Innovation aus Sachsen-Anhalt 2017: 1. Platz in der Kategorie „Innovativste Allianz“ mit dem Thema „Antifouling-Membranspacer in Umkehrosomosemodulen zur Wasserentsalzung“, U. Hirsch, M. Jabłońska, S. Schulze, A. Heilmann, S. Lehmann, C. Schellenberg

Best Poster award for the poster: Antifouling modification of reverse osmosis membrane modules by functional coatings on feed spacers, 3rd International Conference on Desalination using Membrane Technology, MEMDES, Gran Canaria, 02.-05.04.2017

Reviewers:

Prof. Dr. R. Wehrspohn

Prof. Dr. W. Binder

Prof. Dr. J. Vrouwenvelder

Defense date: 03.12.2020